UNIVERSITI TEKNOLOGI MARA

PREPARATION AND CHARACTERIZATION OF ACTIVATED CARBON-SUPPORTED ZINC OXIDE/GRAPHITIC CARBON NITRIDE FOR DEGRADATION OF ACETAMINOPHEN

NURUL IZZATI BINTI IZHAR

MSc

April 2026

UNIVERSITI TEKNOLOGI MARA

PREPARATION AND CHARACTERIZATION OF ACTIVATED CARBON-SUPPORTED ZINC OXIDE/GRAPHITIC CARBON NITRIDE FOR DEGRADATION OF ACETAMINOPHEN

NURUL IZZATI BINTI IZHAR

Thesis submitted in fulfilment
of the requirements for the degree of
Master of Science
(Chemistry)

Faculty of Applied Science

April 2026

CONFIRMATION BY PANEL OF EXAMINERS

I certify that a Panel of Examiners has met on 4 September 2025 to conduct the final examination of Nurul Izzati Binti Izhar on her Masters of Science thesis entitled "Preparation and Characterization of Activated Carbon-Supported Zinc Oxide/Graphitic Carbon Nitride for Degradation of Acetaminophen" in accordance with Universiti Teknologi MARA Act 1976 (Akta 173). The Panel of Examiner recommends that the student be awarded the relevant degree. The Panel of Examiners was as follows:

Nurul Husna Mohd Hassan, PhD
Associate Professor
Faculty of Applied Sciences
Universiti Teknologi MARA
(Chairman)

Norshahidatul Akmar Mohd Shohaimi, PhD
Senior Lecturer
Faculty of Applied Sciences
Universiti Teknologi MARA
(Internal Examiner)

Mohd Saufi Rosmi, PhD
Lecturer
Faculty of Science and Mathematics
University Pendidikan Sultan Idris
(External Examiner)

PROFESSOR DR HJH ZURAEDA IBRAHIM
Dean
Institute of Postgraduates Studies
Universiti Teknologi MARA
Date: 26 April 2026

AUTHOR'S DECLARATION

I declare that the work in this thesis was carried out in accordance with the regulations of Universiti Teknologi MARA. It is original and is the results of my own work, unless otherwise indicated or acknowledged as referenced work. This thesis has not been submitted to any other academic institution or non-academic institution for any degree or qualification.

I, hereby, acknowledge that I have been supplied with the Academic Rules and Regulations for Post Graduate, Universiti Teknologi MARA, regulating the conduct of my study and research.

Name of Student	:	Nurul Izzati Binti Izhar
Student ID. No.	:	2022142405
Programme	:	Master of Science (Chemistry) – AS756
Faculty	:	Applied Sciences
Thesis Title	:	Preparation and Characterization of Activated Carbon-Supported Zinc Oxide/Graphitic Carbon Nitride for Degradation of Acetaminophen
Signature of Student	:	……..
Date	:	April 2026

ABSTRACT

Pharmaceutical waste in wastewater has been causing great environmental concerns as it cannot be degraded with traditional wastewater treatment plants. To address this issue, a cost-effective UV-active photocatalyst, activated carbon-supported ZnO/g-C_3N_4 (AZG), was synthesized using a facile mixing method with different g-C_3N_4 ratios (0.01. 0.03, 0.05, 0.07 and 0.09 g). The photocatalytic performance of the composites was tested for the degradation of acetaminophen (ACE) under low-intensity UV light (7 W). The influence of parameters such as photocatalyst dosage, initial pH, ACE concentration, radical scavengers, and recyclability was also investigated. X-ray diffraction (XRD) confirmed that all AZG samples retained the characteristic ZnO diffraction peaks, indicating that the addition of activated carbon and g-C_3N_4 did not alter ZnO's crystal structure. Scanning electron microscopy with energy-dispersive X-ray (SEM-EDX) analysis showed irregular cubic ZnO particles distributed across the sheet-like g-C_3N_4 surface, while EDX verified the presence of Zn, C, O, and N elements. The reduced photoluminescence (PL) intensity suggested improved charge separation and lower electron–hole recombination. Among all samples, the AZG2 composite (AC:ZnO:g-C_3N_4 = 1.5:1:0.005) achieved the highest photocatalytic activity, removing 96.17% of ACE within 240 minutes with a rate constant of 1.357×10^{-2} min^{-1}, following pseudo-first-order kinetics under the optimal conditions of photocatalyst loading of 0.1 g, initial concentration of ACE of 10 mg/L and initial pH of 5.8. Overall, the results demonstrate that the AC-supported ZnO/g-C_3N_4 photocatalyst is an efficient and low-cost material for removing pharmaceutical contaminants from water.

ACKNOWLEDGEMENT

Firstly, I wish to thank God for giving me the opportunity to embark on my MSc and for completing this long and challenging journey successfully. My gratitude and thanks go to my supervisors Dr. Zul Adlan Mohd Hir, Dr Hartini Ahmad Rafaie and Dr Mohamad Azuwa Bin Mohamed.

My appreciation goes to UiTM Pahang who provided the facilities during the research works. Special thanks to my colleagues and friends for helping me with this project.

Specially, this thesis is dedicated to the loving memory of my very dear late father, Izhar bin Daud, and my dear mother, [redacted] for the determination and support to educate me. This piece of victory is dedicated to both of you. Alhamdulilah ‘ala kulli hal.

The road was indeed rough and bumpy. I lost few loved ones along the journey and yet Allah still blessed me with few beautiful souls that accompany me going through it.

Finally, this thesis would not be here without the support of my dear friends, and I dedicate this thesis to my youth and all those who cheered for me at the lowest point of my life.

TABLE OF CONTENTS

LIST OF TABLES

LIST OF FIGURES

LIST OF SYMBOLS

Symbols

•OH	Hydroxyl Radical
OH^-	Hydroxide Ion
$O_2\cdot$	Superoxide Radical
M	Molarity

LIST OF ABBREVIATIONS

Abbreviations

AC	Activated Carbon
ACE	Acetaminophen
Ag	Silver
AOP	Advanced Oxidation Processes
BBN	CQDs/BiO_2− X/BiOCl
BET	Brunaer-Emmet Teller Surface Area Analysis
$C_8H_9NO_2$	Acetaminophen
CB	Conduction Band
CB	Conduction Band
C-ZnO	Carbon-Doped ZnO
EDCs	Endocrine Disrupting Compounds
FESEM	Field Emission Scanning Electron Microscopy
g-C_3N_4	Graphitic Carbon Nitride
HA	Humic Acid
MB	Methylene Blue
N_2	Nitrogen
NSAID	Non-Steroidal Anti-Inflammatory Drugs
N-ZnO	Nitrogen-Doped Zinc Oxide

N-ZnO/CD	Nitrogen-Doped Zinc Oxide/Carbon Dot
O_2	Oxygen
PAHs	Polycyclic Aromatic Hydrocarbons
PL	Photoluminescence
RhB	Rhodamine Blue
ROS	Reactive Oxygen Species
SEM-EDX	Scanning Electron Microscopy-Energy Dispersive X-Ray
SMX	Sulfamethoxazole
TiO_2	Titanium Dioxide
UVB	Ultraviolet B
UVC	Ultraviolet C
UV-NIR	UV-Visible Near-Infrared
VB	Valence Band
VB	Valence Band
WWTP	Wastewater Treatment Plant
XPS	X-Ray Photoelectron Spectroscopy
XRD	X-Ray Diffraction Analysis
ZnO	Zinc Oxide

LIST OF NOMENCLATURES

Nomenclatures

eV	Bandgap Energy
nm	Nanometer
cm	Centimeter
g	Gram
min	Minutes

CHAPTER 1
INTRODUCTION

1.1 Research Background

Water pollution had already gotten a lot of attention from around the world, due to the presence of a wide variety of emerging contaminants especially the endocrine disrupting chemicals (EDCs) that cause hormonal imbalance (Lauretta et al., 2019). Endocrine disrupting chemicals, a category of exogenous chemicals which can disturb with hormone release in the body, have been linked to endocrine function disruption, which has a negative impact on human health and growth (Lauretta et al., 2019). Industrial chemicals, such as polycyclic aromatic hydrocarbons (PAHs), brominated flame retardants, pesticides, dioxins, parabens, pharmaceutical and personal care products, polyhalogenated and phenolic compounds, phthalates, organic solvents, and some heavy metals, as well as occurring naturally phytoestrogens, are among the causative chemicals of endocrine disruption in wild populations (Munyengabe et al., 2022; Ohore & Songhe, 2019).

EDCs are categorized based on how they affect the body's endocrine system. Based on Lauretta et al., 2019, EDCs can be classified into four categories: industrial (including polychlorinated biphenyls (PCBs), dioxins, and alkylphenols), agricultural (including pesticides, insecticides, herbicides, phytoestrogens, fungicides), residential (phthalates, polybrominated biphenyls, bisphenol A), and pharmaceutical (parabens) (Branco et al., 2021; Lauretta et al., 2019; Munyengabe et al., 2022; Ohore & Songhe, 2019). The extensive list of EDCs may contain even heavy metals like arsenic, cadmium, lead, and mercury (Branco et al., 2021; Nassri et al., 2023). EDCs can act in a variety of ways, including imitating or antagonising the effects of hormones, disturbing natural hormone production pathways, disrupting hormone secretion or metabolism, and meddle with the expression of their nuclear receptors (Stukenborg et al., 2021). Endocrine disruptors are also believed to contribute to the pathogenesis of a variety of disorders, including infertility in both men and women, sexual underdevelopment, congenital abnormalities, endometriosis, and cancer (Nassri et al., 2023; Stukenborg et al., 2021). Some EDCs, in fact, were seen in multiple modes of action, which can have negative consequences for earth ecosystems (Garg et al., 2021).

Numerous examples of reproductive and developmental anomalies in a wide range of wildlife, including invertebrates, fish, amphibians, birds, and mammals (Lauretta et al., 2019; Stukenborg et al., 2021), have been reported over the decade, many of which are linked to EDC exposure. Endocrine disruption in wildlife occurs frequently in animals that live in or are closely associated with the aquatic environment. It is not shocking, given that surface water serves as a sink for both natural and anthropogenic chemicals released into the environment (Munyengabe et al., 2022). Surface water has been contaminated by EDCs through sewage effluents from domestic and industrial amenities, as well as industrial wastewaters discharges (Steplin Paul Selvin et al., 2018). The amount of chemicals in the aquatic system, combined with aquatic life's underlying proneness to the effects of EDCs, has a major effect on aquatic ecosystem biodiversity. Aquatic life could be continuously exposed to a wide range of EDCs at various concentrations in certain water bodies with high anthropogenic chemical inputs.

Acetaminophen (ACE) or commonly known as paracetamol are used to reduce fever or popularized as pain killer. ACE can be bought easily as it requires no prescription from doctors, which makes it very popular. However, due to its wide usage, this drug has been found in various environments including rivers, lakes, groundwater, ocean, and wastewater. This drug possesses toxicity to different organisms. Concerns have been raised about the high ACE dosages used with anti-inflammatory medication, and studies have shown that unmetabolized ACE in humans is eliminated in faeces and urine before being released into the water environment (Jiang et al., 2023; Mirzaee et al., 2019; Soltani et al., 2019; Wilkinson et al., 2022). This would cause bacteria in an aquatic environment may become resistant, making the drug no longer useful. Due to intricate interactions between the chemicals, the impacts are much bigger than simple combinations of the harmful effects of the individual compounds (Wilkinson et al., 2022). Second, chemical processes take place when ACE is heated. High amounts of ACE and its by-products can have a substantial influence on our ecological environment because it was very toxic to the liver and kidneys. ACE can also have this effect if sewage facilities do not completely degrade them. Therefore, the need for more effective and useful degrading techniques is imperative.

Though since traditional wastewater treatment methods aren't designed to remove toxic organic pollutants like EDCs, these toxins have ended up in aquatic life, where they can subsequently make their way into the human food chain (Kodom et al.,

2021). Advanced oxidation processes (AOP) are a common method used for groundwater treatment which has been shown to be an efficient technique for oxidising and removing contaminants from water, given that AOPs are based on the production of reactive oxygen species (ROS), such as superoxide ($\bullet O_2^-$) and hydroxyl ($\bullet OH$) radicals which with a single unpaired electron, they have a brief lifespan (Tisler et al., 2022). As a result, they interact actively and quickly with a variety of chemical species that would be very challenging to break down otherwise.

According to Ameta (2018), AOPs are centred on the production of reactive oxygen species such as hydroxyl radicals with one unpaired electron, they have short lifetimes. As a result, they rapidly and freely react with a variety of chemical species that would otherwise be extremely difficult to degrade. AOPs outperform other traditional techniques because they produce thermodynamically stable oxidation products like carbon dioxide, water, and biodegradable organics. AOPs include the photocatalysis process, which is critical in the harvesting of sunlight by a photocatalyst. Photocatalysts are substances that, when exposed to light, change the rate of chemical reactions. In other word, photocatalysis refers to reactions that occur when light (photon energy) is being absorbed by a semiconductor photocatalyst combined and generate an electron-hole pair (Lauretta et al., 2019; Munyengabe et al., 2022). Photocatalysts can be used for antifouling, antifogging, energy conservation and storage, deodorization, sterilisation, self-cleaning, air purification, wastewater treatment, and many other applications (R. Ameta et al., 2018; Yue et al., 2024). Because of their electronic structure, semiconductors act as photo redox sensitizers. Many organic pollutants, such as aromatics, halo hydrocarbons, insecticides, pesticides, dyes, and surfactants, can be completely mineralized by some semiconductors. Semiconductor-based photocatalysis has received much interest because it helps to solve the problem of fast charge recombination (S. C. Ameta, 2018; Low et al., 2017).

Zinc oxide (ZnO) is a semiconductor metal oxide and widely regarded as the most potential photocatalytic materials for the abatement of pollutant in water. It has a wide bandgap of 3.37 eV, good mechanical, thermal, and chemical stability, nontoxic, and cost-efficient (R. Ameta et al., 2018; S. Kumar et al., 2018; Low et al., 2017; Qi et al., 2017; P. Qiu et al., 2018; Reddy Pullagurala et al., 2018). ZnO, on the other hand, only effective under UV light due to its large bandgap. Besides that, the fast charge carrier recombination in ZnO limits its practical application (S. Kumar et al., 2018; P. Qiu et al., 2018; Reddy Pullagurala et al., 2018). Countless attempts have been made to

help enhance the photocatalytic activity of ZnO-based photocatalysts by doping or compositing with metals, nonmetals, carbon-based materials (graphene, graphene oxide, and reduced graphene oxide) (Chubenko et al., 2019), or combining with visible bandgap semiconductor to heterojunctions (Qi et al., 2017; Youssef et al., 2018; Zhu et al., 2020). However, work on developing a more efficient ZnO-based photocatalyst with higher photocatalytic efficiency is still ongoing (Luu Thi et al., 2021).

One of the simplest ways to improve the photocatalytic property is to combine ZnO with a non-metallic loading to create a binary composite photocatalyst. Carbon-based materials have a broad absorption spectrum in the visible region and are very inexpensive sensitizers (Amornpitoksuk et al., 2018). Wide band gap metal oxides can benefit from the addition of carbon because it can increase both their absorption and their photocatalytic activities even when exposed to visible light (Akir et al., 2017; Amornpitoksuk et al., 2018).

Activated carbons (AC)s are the most commonly used adsorption material due to its excellent physical and chemical characteristics, including its large specific surface area, abundance of functional groups, chemical stability, high mechanical strength, and resistance to acids and alkalis (X. Li et al., 2020). Due to its high adsorption capacity, which is a result of both its large specific surface area and numerous pores, activated carbon (AC) is the most widely used material as an adsorbent (X. Li et al., 2020).

On the other hand, graphitic carbon nitride (g-C_3N_4) is a stable, metal-free, p-conjugative, and n-type polymeric semiconductor with a narrow bandgap (2.7 eV), which could be a good visible-light-responsive photocatalytic composite partner for ZnO (Asadzadeh-Khaneghah & Habibi-Yangjeh, 2020; Inagaki et al., 2019; Lu et al., 2018; Zhao et al., 2019). Since the two materials have very well, overlapping band structures, coupling ZnO with g-C_3N_4 could result in an excellent heterostructure for improving charge separation. These heterostructures have been shown to continue improving photocatalytic activity in previous studies. The transfer of a visible-light induced electron from the conduction band (CB) of g-C_3N_4 to the conduction band (CB) of ZnO explains the improvement (Lia et al., 2021; Ravichandran et al., 2018; Sundaram et al., 2017).

These days, ternary composite photocatalysts attract a lot of attention from researchers due to their superior photocatalytic activity compared to binary composites. In this study, a straightforward production method was used for a UV light driven g-

C_3N_4, activated carbon supported ZnO (AC-supported ZnO/g-C_3N_4) composite photocatalyst.

1.2 Problem Statement

The negative effects of EDCs on human and wildlife reproductive health have become a major source of public concern (Ohore & Songhe, 2019). In addition, chemical compounds of various kinds are released into the aquatic system, represents a major threat. Due to the widespread use of drugs in human activities, the natural environment has been plagued by drug pollution over the past few decades (Basheer, 2018; Guo et al., 2019; Kanakaraju et al., 2018; Sa-nguanprang et al., 2020; Tang et al., 2020). Acetaminophen (ACE), which is praised for its use as an indicator in certain water treatment processes to gauge the level of pollution in the water, has gained attention due to its possible threat to human and environmental health (Behravesh et al., 2020; Feng et al., 2018; Guo et al., 2018; Mashayekh-Salehi et al., 2017; Ramachandran & Jaeschke, 2019; Q. Zhang et al., 2020). ACE has been removed from wastewater using a variety of techniques and technologies up to this point, including chemical oxidation, membrane separation, conventional water treatment, and microbiological technology (K. Li et al., 2021). Unfortunately, the aforementioned technologies have a number of disadvantages that have severely restricted their large-scale application, such as expensive costs, low recycling abilities, and limited removal effectiveness (Behravesh et al., 2020; Kanakaraju et al., 2018; Leng et al., 2020; Maryam et al., 2020). The goal is to create an AC-ZnO/g-C_3N_4 photocatalyst that is both affordable and high-performing by combining inexpensive materials with complementary properties to improve charge separation, increase pollutant adsorption, and facilitate effective photocatalysis in the presence of visible light (Melchionna & Fornasiero, 2020).

Photocatalysis is a phenomenon that occurs when a semiconducting substance is exposed to light and creates an electron-hole pair (R. Ameta et al., 2018). A photocatalyst is a substrate that absorbs light and functions as a catalyst for chemical reactions. All photocatalysts are fundamentally semiconductors. Nevertheless, photocatalysis has been gaining popularity as an up-rising eco-friendly technology that can break down those organic compounds into safer compounds (Sa-nguanprang et al., 2020). To tackle this problem, the majority of countries enacted strict environmental pollution control regulations and due to this concern, numerous treatment processes are

currently proposed for the removal of EDCs, chemically, physically, and biologically (Mashuri et al., 2020). Many heterogeneous photocatalysts have been researched, and the most popular among of them are the semiconductor photocatalysts, ZnO has been widely studied under ultraviolet and/or visible light (Garg et al., 2021; Luu Thi et al., 2021; Sa-nguanprang et al., 2020; Youssef et al., 2018). ZnO is widely recognized as a crucial photocatalyst and has garnered significant interest due to its rich earthly abundance, low cost, biocompatibility, good thermal and chemical stability, and relatively low surface area. Due to its large 3.37 eV bandgap, ZnO exhibits a high ability to absorb exclusively UV light, making it an n-type semiconductor (Feng et al., 2024). In actuality, ZnO photocatalyst has already been successfully applied in a range of possible applications and has shown to be a practical photocatalyst, especially in the production of hydrogen, the removal of pollutants, and the conversion of CO_2 (Ahmad et al., 2024). Many studies published on the use of ZnO for photodegradation, and several types of ZnO-based heterojunctions have been developed to improve ZnO photocatalytic capabilities. Even so, most of the studies were focusing more on improving the properties of ZnO-based photocatalyst and use it for degradation of dyes. Thus, using the capabilities of ZnO-based photocatalysts for other organic pollutants for instance EDCs could also be done.

Due to its large bandgap, ZnO has a lower photocatalytic activity under visible light (Luu Thi et al., 2021). ZnO is among the most popular oxide semiconductor photocatalysts. However, the photo corrosion of ZnO materials caused by the photogenerated holes was found to be severe during the reaction, which could affect the stability and photocatalytic activity of ZnO (Tsai et al., 2022). Regarding this, coupling ZnO with other non-metal carbonaceous materials such as carbon atom and g-C_3N_4 could be a complementary move in preparing a stable yet highly effective photocatalysts. Mesoporous g-C_3N_4 enhances the absorption ability and reactant adsorption capacity of binary ZnO/g-C_3N_4 (Garg et al., 2021). Since the two materials have well-matched, overlapping band structures, coupling ZnO with g-C_3N_4 could result in an excellent heterostructure for improving charge separation (Luu Thi et al., 2021). However, there are not many studies that proposed the photoactivity of ZnO through heterojunction with carbon or g-C_3N_4/C-ZnO photocatalyst in the previous study. Many efforts are being made to improve ZnO photocatalytic efficiency (Sambaza et al., 2020; Sboui et al., 2022). However, its wider bandgap (3.37 eV) inhibits it to absorb light having a wavelength longer than 330 nm. Thus, ZnO can only absorb

ultraviolet (UV) radiations, which is only 5% of the solar spectrum. Another drawback is the faster recombination of excited charge carriers, which renders its inefficient for solar light-driven photocatalysis (Ayoub et al., 2018). ZnO photocatalysts can only be activated and work efficiently under ultraviolet light (UV) irradiation (Youssef et al., 2018). On the other hand, they suffer from high electron-hole recombination, which reduces photonic efficiency significantly (Sa-nguanprang et al., 2020; Yuan et al., 2019). In this case, modifying and grafting of non-metal materials like carbon atom and g-C_3N_4 onto a wide bandgap ZnO photocatalyst could be a complementary strategy for preparing an active and stable low intensity UV light driven photocatalyst which is straight forward and cost-friendly.

1.3 Research Objectives

a) To synthesis different ratio of Activated carbon (AC) supported ZnO/g-C_3N_4 using facile chemical mixing method.
b) To investigate the physicochemical characteristics of AC supported ZnO/g-C_3N_4 photocatalysts on narrowing the band gap and improving photoinduced electron-holes separation efficiency towards low intensity UV light response.
c) To evaluate the photocatalytic activity, degradation rate and kinetic study of the prepared photocatalyst under low intensity UV light and experimental conditions of the study.

1.4 Scope of Study

The working solution used was ACE of 10 mg/L and was irradiated to low intensity UV light (7W). The different ratio of AC to ZnO also the ratio of AC-ZnO to g-C_3N_4 in the preparation of the photocatalysts were studied. The effect of a few variables for the photocatalytic experiment, including the photocatalyst loading (0.1, 0.15, 0.20 and 0.25) g, initial pH of ACE (2,4,6,8 and 10), initial concentration of ACE (5, 10, 15 and 20) mg/L, radical scavenger (•OH, $•O_2^-$ and h^+), and recyclability (up to 5 cycles) as well as kinetic analysis of each variable was also studied during the process. The surface physicochemical properties of AC supported ZnO grafted g-C_3N_4 photocatalyst will be characterized by Scanning Electron Microscopy-Energy Dispersive X-ray analyser (SEM-EDX), Field emission scanning electron Microscopy

(FESEM) and elemental analysis through Energy dispersive X-ray analyzer (EDX), X-ray diffraction (XRD), N_2 adsorption-desorption analysis with Brunaer-Emmet-Teller (BET) surface area analysis, X-ray photoelectron (XPS), Photoluminescence (PL), and UV-vis near-infrared (UV-NIR) spectroscopy.

1.5 Significance of Study

The photocatalytic activity of AC-supported ZnO/g-C_3N_4 photocatalyst is particularly interesting to study because it has the potential to be effectively and continuously applied in a real-life industrial wastewater treatment, particularly for the removal of ACE. Moreover, this research would be an important strategy for gaining a comprehensive understanding of the morphological, structural, and optical properties of a highly stable AC-supported ZnO/g-C_3N_4 photocatalyst coupling system. Furthermore, this research will produce an improved semiconductor photocatalyst that will aid in the development of a cost-effective wastewater treatment process by utilising low intensity UV light irradiation, which is intends to develop a cost-effective and sustainable wastewater treatment process that lowers operating costs in comparison to conventional methods by optimising photocatalytic efficiency under low-intensity UV light irradiation that is less expensive than usual UV light irradiation. It emphasises improving the performance of semiconductor photocatalysts while guaranteeing their resilience and versatility. In addition to aiding in environmental cleanup, this research paves the way for the expansion of photocatalytic technologies into more extensive industrial uses.

CHAPTER 2
LITERATURE REVIEW

2.1 Introduction

This chapter is to give a brief overview among some earlier research on photocatalysis that has already been conducted in order to identify knowledge gaps and guide the structuring of the current study. This provides an understanding of recent research regarding the theoretical, empirical, and methodological issues, as well as a clear and relevant recommendations for the future study. This analysis lays the groundwork for a targeted and creative investigation by critically examining open problems and providing insights into recent advancements in the field. It also highlights areas with a high potential for significant advancements and provides specific, achievable recommendations to direct future research directions.

2.2 Photocatalysis

Photocatalysis is a process when photons generated from any light a source for example UV or visible light react with H_2O or OH^- adsorbed on the photocatalyst surfaces to form hydroxyl radical which is •OH, and electrons in the conduction band react with adsorbed oxygen (O_2) to form •OH radical. Those radicals formed are very reactive and unselective antioxidants (Tahir et al., 2022). Solar photocatalysis is also regarded as a cost-effective and sustainable treatment method due to its use of solar energy which are an abundant source of energy (J. Qiu et al., 2022). Photocatalysis is a technique with high potential for treating contaminated water since it is both eco-friendly and cost-effective, and it can degrade a variety of organic dyes and pollutants (Chauhan et al., 2019; N. B. Singh et al., 2018).

Photocatalytic reaction consists of two categories: homogeneous photocatalysis and heterogeneous photocatalysis. Homogeneous photocatalysis are when both the photocatalysts and reactant are in the same phase, i.e, gas, solid or liquid typically liquid where dissolved species such as O_2 or metal ions involved in the reaction (R. Ameta et al., 2018; Mondal & Sharma, 2016). For example, Loaiza-ambuludi et al., used Fenton's reagent in conjunction with UV-C radiation to catalyse the in situ production of

hydroxyl radicals, a potent oxidising agent that causes ibuprofen to degrade until complete mineralisation (Loaiza-ambuludi et al., 2014). On the other hand, in heterogeneous photocatalysis, the reactants are in liquid or gas phases, and the photocatalyst is in a different phase, typically a solid. Solid-phase catalysts, such as ZnO or TiO_2, effectively break down contaminants when exposed to UV or visible light, providing special benefits for air and water purification systems (R. Ameta et al., 2018). The primary benefit of employing a heterogeneous catalyst is that it uses a solid catalyst that is simple to separate from the gas and liquid reactants and products (Jacques, 2017; S. Singh et al., 2021).

2.2.1 Heterogeneous semiconductor Photocatalyst

Heterogeneous semiconductor photocatalyst, which utilizes solar radiation as a source of photons to activate the catalyst, has gotten a lot of interest in recent years. Some heterogeneous photocatalysts have been studied in previous research such as TiO_2 that has been widely studied under ultraviolet and/or visible light meanwhile ZnO, with a gap energy of 3.37 eV, is another photocatalyst that absorbs a considerable portion of the sunlight spectrum (S. Singh et al., 2021). Photocatalysts like TiO_2 and ZnO are broadly used by researchers. This is because of their high photocatalytic activity and exceptional chemical and mechanical stability, as well as the fact that they are harmless and affordable (Phuruangrat et al., 2014). Xu and Ma (2023) synthesized a series of Ag/g-C_3N_4/TiO_2 nanocomposites using post-hydrothermal and spinning techniques to degrade Rhodamine B (RhB) that achieves a significantly higher photocatalytic efficiency in which RhB can be totally broken down in 110 minutes (Xu & Ma, 2023). Meanwhile, the sol-gel method was used to create silver (Ag)-decorated microstructures and ZnO photocatalyst with Ag. The samples were utilised to break down methylene blue (MB) in aqueous solution via photocatalysis. The maximum degradation after 60 minutes rose up to 87.74% (Rafaie et al., 2017).

Since both ZnO and TiO_2 have broad band gaps (~3.2–3.3 eV), they are mostly active in UV light, which makes up a very minor portion of sunlight. Improving their visible light activity is still very difficult (Raza et al., 2020). Although methods like as sensitisation, heterojunction creation, and doping have been investigated, effective and scalable approaches are still missing. One major drawback is that photogenerated electron-hole pairs quickly recombine, lowering photocatalytic effectiveness. Even

though many modifications have been employed to enhance charge separation, additional effort is required to create reliable and long-lasting solutions. Certain improvement techniques restrict scalability and environmental friendliness by utilising costly or hazardous ingredients. The demand for affordable, environmentally friendly synthesis methods that make use of plentiful, secure ingredients is rising (Mehta et al., 2022).

2.2.1.1 Zinc oxide (ZnO)

Specifically for this study, ZnO will be used due to its strong electrical conductivity and optical transmittance in the solar spectrum (Pant et al., 2020). ZnO owns great potential in alteration of bandgap, yet it is easier to crystallize and manufactured (Behravesh et al., 2020; Krishnakumar et al., 2021; Tsai et al., 2022). ZnO bandgap can be adjusted by doping it with either i) transition metal or non-metal, or ii) hybridization with other of those with small bandgap semiconductor or metal to create Shockley junctions, iii) create vacancies in structure (Garg et al., 2021; Sa-nguanprang et al., 2020; Youssef et al., 2018).

ZnO is an n-type semiconductor by nature, but carbon doping converts it to a p-type semiconductor (Girija Shankar et al., 2021). The electrical and optical properties of p-type ZnO fluctuate dramatically, and it even develops new properties (Yu et al., 2023). ZnO may be doped to add new features or improve ones that already exist, making it a material that can be used in a variety of ways. To alter the characteristics of the ZnO crystal lattice, doping entails adding particular ions (Mehwish et al., 2025). Doping plays a distinctive role in enhancing ZnO's functionality and performance (Carofiglio et al., 2020). Doping enables the modification of ZnO's optical, electrical, electromechanical, and catalytic characteristics, among other physical and chemical characteristics. ZnO's characteristics are changed, and its photocatalytic efficacy is increased by doping it with metal, non-metal, or noble metal components (Y. Sun et al., 2023). Doping carbon, for example, will expand ZnO's optical absorption to the visible-light region (Garg et al., 2021; Sa-nguanprang et al., 2020; Youssef et al., 2018). The porous carbon-doped ZnO (C-ZnO) was produced by the calcination of zinc compounds produced by the hydrothermal reaction of zinc gluconate (Haibo et al., 2013). The absorption edge of the C-ZnO clearly redshifts, and its absorption in the UV and visible light regions is noticeably increased. The photocatalytic activity of the produced C-

doped ZnO demonstrated a significant photodegradation rate of RhB (98%) after 25 minutes of sun light irradiation (Haibo et al., 2013). On the other hand, Ayu et al., (2023) successfully synthesized nitrogen-doped zinc oxide (N-ZnO) and nitrogen-doped zinc oxide/carbon dot (N-ZnO/CD) nanocomposites and degraded methylene blue efficiently (83.4% in 60 minutes) (Ayu et al., 2023).

However, due of its large band gap (3.37 eV), ZnO can only be used for photocatalysis in the UV spectrum. ZnO's capacity to harness solar energy is constrained since UV light only makes up a small percentage of sunlight. Effective methods to improve its reaction to visible light are still required. ZnO's vulnerability to photocorrosion, particularly in acidic or alkaline conditions, is another disadvantage. As a result, it becomes less stable and reusable in aqueous photocatalytic systems. There is continuous research to determine how to increase ZnO's resilience to extended light. ZnO's photocatalytic effectiveness is reduced by the rapid recombination of photogenerated electron-hole pairs. Stable and long-lasting charge separation is still difficult to achieve, despite the use of heterojunctions and doping to solve this (Krishnakumar et al., 2021).

2.2.1.2 Activated carbon (AC)

Activated carbon (AC) has drawn the attention of numerous researchers due to its low cost, higher surface area, and potential as a supporting material for polymers to enhance the mechanical, thermal, and physicochemical properties of composite materials in comparison to pure polymer (R. Kumar et al., 2023; Mariana et al., 2021). Due to its excellent adsorption ability, which is caused by a combination of its substantial specific surface area and the existence of many pores, AC is the most often employed material as an adsorbent (Kim et al., 2023; Sushant Kumar et al., 2023; X. Li et al., 2020; Oyim et al., 2022). As a result, AC is frequently used to remove VOCs from water and the vapor phase (M. S. Reza et al., 2020). The three-component method was created to boost activity and expand the photocatalyst's surface area. Additionally, AC helps the catalyst adsorb more pollutant molecules and speeds up the degradation of the material (Steplin Paul Selvin et al., 2018). Additionally, a bigger surface area catalyst is required for photocatalytic reactions so that the pollutant can be contacted by the catalysts more easily, increasing the photocatalyst's catalytic efficiency. Therefore, AC is used to be coupled with ZnO in this study to increase the efficiency of ZnO as a

photocatalyst. Yue et al., (2024) successfully synthesized TiO_2/AC nanocomposites with long-lasting simultaneous adsorption and photocatalysis properties (Yue et al., 2024). The synthesized TiO_2/AC also showed dye degradation efficiency of 99.6% after the exposure of natural. These findings showed that the TiO_2 and AC has good synergistic adsorption and photocatalytic characteristics, which make it a powerful catalyst combination for the degradation of organic contaminants (Yue et al., 2024).

2.2.1.3 Graphitic carbon nitride (g-C_3N_4)

Graphitic carbon nitride (g-C_3N_4) is a photocatalytic material that is frequently used to absorb visible light (Lia et al., 2021; Mukhair et al., 2023; Ravichandran et al., 2018; Xu & Ma, 2023). g-C_3N_4 has attracted much interest as a possible visible light photocatalyst for water photo-splitting and organic pollutant degradation, because it has a lot of thermal and chemical stability and interesting electronic properties (K. Li et al., 2021; F. Liu et al., 2019; Munusamy et al., 2021; Ouriques Brasileiro et al., 2023). g-C_3N_4 have excellent photocatalytic performance for the removal of organic dyes under visible light irradiation when heated with cyanamide (Inagaki et al., 2019).

The g-C_3N_4 has the smallest direct band gap (2.7 eV) and the most stable of all the carbon nitride allotropes, resulting in high photocatalytic efficiency under visible light irradiation. It is composed of π-conjugated graphitic planes formed by the sp^2 hybridization of carbon and nitrogen atoms (MuthuKathija et al., 2023a). Even so, due to its low quantum efficiency and high recombination rate of photogenerated electron hole pairs, pure g-C_3N_4 photocatalytic efficiency is limited (Xu & Ma, 2023). Many methods have been discovered to improve the photocatalytic activity of g-C_3N_4, including the preparation of mesoporous structures, doping and coupling with metal, and non-metal species (L. Li et al., 2018; Mukhair et al., 2023; MuthuKathija et al., 2023; Q Alfaifi & A Bagabas, 2019). Xu and Ma, (2023) narrated when small amounts of Ag were distributed over pure g-C_3N_4 photo-catalysts under visible light irradiation, g-C_3N_4 showed enhanced photocatalytic activity. Furthermore, g-C_3N_4 can be made using a simple thermal decomposition method from low-cost, widely available precursor materials like urea and thiourea (Akhundi et al., 2019).

Combining ZnO with a visible light sensitizer is advantageous, not only because it improves light harvesting, but also because it facilitates charge separation in photoexcited electron–hole pairs (excitons) (Luu Thi et al., 2021). Since the two

materials have well-matched, overlapping band structures, coupling ZnO with g-C_3N_4 could result in an excellent heterostructure for improving charge separation (Jianxin Li et al., 2023). Indeed, previous research has demonstrated that such heterostructures have managed to improve photocatalytic activity since the initial electron excited from the valence band (VB) to the conduction band (CB) of the g-C_3N_4 by visible light irradiation could now transfer to the CB of ZnO (Garg et al., 2021; L. Li et al., 2018; Luu Thi et al., 2021; Ravichandran et al., 2018). Ravichandran et al., (2018) revealed that mesoporous g-C_3N_4 enhances the visible light absorption ability and reactant adsorption capacity of binary ZnO/g-C_3N_4. Despite these benefits, there are few reports on ZnO/g-C_3N_4 composites in thin film form in the literature (Uma et al., 2017).

2.3 Endocrine Disrupting Compounds (EDCs)

Endocrine disrupting compounds (EDCs) develop a crucial category of arising environmental contaminants in which brings threats to aquatic creatures and also to human beings (Garg et al., 2021). Endocrine disruptors are assumed to be responsible for the rising rate of cancer and the hypothesis that men's reproductive fitness is deteriorating (Gunnarsson et al., 2019; Stukenborg et al., 2021). Industrial additives, persistent organic pollutants, pharmaceutical products (drugs of abuse, stimulants, analgesics, antibiotics, non-steroidal anti-inflammatory drugs (NSAIDs), antihistamines, and hormones), personal care products (fragrances, parabens), plasticizers, flame retardants, and surfactants are among the contaminants of emerging concern found in surface waters (Nilsen et al., 2019). Certain contaminants are categorised as endocrine disrupting compounds (EDCs), which are substances that interfere with the functioning of the endocrine system (Branco et al., 2021). These substances alter the synthesis, secretion, transport, and/or action of hormones that are naturally secreted by the organisms, changing their physiology, including reproduction (Branco et al., 2019). These substances also change the hormones that are part of the reproductive axis, such as those released by the hypothalamus, pituitary, and gonads (HPG) (Branco et al., 2019). Pharmaceutical products are frequently identified as potential EDCs (Branco et al., 2021). When released into aquatic environments, these products pose a global threat (Gunnarsson et al., 2019). This is because, although they have been found in water at concentrations ranging from ngL^{-1} to μgL^{-1}, the majority of them are resistant to conventional water treatment (Branco et al., 2021). However,

due to their widespread use in aquatic environments, nonsteroidal anti-inflammatory drugs (NSAIDs) have drawn special attention. They are unique primarily in that they can be used without a prescription and are consumed at the highest rate globally (Michelon et al., 2022). NSAIDs have a short half-life, but they persist long enough to enter water supply systems, which exacerbates the problem (S. C. Ameta, 2018; Low et al., 2017). Branco et al. (2021) also noted that NSAID removal from sewage treatment plants is limited (Branco et al., 2021).

2.3.1 Acetaminophen (ACE)

Acetaminophen (ACE) is a well-known antipyretic and analgesic that is frequently prescribed to treat fever and mild to moderate pain, also known as paracetamol (Brillas & Manuel Peralta-Hernández, 2023). The chemical formula for this compound, which has the CAS number 130-90-2, is $C_8H_9NO_2$, with M = 151.165 g mol^{-1}, solubility in water of 14 gL^{-1} at 20°C, and pKa = 9.53. Following the consumption by humans and animals, it goes through partial metabolism before being eliminated through the urine and contaminating aquatic and natural environments, including wastewater treatment plants (WWTPs) (dos Santos et al., 2021).

Acetaminophen is categorized under non-steroidal anti-inflammatory drugs (NSAID) and it is among the endocrine disrupting chemicals (EDCs) (S. Kumar et al., 2018; Low et al., 2017; K. Qi et al., 2017). Acetaminophen, polybrominated diphenyl ethers (PBDE), vinclozolin and phthalates appear to be crucial etiopathogenetic factors in the occurrence of testicular dysgenesis syndrome (TDS) (Lauretta et al., 2019). The industrial manufacturing process of ACE and the disposal of overdue or unused drugs are significant additional factors that contribute to its environmental release (Phong Vo et al., 2019). Unfortunately, because wastewater is frequently not collected and treated properly, ACE dominates in surface water in developing countries. Rivers in Asia have been found to contain up to 33 ngL^{-1} of this drug, while rivers in Spain and France have been reported to contain between 0.4 and 71 ng/L (Phong Vo et al., 2019).

Human waste and wastewater from homes and businesses are the main sources of ACE, a persistent micropollutant found in the environment (Phong Vo et al., 2019). ACE is gathered in WWTPs and is disposed of in sewage systems by a variety of domestic activities. Following the treatment process or processes in WWTPs, ACE is still present in the effluent and is discharged into water reservoirs, where it contaminates

groundwater, soil, and sediment. Therefore, surface water, groundwater, soil, and sediments are the four environments where ACE is primarily found. Sewage and WWTPs are another (Phong Vo et al., 2019).

The majority of the time, conventional WWTP techniques like membrane filtration, sedimentation, activated sludge adsorption, biodegradation, and solar photolysis are ineffective for completely eliminating drug residue. Since this drug can oxidise cell lipids and denature proteins with damage to their genetic codes, long-term exposure to trace amounts of it over bacteria, plants, animals, and humans may cause endocrine disruption and chronic disease (Phong Vo et al., 2019). Thus, it is well established that certain bacteria, algae, fish, protozoa, and macrophytes are toxic to ACEs (Brillas & Manuel Peralta-Hernández, 2023).

2.3.2 ACE Degradation Using Heterogenous Semiconductor Photocatalyst

Various conventional techniques for the treatment of pharmaceutical wastes including ACE have been used over the years, but their overall effectiveness and convenience have been continually affected. Seeing as ACE found in wastewater has endocrine disrupting properties and is unsafe to humans and the environment even at very low concentrations, it is necessary to eliminate or limit its use in the production process, or to effectively treat any waste to guarantee its removal (S. C. Ameta, 2018; Low et al., 2017). Due to the obvious drawbacks of traditional treatment procedures, such as the formation of chlorinated metabolites, other alternatives, such as photocatalysis, have been thoroughly investigated (Reddy et al., 2018). Throughout this context, plenty of studies have recently been carried out in order to find new photocatalysts for the efficient degradation of ACE (S. Kumar et al., 2018; Low et al., 2017; Qi et al., 2017). Such photocatalysts were modified to increase their light absorptivity and/or to reduce electron/hole recombination (such as, via coupling, doping, morphological alterations, and other similar processes).

Hojamberdiev et al. (2020) reported that the heterojunction that developed between tin oxide (SnO_2) and zinc sulfide (ZnS) facilitate the effective separation of photogenerated charge carriers. Thus, SnO_2@ZnS composite photocatalysts degraded 70% of ACE under visible light irradiation sourced high pressure mercury lamp (emission was centered at 500-550 nm, light intensity was 7.31-7.53 mW cm^{-2}) (Hojamberdiev et al., 2020). On the other hand, Kumar et al. (2021) successfully

degraded (>99%) ACE using synthesized poly(3,4-ethylenedioxythiophene) (PEDOT) under UVB light irradiance of 16 mW/cm^2. In addition, by using the phase-inversion method, PES-ZnO (Polyethersulphone-Zinc Oxide PZ) photocatalyst sheets were synthesized and utilized in the oxidative breakdown of ACE (Chijioke-Okere et al., 2023). As a result, the maximum ACE degradation efficiency of 92% was recorded when four PZ-15 photocatalyst sheet pieces were used under 420 minutes of UV irradiation.

2.4 Mechanism of Photodegradation

Photocatalysis, also known as photocatalytic reaction, is a chemical reaction that occurs when light interacts with a photocatalyst (Yuan et al., 2019; F. Zhang et al., 2019). Since the reaction can be controlled using light or photon sources, this technique requires the use of light energy to activate the photocatalyst (Melchionna & Fornasiero, 2020). The energy of incoming visible or UV photons, and the crystal structure of the catalyst, decide the reaction rate (Yuan et al., 2019). The photocatalytic process generally uses light energy from the sun to drive an upward thermodynamic reaction that produces highly energetic chemical fuels, such as the water splitting reaction to produce hydrogen (de Moraes et al., 2020). Besides, there are a numerous advantage to this technique, including ecological sustainability, complete pollution degradation, as well as no secondary contamination (Chijioke-Okere et al., 2023).

The energy band of semiconductor contains a conduction band (CB) of high-energy, a valence band (VB) of low-energy and a forbidden energy gap that separates those two bands. Electrons on a VB are motivated and leap onto a CB at a specific light energy, whereas holes remain on the VB. The holes on the VB diffuse to the photocatalyst surface, where they actively engage in an oxidation process, while the electrons on the CB travel to the catalyst's surface and participate in a reduction process (Chijioke-Okere et al., 2023). In a photocatalytic process, the oxidation and reduction reactions occur simultaneously (Yuan et al., 2019). When dissolved oxygen (O_2) in water undergoes reduction in the presence of electrons, superoxide radical anions ($\bullet O_2^-$) are produced, which react with the water in the solution to produce hydrogen peroxide (H_2O_2). The photon energy from the light irradiation will be absorbed by this H_2O_2, which will then be reduced and separated into two hydroxyl radicals (•OH). In the meantime, the holes can produce hydroxyl radicals (•OH) by oxidising the hydroxide

ion (OH-). As a result, the •OH is responsible for the degradation of contaminants (S. C. Ameta, 2018; Low et al., 2017). The redox reactions are triggered by these electrons, and the holes and electrons are adsorbed on the semiconductor's surface where they undergo progressive oxidation and reduction reactions to produce the desired products. These reactions continue until light is available (Mandade, 2021). Equations (1.1-1.8) and Figure 2.1 provide a summary of the entire mechanism. Given that reduction and oxidation happen at the photocatalyst's valence and conduction bands, respectively, the reactions that take place on its surface are redox in nature (Ajiboye et al., 2021).

$$\text{Photocatalyst (PTC)} + \text{Pollutant (X)} \rightarrow \text{PTC (X adsorption)} \quad (1.1)$$

$$\text{PTC} + h\nu \rightarrow \text{PTC}\,(e^- + h^+) \quad (1.2)$$

$$O_2 + e- \rightarrow \bullet O_2^- \quad (1.3)$$

$$2\bullet O_2^- + 2H_2O \rightarrow H_2O_2 + 2OH^- + O_2 \quad (1.4)$$

$$H_2O_2 + e^- \rightarrow \bullet OH + OH^- \quad (1.5)$$

$$\bullet O_2^- + X \rightarrow \text{non-toxic or less-toxic products} \quad (1.6)$$

$$h^+ + X \rightarrow \text{non-toxic or less-toxic products} \quad (1.7)$$

$$\bullet OH + X \rightarrow \text{non-toxic or less-toxic products} \quad (1.8)$$

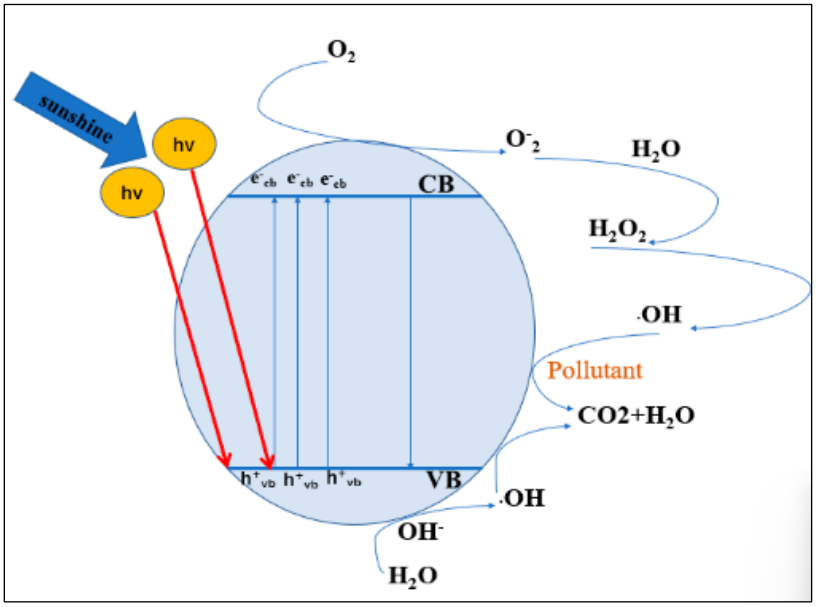

Figure 2.1 Photocatalytic Reaction Mechanism (F. Zhang et al., 2019)

The fundamental mechanism of a photocatalytic reaction is depicted in Figure 2.1 (F. Zhang et al., 2019). In simple words, a photocatalytic process on a semiconductor involves at least five major stages: (i) absorption of light by the semiconductor, (ii) formation of photogenerated electron–hole pairs, (iii) migration and recombination of photogenerated electron–hole pairs, (iv) adsorption and desorption of reactant, and finally the (v) appearance of redox reactions on the semiconductor in accordance to Figure 2.1, as shown in Figure 2.1 and 2.2 (Low et al., 2017).

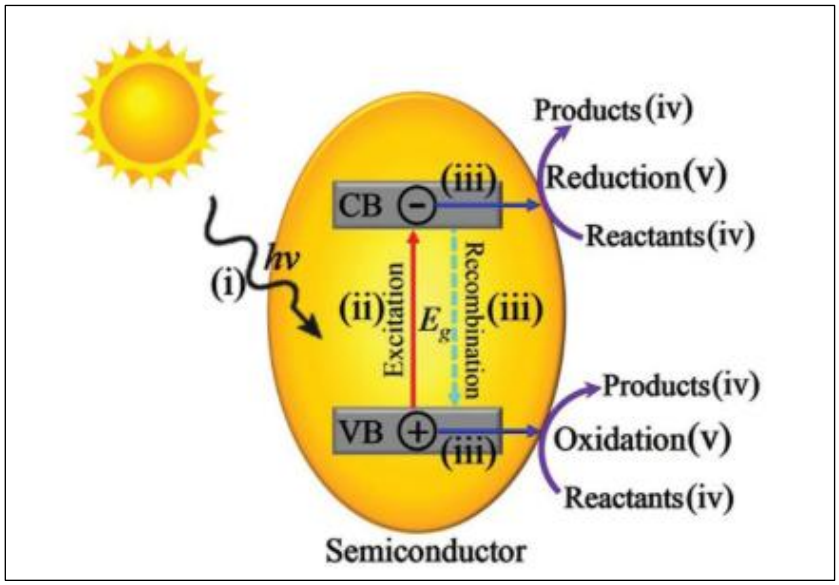

Figure 2.2 Photocatalytic Reactions Schematic Illustration on Semiconductor (Low et al., 2017)

2.5 Synthesis of Photocatalysis

2.5.1 Technique of Synthesis

Photocatalyst can be manufactured in a variety of ways. In recent years, various photocatalyst prepping methods and procedures have been introduced, including hydrothermal, electrospinning, impregnation, co-precipitation, solid-state, sonication, microemulsion, thermal evaporation, and sol-gel (Melchionna & Fornasiero, 2020). According to (Chijioke-Okere et al., 2023), various preparation techniques can be categorized into a few classifications of methods as shown in Figure 2.3.

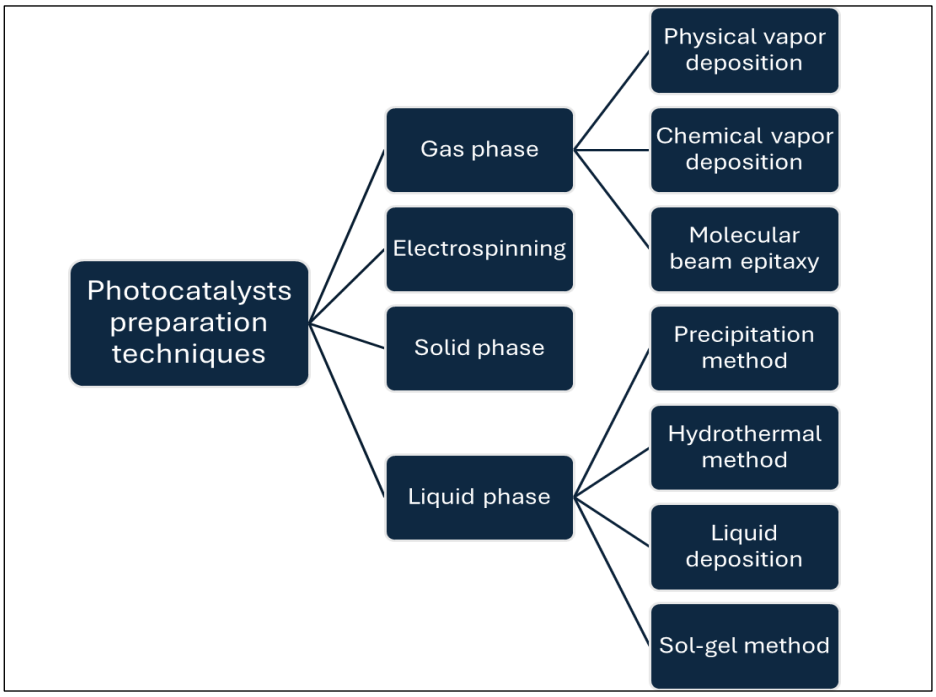

Figure 2.3 Techniques of Preparing Photocatalysts (Chijioke-Okere et al., 2023).

The methods used to make the photocatalyst are well known to have a significant impact on the photocatalytic properties and performances. According to Zhang et al., (2019), the efficiency of the synthesised photocatalyst can be adjusted by controlling the operating parameters. Because of the various compositions, forms, and sizes of the photocatalyst produced, the parameters used in the process design may influence on the photocatalyst's performance (Melchionna & Fornasiero, 2020). The solution-based approach is the most widely used method of creating photocatalysts due to its many benefits, which include being environmentally friendly, using low-cost chemicals, and

requiring such little energy. As a result, the liquid phase method is preferred over solid-based and gas-based techniques (Melchionna & Fornasiero, 2020).

2.5.2 Chemical Mixing

Groeneveld et al., (2022) stated that the liquid-phase/solution-based technique is the most widely used approach to creating photocatalysts due to its many benefits, including its low energy requirements, affordability of reagents, and environmental friendliness (Melchionna & Fornasiero, 2020). According Groeneveld et al., adjusting the operating parameters can regulate the generated photocatalyst's efficiency. The process design variables may lead to varying compositions, forms, and sizes, which may have an impact on the photocatalyst's performance (Melchionna & Fornasiero, 2020).

Chemical mixing technique is one of the techniques used to prepare photocatalysts. However, this technique is not widely used due to its unsuitability towards certain compounds. This technique includes two most crucial steps: i) mixing and ii) drying (S. Kumar et al., 2018; Low et al., 2017; K. Qi et al., 2017). The compound will be added to a media solution such as distilled water or organic solvent. The mixture will undergo continuous stirring for few hours to ensure it is homogeneous. Lastly, the mixture will undergo drying process to obtain the photocatalysts in powder form. Latha et al., (2017) utilized chemical mixing method to synthesize CeO_2/alumina nanocomposite and tested its photocatalytic activity performance towards degradation of Congo Red (CR) and Methylene Orange (MO) dye (Latha et al., 2017). CeO_2/alumina nanocomposite was prepared by mixing synthesized cerium oxide (CeO_2) nanoparticles and aluminium oxide (Al_2O_3) in deionized water and calcinated at 600°C for four hours (Latha et al., 2017). The photocatalytic activity of CeO_2/alumina nanocomposite was recorded to be at 90% of degradation rate of CR within 120 mins and 92% within 90 minutes of visible light irradiation (300W Tungsten lamp).

2.6 Factors Affecting Photocatalytic Degradation

For effective planning and implementation of photocatalysis processes in wastewater treatment, recognising the roles of various operational factors is crucial. A variation of operational factors that affect the breakdown of EDCs in wastewater, like initial substrate concentration, catalyst loading, pH value of the solution, reaction

temperature, light intensity, and wavelength, along with dissolved oxygen in solution, determine the rate and efficiency of a photocatalytic activity (Jiade Li et al., 2015). Some factors that influence the photocatalyst's effectiveness in photocatalytic degradation such as the photocatalyst's composition, crystal structure, and morphology, among many others (Jiade Li et al., 2015). The pH of the solution is important because it influences the photocatalyst's surface charge and how it interacts with contaminants; a basic pH encourages the formation of hydroxyl radicals as the main oxidant, while an acidic pH increases the adsorption of anionic species (J. Liu et al., 2023). Because higher concentrations may saturate active sites and prevent light penetration, the initial pollutant concentration also affects efficiency (Rafiq et al., 2021). The production of reactive species is also controlled by the characteristics of the photocatalyst, such as its surface area and bandgap energy, as well as the wavelength and intensity of the light. By promoting or suppressing the production of reactive species, scavengers like oxygen have an additional impact on the overall degradation performance (S. Kumar et al., 2018; K. Qi et al., 2017). According to Zhang et al. (2019), they listed six influencing factors that can affect photocatalysis including catalyst concentration, light source and light intensity, pH value, rate of electron-hole pair separation and oxygen presence, inorganic ions and temperature (Table 2.1). However, in this study we chose only 5 parameters which are the effect of photocatalyst loading, effect of initial pH, effect of initial concentration, radical scavenger and recyclability.

Table 2.1
Affecting Factors of Photocatalytic Activity and its Effects on Photocatalytic Reaction.

Affecting factors	**Effects on photocatalytic activity**
Catalyst concentration	- As the catalyst concentration increase, the photocatalytic activity also increases. - However, the photocatalytic activity decrease once it goes above the optimum amount.
Light source and light intensity	- Provide light of different wavelengths. - Improving light intensity and boost photocatalytic activity.
pH value	- The amount of hydrogen (H_2) generated by water splitting is dependent on the pH of the solution, or the

Affecting factors	Effects on photocatalytic activity
	proton concentration, as the electron generated by photolysis lowers the proton. - Strong basic medium produces the most H2 thus improving photocatalytic activity.
Plus oxidants	- Enhancing photocatalytic activity by reducing the recombination of electron and holes.
Inorganic ion	- Enhances photocatalytic process and speeds up the separation of photogenerated electrons and holes. - Scavenges hydroxyl radicals to create anion radicals. The photocatalytic degradation of organics may be impacted by the competing adsorption of active sites on the catalyst's surface.
Temperature	- Photocatalytic activity increase as the temperature increase.

2.6.1 Catalyst Concentration

Catalyst concentration or loading do contribute to the degradation rate which by increasing the catalyst concentration, the reaction rate will also increase. However, increasing catalyst concentration above certain dose can cause the degradation rate to decrease. Weldekirstos et al., (2024) studied on the degradation of MB using synthesized g-C_3N_4/$CoFe_2O_4$ and reported that as methylene blue (MB) concentration rises, more reactant molecules are adsorbed on the g-C_3N_4/$CoFe_2O_4$ surface, which lowers the production of ·OH radicals because there are fewer active sites available for hydroxyl anion adsorption (Weldekirstos et al., 2024). However, the contaminants absorb the photons before they can reach the catalyst surface at higher MB concentrations (K. M. Reza et al., 2017). Consequently, the g-C_3N_4/$CoFe_2O_4$ composite surface's absorption of light reduces the photocatalytic efficiency and the photocatalyst may also become deactivated due to a high substrate concentration (Weldekirstos et al., 2024).

Similarly, Sanjeev and Valsan., (2024) stated that as ACE and sulfadiazine (SFZ) concentrations were raised from 5 mgL^{-1} to 100 mgL^{-1}, the percentage removal

of each decreased from 80.3% to 40.49% and 78.6–34.74%, respectively (Sanjeev & Valsan, 2024). As a result, when ACE and SFZ concentrations rise, the percentage removal falls. The likelihood of ·OH formation and reaction with the target pollutant determines the rate of reaction degradation (K. M. Reza et al., 2017). More adsorptions occur onto the N-ZnO surface as the pollutant concentration rises. This reduces the production of ·OH by limiting UV ray penetration to the photocatalyst surface (Mirzaei et al., 2018).

2.6.2 Light Source and Light Intensity

Light source and light intensity can also affect the photocatalytic activity of photocatalyst. Different light sources provide different wavelengths. For example, Mirzaei et al. (2018) utilized UVC light source to degrade sulfamethoxazole (SMX) which provides wavelength in range between 100 – 280 nm. Zhu et al. (2014) on the other hand, used Xenon lamp with a 400 nm cutoff filter for the visible light source for the degradation of methylene blue (MB). On the contrary, light intensity improve the photocatalytic reaction of photocatalyst. Low intensity light source helped in improving the photo-removal efficiency and minimise energy waste in accordance with its smaller energy band structure (Carofiglio et al., 2020). Given that photocatalysis has two systems the intensity of the light source is crucial. The first system, by increasing the intensity of irradiated light with energy roughly equal to or above the band gap energy or threshold energy generally improves activity given that the forward reaction rate; the rate at which photo electrons and holes are consumed to produce hydrogen and oxygen—is higher than the backward reaction (Yuan et al., 2019). The second system is a half order reaction. Since the rate of backward reaction is higher than the rate of forward reaction, increasing the intensity results in a decrease in activity and finally, we obtain less hydrogen (Yuan et al., 2019). Lu et al., (2022) degraded CR dye using ZnO-CoOx-CeO_2 nanocomposites with 500 W xenon lamp and resulted to 98.8% within 65 min of irradiation while Wang et al., (2024) degraded RhB using sulfur vacancy-rich (α/β-CdS)/SiO_2 (α: hexagonal & β: cubic) photocatalysts with lower intensity visible light irradiation (113.7 mW) which achieved 93.37% degradation percentage.

2.6.3 pH of Solution

Next, pH values of solution also take part in factors that influence photocatalytic reaction. The pH of the solution, or the proton concentration, determines the amount of hydrogen (H_2) produced by water splitting because the electron produced by photolysis lowers the proton. When compared to acidic media, the production rate of H_2 in basic medium is generally higher in reported papers (pH>10) (Yuan et al., 2019). However, according to Nada et al., (2008) who used $TiO_2/RuO^{2-}MV^{2+}$ photo-catalyst in a methanol water mixture, the production of H^+ in acidic media is higher than in basic medium. In strong acidic media, more H^+ are absorbed on the photo-catalyst, which increases the possibility of reducing H^+ to H_2 by e^-. In general, maximum H_2 production occurs at strong basic medium.

2.6.4 Rate of Electron-Hole Pair Separation

The rate of electron-hole pair separation is also one of the influencing factors. The lifetime of an electron-hole (e-h) pair in a semiconductor catalyst is very short (Yuan et al., 2019). Therefore, to increase photocatalytic activity, oxidants can be added to lower the recombination of photogenerated electrons and holes (Chijioke-Okere et al., 2023). According to Selvaraj et al. (2021), the rate-managing step of the reaction mechanisms is the recombination of electron and electron-hole pairs during photocatalysis (Selvaraj et al., 2021). The reaction is proportional to the light intensity. Hung et al., 2001 stated that the photocatalytic degradation of Orange G may be significantly influenced by the recombination of electron-hole pairs and they also suggested that to increase the degradation rates of Orange G by altering the photocatalyst to lower the recombination rates of electron-hole pairs (Hung et al., 2001). Zhang et al., (2019) synthesized an efficient hybrid photocatalyst $Ag/AgCl/NH_2$-UiO-66 hexavalent chromium (CrVI) reduction with UiO-66 metal organic framework (Hung et al., 2001). The study reported that Ag nanoparticle surface plasmon resonance improved electron-hole separation and photo-response range, enhancing structural stability and CrVI reduction photocatalytic performance and the hybridisation enhanced the efficiency of charge separation and transfer, resulting in 1.7 times the photo-catalytic activity of UiO-66 metal organic framework (S. Kumar et al., 2018; K. Qi et al., 2017).

2.6.5 Presence of Oxygen

O_2 is one of the crucial oxidants in the photocatalytic reaction system and a major factor influencing the rate of the photocatalytic reaction (Chijioke-Okere et al., 2023). As an electron acceptor, O_2 easily adsorbs on the photocatalyst surface, preventing electron-hole recombination (Gao et al., 2022). Furthermore, the produced $\bullet O_2$ can be utilised as an active species to break down contaminants. Thus, the addition of O_2 generally helps speed the reaction (Chen et al., 2020). An additional agent that traps electrons is H_2O_2. The production of •OH radicals and the breakdown of contaminants are aided by the addition of H_2O_2. ZnO/CQDs/AgNPs composite catalysts were synthesised by (Bozetine et al., 2021) and used in a hydrothermal method to degrade methylene blue. An investigation was conducted into the impact of incorporating H_2O_2 on the rate of photocatalytic degradation of MB. The findings demonstrate that H_2O_2 can greatly increase ZnO/CQDs/AgNPs' catalytic activity and quicken the rate of reaction. The addition of H_2O_2 shortened the MB's overall degradation time by 20 minutes. This is due to the fact that H_2O_2 produces ·OH, an active ingredient for MB degradation, when it reacts with e^- produced by the photocatalyst conduction band. Naturally, a few photocatalytic reactions are also inhibited by H_2O_2. Di et al.'s (Di et al., 2020) study investigated the impact of CQD/g-C_3N_4 on the photocatalytic degradation of sulfamethazine (SMZ) at various H_2O_2 concentrations. According to the results, the photocatalytic degradation rate of SMZ gradually decreased as the H_2O_2 concentration increased (1 mM, 2 mM, and 5 mM). This is due to the fact that H_2O_2 poisons g-C_3N_4, preventing it from acting as a photocatalyst.

2.6.6 Presence of Inorganic Ions

Next, the presence of inorganic ions also listed in the influencing factors of photocatalytic reactions (Chijioke-Okere et al., 2023). The photocatalytic reaction rate can be influenced by humic acids (HA) which are the complex organic molecules that were created when plant and animal wastes decompose; they are commonly found in compost, peat, lignite, leonardite, and organic wastes (Biswas et al., 2025), halogen ions, and common acid ions present in the solution. This could have something to do with the pollutant and catalyst adhering to one another. According to reports, acid ions

and pollutants have a competitive adsorption relationship. Wu et al. (2021) investigated the effects of four distinct acid ions (SO_4^{2-}, CO_3^{2-}, NO_3^-, and HCO_3^-) on the reduction rate in addition to the effects of CQD loading, catalyst dosage, and pH on the photocatalytic reduction of Cr(VI) (Wu et al., 2021). The findings show that the reaction rate is slowed down by all four of the acid ions, which is in line with the pH experiments above that show that the reaction is not favoured by alkaline conditions. The effects of varying anion concentrations (SO_4^{2-}, Cl^-, and NO_3^{2-}) and HA on the photocatalytic degradation of sulfamethoxazole (SMX) by CQDs/BiO_2− X/BiOCl (BBN) in natural water were examined by Qi et al. (Kemin Qi et al., 2022). The inferences that follow can be made as follows: (1) The photocatalytic activity of BBN is significantly reduced when varying concentrations of SO_4^{2-} are present. Upon adding 2 mM SO_4^{2-}, the rate of SMX degradation dropped from 96.48% to 38.86%. This could be because H^+ and SO_4^{2-} form $\cdot SO_4^-$, which eats up the active ingredients in the reaction system and takes up the active sites on the catalyst surface. The incorporation of Cl^- results in a marginal reduction in the rate of SMX degradation, potentially impacting the catalyst's ability to adsorb pollutants. (3) NO_3^{2-} hardly affects SMX photodegradation at all. (4) The concentration of HA affects how it affects the photocatalytic degradation of SMX. Low HA concentrations prevent BBN from being photocatalytically active, which may be connected to free radicals' utilisation of unsaturated functional groups. High HA concentrations, however, neither affect it nor help it. A high concentration of HA is advantageous to promote the generation of reactive oxygen species because it is a photosensitive organic matter (Kemin Qi et al., 2022).

2.6.7 Temperature

Researchers have looked into how the temperature of the reaction affects the photo-catalytic rate's efficiency. Typically, the reaction rate will increase as the temperature increase (Mashuri et al., 2020). For instance, Chegeni et al., (2020), found that as the temperature increased from 15 to 45°C, the adsorption process also increased. However, as the temperature reached beyond 45°C, the adsorption depleted making 32°C as the optimum temperature for the removal of aspirin (Chegeni et al., 2020). On the other hand, Tahir et al., (2022) stated that the reaction rate of TiO_2 decreases at 80 °C due to an increase in the rate at which electrons and holes recombine as well as a

decrease in the catalyst's absorption rate at this temperature. The maximum reaction rate is obtained at the ideal temperature range of 20 – 80°C (Yuan et al., 2019).

2.6.8 Effect of Photocatalyst Loading

According to Sin et al., (2021) the rate as well as efficiency of photocatalytic degradation would increase with increased catalyst which it appears to be due to the catalyst's effective surface area and light absorption (Sin et al., 2012). However once the optimum limit is reached, , the increase in photocatalyst loading will no longer be effective because it is difficult for light to penetrate through causing most of the catalyst surfaces remains in-active (Tahir et al., 2022). Given the limited catalyst surface area, the photocatalytic process was controlled by light absorption at lower catalyst loadings. As stated from Elhalil et al. (2018), the degradation percentage of caffeine showed an increment from 69.42% to 98.9% with photocatalyst loading around 0.1 to 0.3 g/L. As the photocatalyst loading increased over 0.3 g/L, the degradation percentage reduced. This was caused by the overabundance of photocatalyst resulted to disperse the light and decreasing its penetration into the solution (Elhalil et al., 2018).

2.6.9 Effect of Initial pH

The efficiency of the photodegradation process is strongly influenced by the pH of the solution (Melchionna & Fornasiero, 2020; Tsai et al., 2022). The initial pH of solution affects the adsorption−desorption of the organic molecules on the photocatalyst's surface (Tsai et al., 2022). pH also affects the activity of photocatalyst by affecting its surface charges (Yuan et al., 2019). This can be viewed in term of electrostatic phenomenon between pollutant and charge particles. Tahir et al. (2022) disclosed that lower photocatalyst efficiency is observed for acidic medium, due to the high concentration of proton in this pH, causing pollutant degradation to lag because there are fewer OH- available. Meanwhile, the photoactivity of the catalyst increases in the pH range of 5–10, and the efficiency is highest at pH 10 (alkaline medium), because the OH- produced reacts with the organic pollutant and degrades it. The efficiency drops in the pH range 11–13 because the concentration of hydroxyl ions is very high and thus, they are scavenged. The OH- don't have time to react with the pollutant. As a result, the efficiency in this pH range is extremely low.

2.6.10 Effect of Initial Concentration

The initial substrate concentration can affect the degree of photocatalytic reaction rate on the surface of the catalyst (Chegeni et al., 2020). This is due to the fact that as the concentration of pollutant increases, more and more molecules of the pollutant compound adsorbed on the catalyst's surface causing fewer photons that are able to reach the photocatalyst's surface, resulting in fewer hydroxyl radicals being produced and lower photodegradation efficiency (Luu Thi et al., 2021; Tsai et al., 2022). Higher concentrations may cause the photocatalyst's active sites to become saturated, which would reduce the efficiency of degradation by producing insufficient amounts of reactive species like •OH and $•O_2$ radicals. On the other hand, low starting concentrations promote better generation of reactive species and light absorption. Higher concentrations result in lower degradation rates because of active site blockage and limited photon penetration, according to studies like those looking at TiO_2-based photocatalysts (Rafiq et al., 2021). By assessing its effectiveness under various pollutant loads, the impact of initial concentration on photocatalytic degradation aids in the selection of the optimal photocatalyst.

2.6.11 Radical Scavenger

Photo-generated holes (h^+), •OH, and $•O_2$ are usually the primary reactive species in the photocatalytic process (Luu Thi et al., 2021; Tsai et al., 2022). Other oxygen-derived radicals, such as $•O_2$, are produced by the capture of photogenerated electrons (Das et al., 2021). Brillas and Manuel Peralta-Hernández, (2023) showed that the degradation of ACE is aided primarily by positively charged holes, followed by superoxide radicals, and the least dominant reactive species is hydroxyl radicals.

2.6.12 Recyclability

To ensure the efficiency and quality of the synthesised catalyst, the photocatalyst's stability and durability are critical (Melchionna & Fornasiero, 2020). Besides that, due to the ability of electrons and holes in the composite material to separate efficiently, a heterojunction photocatalyst could maintain a high efficiency of photocatalytic performance even after a few cycles due to the formation of an

appropriate or suitable heterojunction structure (C. Wang et al., 2014). This appears to be in consensus with what Low et al., (2017) have stated which photocatalysts with heterojunctions have been shown to have an efficient spatial separation of electron–hole pairs for effective photodegradation (Munyengabe et al., 2022; Zhu et al., 2020).

CHAPTER 3
RESEARCH METHODOLOGY

3.1 Introduction

In this chapter, the experimental setup, the procedure for synthesis and the photocatalysis evaluation of AC-supported ZnO/g-C_3N_4 photocatalyst were explained. The instruments and equipment as well as details on materials used and the measurement techniques and procedure to determine the photocatalytic performance were also specified below.

3.2 Materials

The reagents that are used for the preparation of AC-supported ZnO/g-C_3N_4 composite photocatalysts and the pollutant are listed. Activated carbon (AC), zinc oxide (ZnO, purity > 99%) powder and dicyandiamide ($C_2H_4N_4$, purity > 99%) powder of analytical grade were supplied by R&M Chemicals (Selangor, Malaysia) and Sigma-Aldrich (Selangor, Malaysia), respectively. Acetaminophen (ACE) was obtained from a local pharmacy in Malaysia. All the reagents used for the syntheses of photocatalysts were directly purchased with analytical grade and used without further purification. The dicyandiamide was used as a precursor for the photocatalyst preparation. Furthermore, deionized water was also used throughout this research study.

3.3 Preparation of AC-Supported ZnO Composite Photocatalysts

The preparation of AC-supported ZnO composite photocatalysts started with 0.05 g of activated carbon were added to 50 mL of distilled water. ZnO powder of different mass then were added to the solution and magnetically stirred for 1 hour. Next, the mixture was dried in the oven at 120°C for 6 hours. Then, the resulted powder will be grinded in a mortar for approximately 30 minutes. Different composition ratios of AC-supported ZnO composite photocatalysts were shown in Table 3.1. The fine resulted AC-supported ZnO composite photocatalysts will then be stored in desiccator and labelled.

Table 3.1
The Composition for the Preparation of AC-Supported ZnO Composite Photocatalysts.

Activated Carbon, g	Zinc Oxide, g	Label
0.05	0.5	AZ1
0.05	1.0	AZ2
0.05	1.5	AZ3
0.05	2.0	AZ4
0.05	2.5	AZ5

3.4 Preparation of AC Supported ZnO/g-C_3N_4 Composite Photocatalysts

Prior to the addition of g-C_3N_4 onto AC-supported ZnO composite photocatalysts surfaces the AC-supported ZnO composite photocatalysts, g-C_3N_4 were synthesized beforehand. A 10g of dicyandiamide were be calcined at 550°C for 2 hours. The prepared AC-supported ZnO composite photocatalysts will be added to the synthesized g-C_3N_4. A 1.5 g of the prepared AC-supported ZnO photocatalysts was added to a beaker containing 50 mL of deionized water. 0.005 g of g-C_3N_4 were added to the mixture. Next, the mixture was stirred on a magnetic stirrer for 1 hour without any heat. After 1 hour, the mixture was dried in the oven at 120°C for 6 hours. In this work, 1.5 g of AC-supported ZnO composite photocatalysts (the optimum amount) with different compositions of g-C_3N_4 as presented in Table 3.2. For comparison purposes, the pristine g-C_3N_4 was prepared via the same route without AC-supported ZnO composite photocatalysts added.

Table 3.2
The Composition for the Preparation of AC-supported ZnO/g-C_3N_4 Composite Photocatalysts

AC-supported ZnO composite photocatalyst, g	Graphiti carbon nitride (g-C_3N_4), g	Label
1.5	0.005	AZG1
1.5	0.010	AZG2
1.5	0.015	AZG3
1.5	0.020	AZG4

3.5 Characterization of AC Supported ZnO/g-C_3N_4 Composite Photocatalyst

The samples of pristine AC, pristine ZnO, pristine g-C_3N_4 and AC-ZnO/g-C_3N_4 at different mass was characterised for a comprehensive understanding on morphological, structural, and optical characteristics of the photocatalysts. In this research, the three properties of the photocatalysts samples were investigated by using Powder X-ray Diffraction (XRD) analysis, Scanning Electron Microscopy (SEM) and Field Emission Scanning Electron Microscope equipped with Energy Dispersive X-ray (FESEM-EDX), N_2 adsorption-desorption analysis and Bruennaur Emmet (BET) surface area, X-ray Photoelectron Spectroscopy (XPS), Photoluminescence analysis (PL) and UV-Vis Diffuse Reflectance Spectrophotometer (UV-DRS).

3.5.1 Powder X-ray Diffraction (XRD)

The crystalline phase and particle size of the photocatalyst samples were analysed by using XRD analysis (PANalytical X'pert PRO / DY 2536). The instrument uses an X-ray source of Cu Kα-radiation beam with an excitation wavelength of 0.15406 nm for the analysis. The X-rays focused on the fixed sample first, before being diffracted by the 2θ range of 10° to 90° at a rate of 4°/min. The changes in the intensity of diffracted x-ray were measured, recorded, and plotted against the rotation angles from the samples. Then, the resulting x-ray diffraction pattern was evaluated qualitatively based on the peak height or area. From these findings, the particle sizes and degree of crystallisation were calculated using Scherrer.

The average crystallite size (D) of AC-supported ZnO and Ac-supported ZnO/g-C_3N_4 composite photocatalysts particles were calculated using Debye-Scherrer's formula (Yin et al., 2015) given by Equation 3.1 below:

$$D = K\lambda/(\beta \text{Cos } \theta) \tag{3.1}$$

whereas K is the is the Scherrer constant (0.94), λ is the X-ray wavelength (0.154 nm), β is the line broadening at full width at half maximum (FWHM) and θ is the Bragg's angle in degree (half of the peaks' position).

3.5.2 Scanning Electron Microscopy Equipped with Energy dispersive X-ray (SEM-EDX)

The surface morphology and particle size of the eight photocatalyst samples was observed by using SEM (Tescan Vega3 / 1190134), while its elemental compositions were determined by using EDX. The samples were mounted first onto an appropriately sized pin stub before being inserted into the brass carrier. After that, using the provided height measuring equipment, the sample height was measured with respect to the standard height and the overall size of the specimen was also recorded. The SEM started by turning on the beam, then the image was viewed on the screen and further be analysed. The EDX was used together with SEM. SEM and FESEM were both used for the surface morphological and structural analysis in which FESEM were used to further analyze the surface morphological and structure of the best photocatalysts composites of AC-supported ZnO and AC-supported ZnO/g-C_3N_4 after SEM.

3.5.3 Field Emission Scanning Electron Microscope Equipped with Energy Dispersive X-ray (FESEM-EDX)

The surface morphology and particle size of only the best among AC-supported ZnO (AZ3) and the best among AC-supported ZnO/g-C_3N_4 (AZG2) composite photocatalyst samples was observed by using FESEM (JEOL JAPAN JSM-7800 F / SM1881000120012), while its elemental compositions were determined by using EDX. FESEM-EDX were done to further examine the surface morphology and structure of the best composite photocatalysts (AZ3 and AZG2). The samples were mounted first onto an appropriately sized pin stub before being inserted into the brass carrier. After that, using the provided height measuring equipment, the sample height was measured with respect to the standard height and the overall size of the specimen was also recorded. The FESEM started by turning on the beam, then the image was viewed on the screen and further be analysed. The EDX was be used together with FESEM.

3.5.4 N_2 Adsorption-Desorption Analysis

The nitrogen (N_2) adsorption and desorption isotherms and BET surface area were measured at 77 K after degassing the samples using surface area analyzer

(Micromeritics / ASAP2020). Electrochemical and photoelectrochemical measurements was performed in three-electrode quartz cells with a 0.1 M Na_2SO_4 electrolyte solution. Platinum wire was used as the counter electrode, and saturated calomel electrodes (SCE) were used as the reference electrodes, respectively. The prepared photocatalyst film electrodes on ITO served as the working electrode. The photoelectrochemical experiment results was recorded using an electrochemical system (CHI-660B, China). The intensity of light is 1 $mWcm^{-2}$ given with reference to the SCE. This analysis was done on all of AC-supported ZnO composite photocatalyst and only on the most optimum ratio of AC-supported ZnO/g-C_3N_4 composite photocatalyst (AZG2).

3.5.5 X ray Photoelectron Spectroscopy (XPS)

A VSW HA-100 spherical analyzer (ULVAC-PHI / PHI 5000 VersaProbe II) was used to obtain the XPS spectra, employing AlKα radiation (hv =1486.6 eV). The analyzer was operated in the fixed transmission mode with a pass energy of 44 eV. During the measurements, the pressure was maintained below 2×10^{-8} mbar. The powdered samples are fixed to a stainless-steel sample holder with carbon tape and was analysed without further preparation.

3.5.6 Photoluminescence Analysis (PL)

The separation and recombination processes of the photo-induced electron-hole pairs were examined using the steady-state Photoluminescence (PL) spectroscopy (FP-8500 / JASCO). PL spectra were recorded at room temperature. The excitation wavelength was set at 325 nm. Samples were coated onto quartz cuvettes for solid fluorescence testing.

3.5.7 UV-Visible Near Infrared Spectrophotometer (UV-NIR)

The UV–Vis NIR spectrum was be used to assess the optical response of the photocatalyst samples in the visible light range using PerkinElmer Lambda 1050. This characterisation was conducted in total reflection mode from 200 to 800 nm. The optical

transition fitted at the absorption edges using the Tauc's model stated in Equation 3.2 below to estimate the band gap energies of the samples (Girija Shankar et al., 2021).

$$(\alpha hv)\, n = A(hv - Eg) \tag{3.2}$$

Where, h is the Planck's constant, v is the absorption of photon frequency, α is the coefficient of optical absorption, Eg is the optical band gap energy, A is a proportional constant and n n represents the power factor transition mode, which is contingent on the material's crystalline or amorphous nature. Furthermore, the value of the exponent n is influenced by the type of electronic transition between the semiconductor bands (Su et al., 2021).

3.6 Photodegradation Evaluation of AC-Zupported ZnO and AC-Supported ZnO/g-C_3N_4 Composite Photocatalysts

3.6.1 Calibration of ACE

Prior to the photocatalytic measurement, the calibration plot ACE in aqueous phase under normal and acidic/basic condition will be performed using UV-Vis Spectrophotometer. The calibration curve will be plotted according to the various concentrations of the targeted EDCs, ranging from 5 to 25 mgL^{-1}. From this calibration plot, the linear equation will be determined by measuring the absorbance of each sample at maximum wavelength (λmax).

3.6.2 Photodegradation of ACE

The photocatalytic performance of a developed system is usually evaluated by measuring the time dependence of the concentration loss of a degraded compound. The photocatalytic performance of AC-supported ZnO/g-C_3N_4 composite photocatalysts using ACE in aqueous phase will be conducted in a glass photoreactor as presented in Figure 3.1. A 0.1 g of AC-supported ZnO/g-C_3N_4 composite photocatalysts was added in the photoreactor containing a known concentration (10 ppm) of ACE solution (200 mL). The photoreactor was supplied with air to warrant a constant supply of oxygen with a fixed flow rate of 4 $Lmin^{-1}$ and left in dark for 60 minutes before starting the photodegradation testing to achieve adsorption–desorption equilibrium. The

photoreactor then was exposed to a visible light irradiation. The liquid (5–10 mL) then was collected at every 30 minutes time interval and will be filtered to remove the photocatalyst. The interval and the effect of photocatalyst loading, initial concentration, initial pH, radical scavengers and recyclability on photodegradation of ACE was monitored by using Perkin-Elmer UV-Visible spectrophotometer. Photolysis and adsorption were done in prior the photodegradation to verify whether the degradation of ACE was due to photocatalytic activity of the photocatalyst composite. Photolysis is when the reactant absorbs light and broken down into smaller molecules (Kanakaraju et al., 2018). On the other hand, adsorption is when a mass transfer process occur, gases or solutes are adsorbed onto solid or liquid surfaces (Das et al., 2021). In this study, both photolysis and adsorption were done using 10 mg/L of ACE in aqueous phase. Photolysis was conducted in the absence of photocatalyst composite and irradiated with low-intensity UV light for 240 min. Meanwhile, adsorption was carried out in the dark in the presence of the best photocatalyst composite (AZ3 and AZG2) for 240 minutes.

In this study, all the degradation percentage and amount of organic pollutant degraded was calculated using the following equation 3.3 and 3.4 as seen below (Hir, Nik Badrul Alam, et al., 2022):

$$\text{Degradation percentage, (\%)} = \frac{((Co - Ct))}{Co} \text{ x } 100\% \quad (3.3)$$

$$\text{Acetaminophen degraded } \left(\frac{mg}{g}\right) = \frac{(C_o - C_t)\left(\frac{mg}{L}\right) \text{x volume (L)}}{\text{weight of photocatalyst (g)}} \quad (3.4)$$

Where, C_o is the concentration of pollutant before irradiation and C_t is the concentration of pollutant at 't' min.

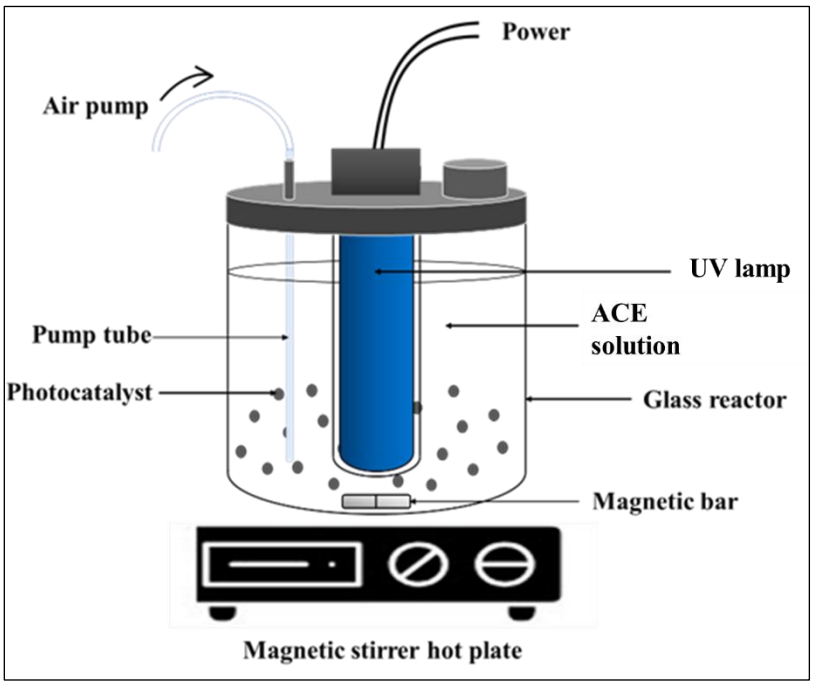

Figure 3.1 Schematic Illustration of the Photoreactor Setup for Photodegradation of ACE Using AC-supported ZnO/g-C_3N_4 Composite Photocatalysts.

3.6.3 Effect of Photocatalysts Loading

AC-supported ZnO/g-C_3N_4 composite photocatalysts underwent screening tests to determine the optimum loading of the material varied from 0.10 – 0.25 g which was the same as in Table 3.2. Under the irradiation of low intensity UV light (7W), the photocatalyst composite was utilized to degrade ACE in aqueous phase at a concentration of 10 mg/L. For additional testing, the photocatalyst composite with the highest percentage of degradation for each series was selected.

3.6.4 Effect of Initial Concentration

A significant parameter to investigate was the effect of varying initial concentrations of ACE on performance degradation. In this work, the best photocatalyst composite irradiated to low intensity UV light (7W) was used to degrade ACE at concentrations ranging from 5 to 20 mgL^{-1}.

3.6.5 Effect of Initial pH

The pH of dispersions is a crucial factor influencing the rate of reaction occurring on the surface of the photocatalyst, as most semiconductor oxides exhibit amphoteric behaviour. Given that the pH of the solution affected the surface-charge characteristics of the photocatalysts, this parameter was investigated. Using a composite photocatalyst, the photodegradation step was carried out in this work within a pH range of 2 to 10. 1.0 M of nitric acid (HNO_3) or sodium hydroxide (NaOH) was added to the ACE solution to bring its initial pH to the desired level in each experiment. Throughout the degradation process, the pH of the solution was not changed. Irradiation with low intensity UV light (7W) aided in the degradation process.

3.6.6 Effect of Radical Scavenger

To investigate the active radical species responsible for ACE photodegradation, three radical scavengers were added to the working solution separately: tert-butanol (tBuOH), ethylenediaminetetraacetic acid (EDTA), and 1,4-benzoquinone (p-BQ). tBuOH was used to scavenge the hydroxyl radicals (•OH), EDTA for holes (h^+), and p-BQ for superoxide radical anions ($\bullet O_2^-$). Under low intensity UV light (7W) irradiation, 200 mL of working solution contained 10 mg/L of ACE.

3.6.7 Kinetic Study on the Operational Parameters

The kinetic study was done for each operational parameter which includes the effect of photocatalyst loading, initial concentration, pH and radical scavenger. This following equation was used to study the kinetics of ACE degradation by the produced photocatalysts using the Langmuir-Hinshelwood (L-H) kinetic model (Hir, Nik Badrul Alam, et al., 2022):

$$r = \left(\frac{dC}{dt}\right) = k_{obs}C \tag{3.5}$$

which is equivalent to

$$ln\left(\frac{C_o}{C_t}\right) = k_{obs}t \quad (3.6)$$

where r is the reaction rate, k_{obs} is the rate constant (min^{-1}), and C_o and C_t are the concentration (mg/L) of ACE initially and at different irradiation times, respectively.

3.6.8 Recyclability

In order to examine the long-term stability and practicality of the potential AC-supported ZnO/g-C_3N_4 composite photocatalyst, the best composite photocatalyst was filtered and recycled without undergoing any pre-treatment steps in between cycles. After stopping each of the reaction, fresh ACE aqueous solution (10 mg/L) was added to the new cycle.

3.7 Research Flow Diagram

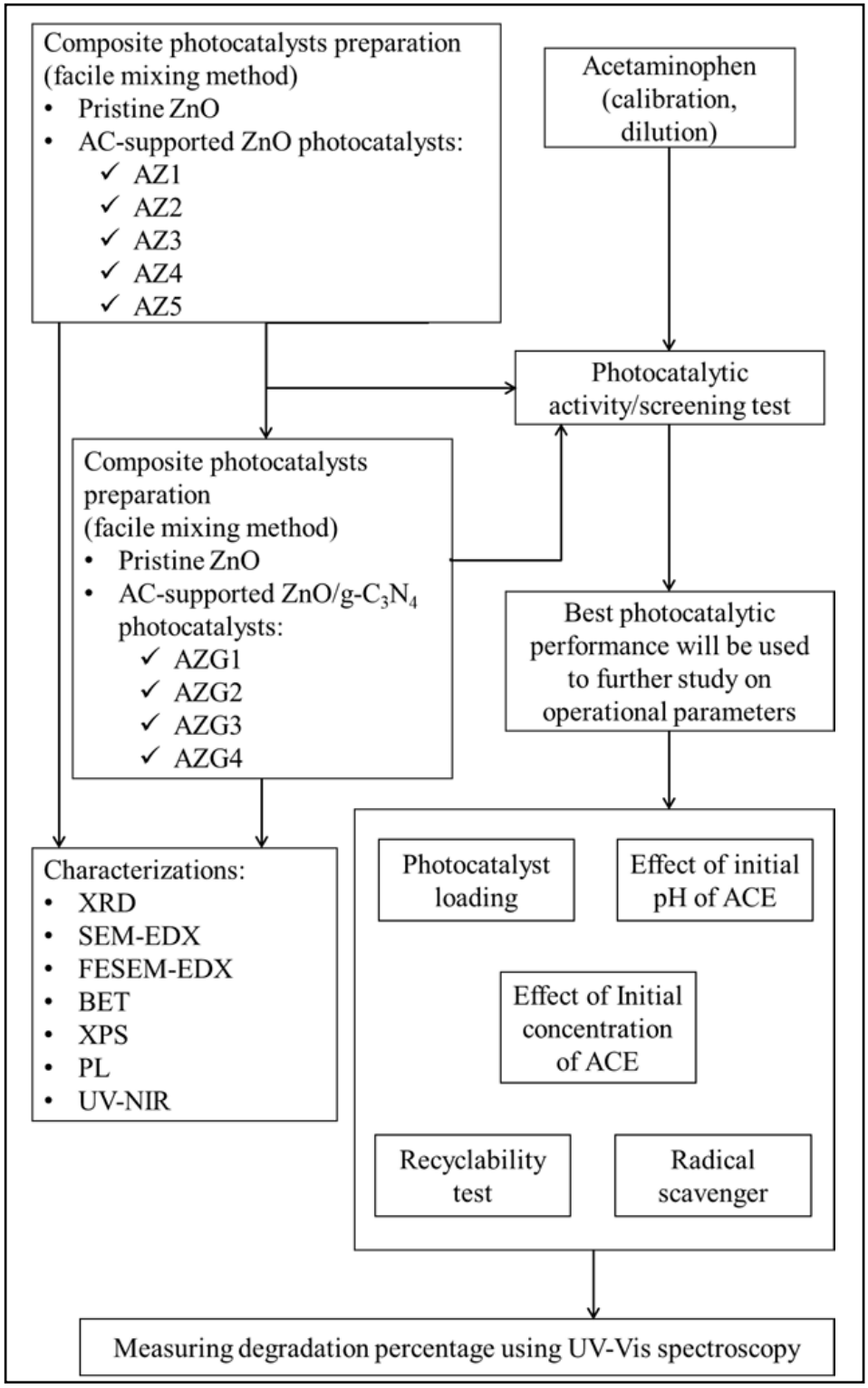

Figure 3.2 Research Flow Diagram of the Study.

CHAPTER 4
RESULTS AND DISCUSSION

4.1 Introduction

In this chapter, there are three stages that encompassed the whole study. The first stage is the preparation of AC-supported ZnO/g-C_3N_4 composite photocatalysts using a facile chemical mixing method. The second stage involved the physicochemical characterization of the prepared composite photocatalysts using X-ray Diffraction Analysis (XRD), Scanning Electron Microscopy (SEM), and Field Emission Scanning Electron Microscopy (FESEM) along with elemental analysis via Energy Dispersive X-ray Analyzer (EDX), N_2 adsorption-desorption analysis and Brunaer-Emmet-Teller (BET) surface area, X-ray Photoelectron Spectroscopy (XPS), Photoluminescence Spectroscopy (PL), and UV-vis Near Infrared (NIR) spectrophotometer. The third stage involved testing the prepared composite photocatalysts in the acetaminophen (ACE) aqueous phase UV-induced degradation system and analyzing the data from the UV-Vis Spectrophotometer to examine the composite photocatalysts' photocatalytic performance. Further investigations were also carried out on the effects of several parameters on the photocatalytic degradation process using the best ratio of the composite photocatalyst, including photocatalysts loading, initial concentration and pH of the working solution, radical scavengers, and recyclability study. The kinetics of the ACE degradation using pristine ZnO and all prepared composite photocatalysts were also discussed in detail concerning the effects imposed during the degradation process.

4.2 Surface Morphological, Composition & Structural Analysis

4.2.1 X-ray Diffraction (XRD) Analysis

The X-ray diffraction (XRD) analysis was used to investigate the phase structure and crystallinity of the as-prepared samples (Figure 4.1-4.2). The peak observed at 27.0°, 29.7° and 44.6° are corresponding to the (002), (113), and (100) planes of pristine activated carbon (AC), respectively (Figure 4.1a) (Hir, Alam, et al., 2022; Su et al., 2021; C. Wang et al., 2014). The peaks suggest that the structure of AC is a mixture of

crystalline and amorphous phases (Mehta et al., 2022) and the stronger peak at 44.6° is associated to a more ordered carbon structure (Hir et al., 2022). On the other hand, pristine ZnO showed the typical diffraction peaks at 31.78°, 34.40°, 36.25°, 47.54°, 56.58°, 62.82°, 67.94°, and 69.04°, with corresponding crystal planes of (100), (002), (101), (102), (110), (103), (200), (112), (201), and (202), signifying the ZnO hexagonal wurtzite structure (Figure 4.1b) (JCPDS card 36–1451) (Hir, Alam, et al., 2022; M. S. Reza et al., 2020). The AC-supported ZnO composite photocatalysts depicts the identical pattern with pristine ZnO, and no peaks of AC being detected due to low concentration of AC in the composite photocatalysts. The addition of AC did not alter the phase structure of ZnO and the absence of new diffraction peaks indicates the high purity of the prepared samples. The crystallite size of AC-supported ZnO composite photocatalysts was found to be averaged of 35.40 nm.

On the other hand, two distinct diffraction peaks at 13.8° and 27.8°, which are typical of g-C_3N_4 (Khezami et al., 2024; Kim et al., 2023), can be indexed as (100) and (002) diffraction planes, as shown in Figure 4.2a. The AC-supported ZnO/g-C_3N_4 composite only exhibits the characteristic diffraction peaks of ZnO, as depicted in Figure 4.2(b-e). This is due to very small amount of g-C_3N_4 was added to the AC-supported ZnO composite photocatalyst which results to no g-C_3N_4 peaks was detected in the AC- supported ZnO/g-C_3N_4 composite. Moreover, no additional crystal phases during the preparation procedure are discovered. Furthermore, the positions of the characteristic peaks for the AC-supported ZnO/g-C_3N_4 composite remain unchanged when compared to pristine ZnO and pristine g-C_3N_4. This proves that the prepared ZnO/g-C_3N_4 composite has no effect on the g-C_3N_4 and ZnO lattice structures (Kim et al., 2023). The average crystallite size of AC-supported ZnO/g-C_3N_4 composite photocatalysts was 35.16 nm.

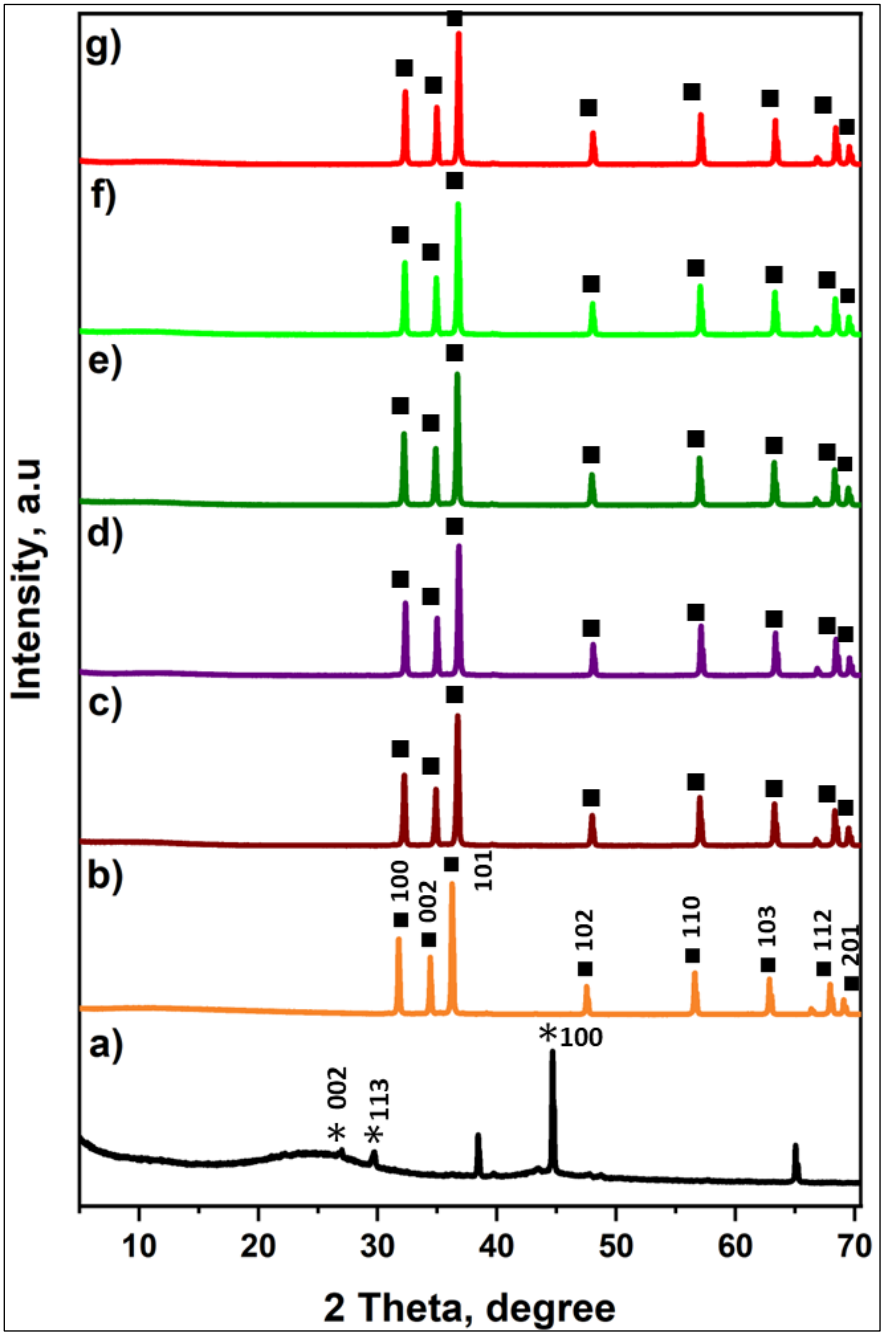

Figure 4.1 XRD Analysis of (a) Pristine AC, (b) Pristine ZnO, (c) AZ1, (d) AZ2, (e) AZ3, (f) AZ4 and (g) AZ5 Composites with Different ZnO Contents.

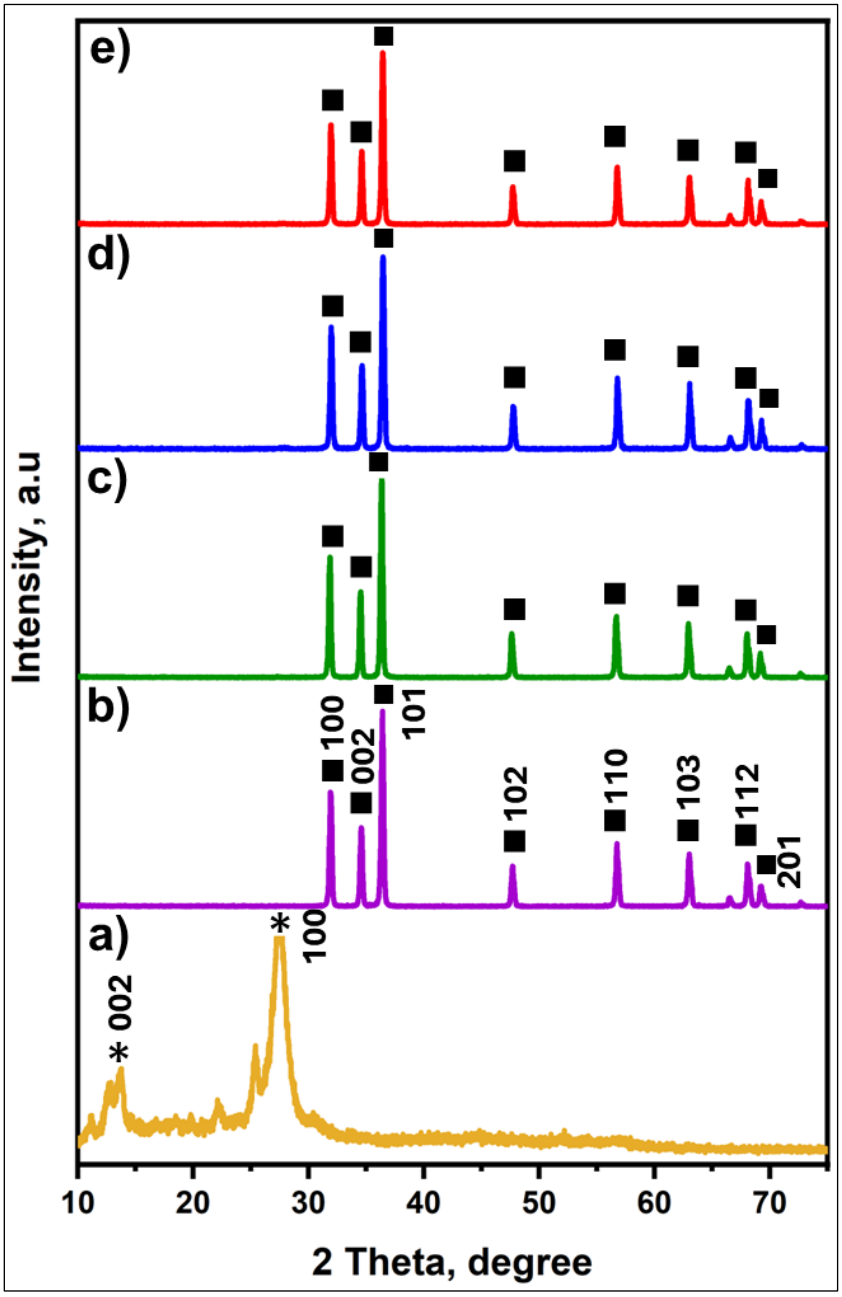

Figure 4.2 XRD Analysis of (a) Pristine g-C_3N_4, (b) AZG1, (c) AZG2, (d) AZG3 and (g) AZG4 Composites with Different g-C_3N_4 Contents.

4.2.2 Scanning Electron Microscopy Equipped with Energy Dispersive X-ray (SEM-EDX)

Scanning electron microscopy equipped with energy dispersive X-ray (SEM-EDX) analyzer was used to examine the morphology and compositions of the prepared photocatalysts. The SEM morphology for pristine AC, pristine ZnO, pristine g-C_3N_4, AC-supported ZnO and AC-supported ZnO/g-C_3N_4 composite photocatalysts with various ratio compositions are shown in Figure 4.3-4.4.

The pristine AC presents rod-like shaped porous structures along the surface. AC reveals non-homogeneous flake shape porous structure with the particle size ranging from 2 to 20 µm (Figure 4.3a). On the other hand, pristine ZnO reveals that it is made up of densely packed agglomerated and irregularly shaped particles which are uniformly distributed particles around 100 nm (Figure 4.3b). Figure 4.3a-g showed that ZnO are deposited onto AC with gradually higher content of ZnO; which higher ZnO content led to their emergence in SEM images. It is evident that AC and ZnO were blended somewhat well, but as the ZnO content increased in each ratio, ZnO was seen to accumulate. AC served as a support material in the AC-supported ZnO composite photocatalyst.

The EDX analysis was conducted to support the results from the SEM examination and to further confirm the presence of AC and ZnO in the AC-supported ZnO composite photocatalyst. The atomic percentages of Zn, C and O are as shown in Figure 4.3a-g. Gold coating (Au) was used in the EDX analysis which included in the atomic percentage (5%). ZnO could be identified by the constituent element O having the same distribution as Zn, as shown in Figure 4.3a-g. The existence of zinc, carbon and oxygen has been established for every photocatalyst, confirming the composition of AC-supported ZnO composite photocatalyst, as illustrated in Figure 4.3a-g. The EDX spectra are in line with the composition of each composite as the increasing amount of ZnO for each ratio.

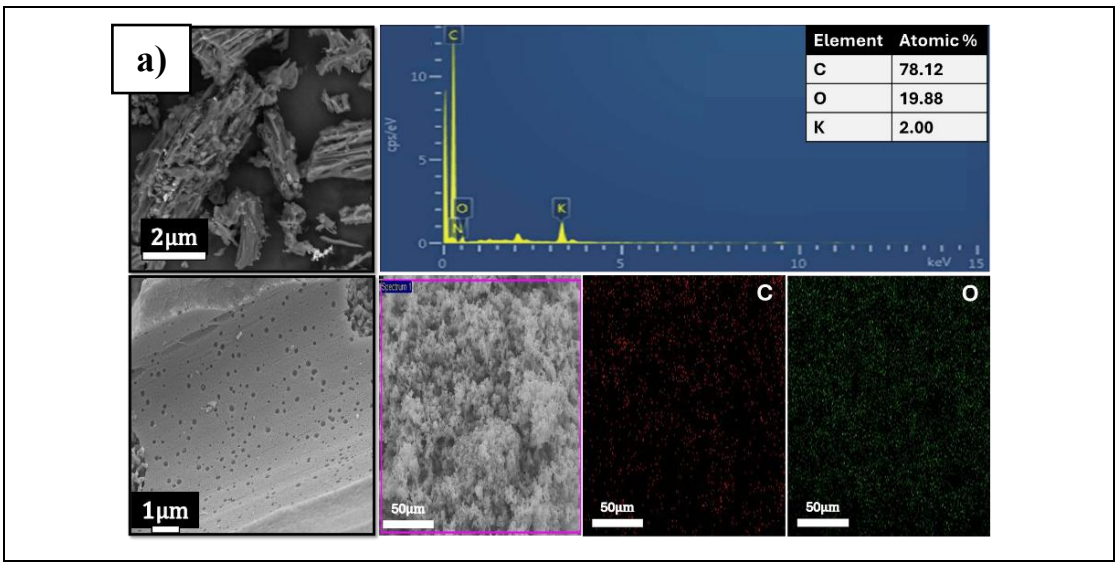

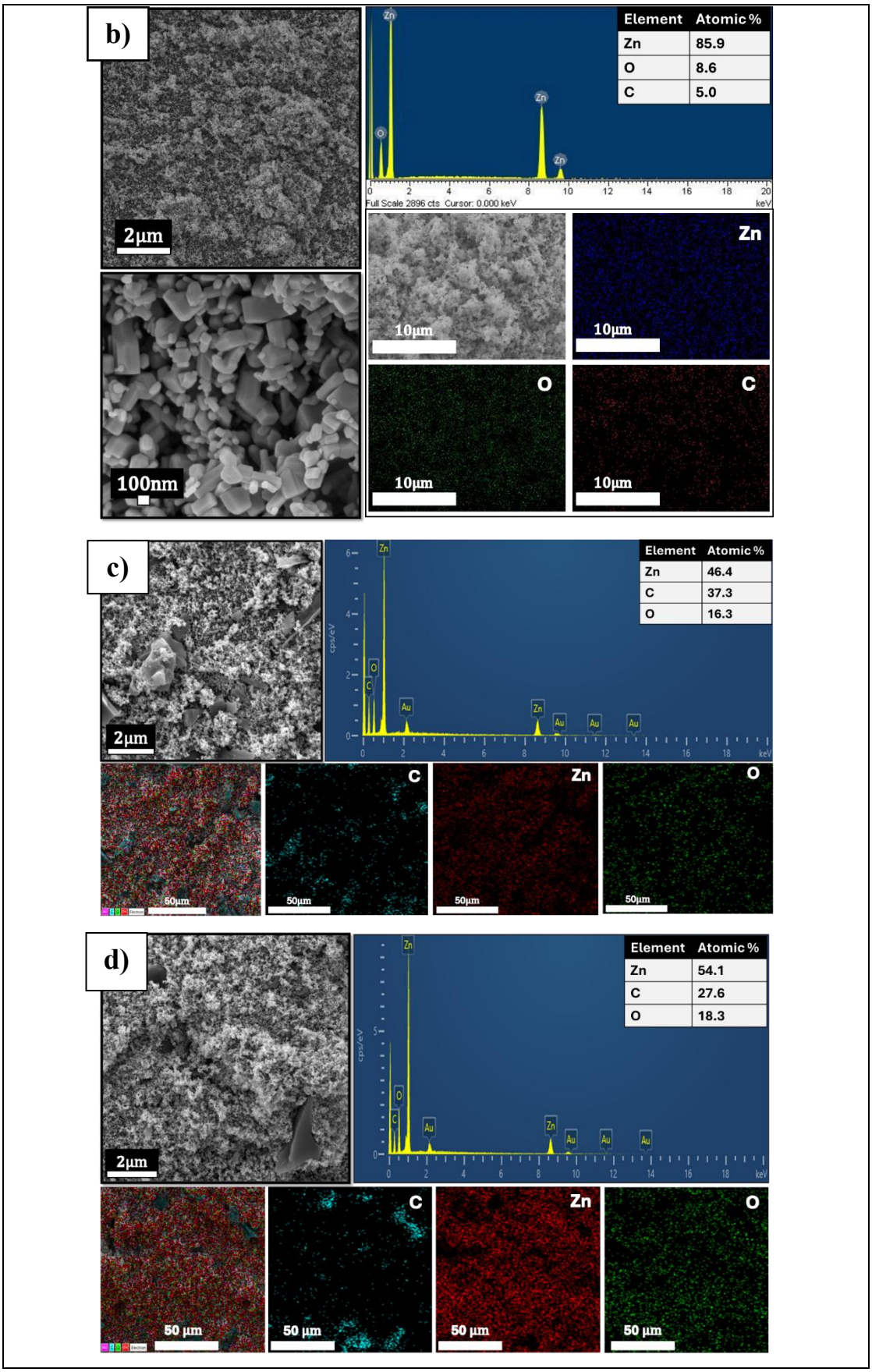
b)
2µm
100nm
Element Atomic %
Zn 85.9
O 8.6
C 5.0
Full Scale 2896 cts Cursor: 0.000 keV
keV
10µm
Zn
O
C
c)
2µm
Element Atomic %
Zn 46.4
C 37.3
O 16.3
cps/eV
50µm
d)
2µm
Element Atomic %
Zn 54.1
C 27.6
O 18.3
50 µm

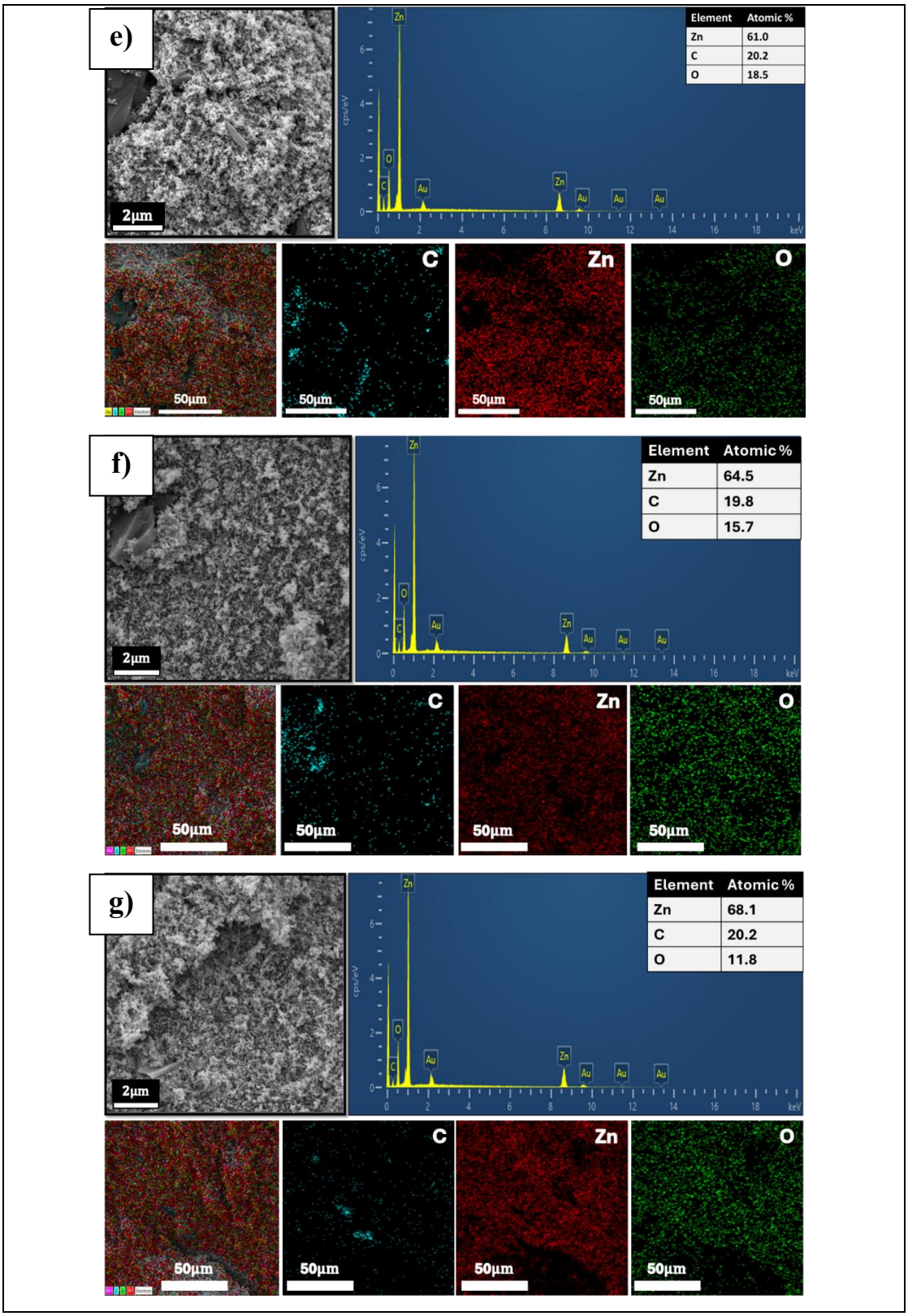

Figure 4.3 SEM-EDX and Mapping Analyses of (a) Pristine AC, b) Pristine ZnO, c) AZ1, d) AZ2, e) AZ3, f) AZ4 and g) AZ5 Composites with Different ZnO Contents. .

Meanwhile, pristine g-C_3N_4 presented irregular sheet-like structure with the particle size around 2-4 µm (Figure 4.4a). However, g-C_3N_4 cannot be spotted easily in the AC-supported ZnO/g-C_3N_4 composite photocatalysts due to the quite small content of g-C_3N_4 (0.005-0.05 g) was added to the composite photocatalysts. Figure 4.4b-e) clearly showed g-C_3N_4 was distributed in a non-uniform manner and ZnO particles were laid onto the surface of g-C_3N_4. The g-C_3N_4 sheet-like structure provides the medium for excited electrons of ZnO to fall onto instead of falling back to ZnO's VB (Garg et al., 2021; Kim et al., 2023; Lia et al., 2021; Youssef et al., 2018). This attribute will improve the photocatalytic activity of composite photocatalysts by preventing hole recombination.

The EDX analysis was carried out on AC-supported ZnO/g-C_3N_4 composite photocatalysts to demonstrate the element composition and distribution of the composite photocatalysts. Each composite photocatalysts has been shown to contain zinc, carbon, oxygen, and nitrogen, indicating the successful preparation of AC-supported ZnO/g-C_3N_4 composite photocatalysts with uniform distribution as shown in Figure 4.4a-e). The increasing quantity of g-C_3N_4 for each ratio is consistent with the composition of each composite photocatalyst as shown by the EDX spectra.

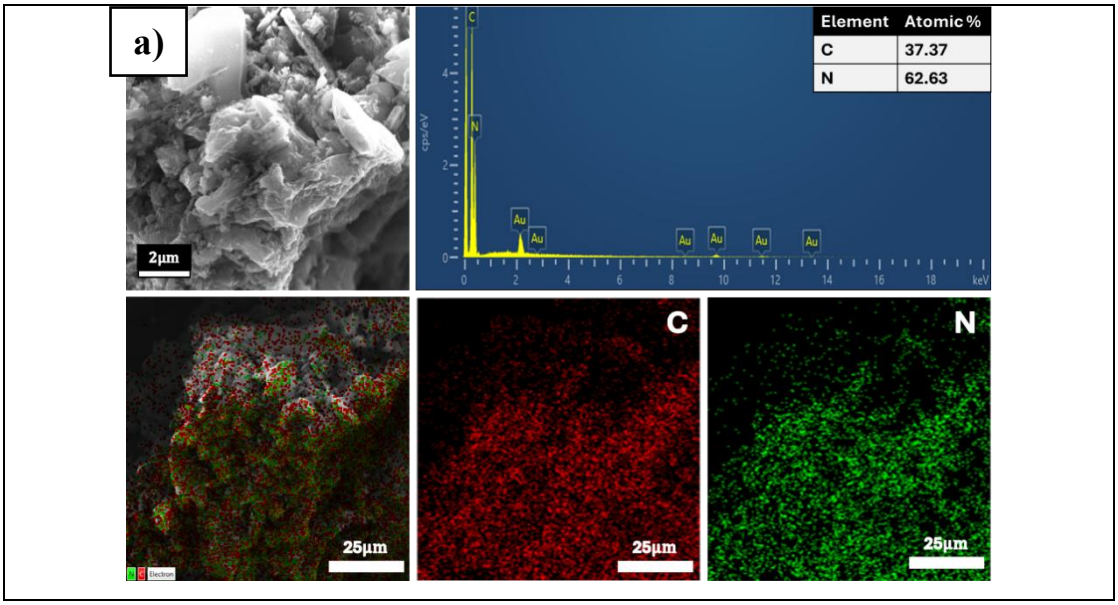

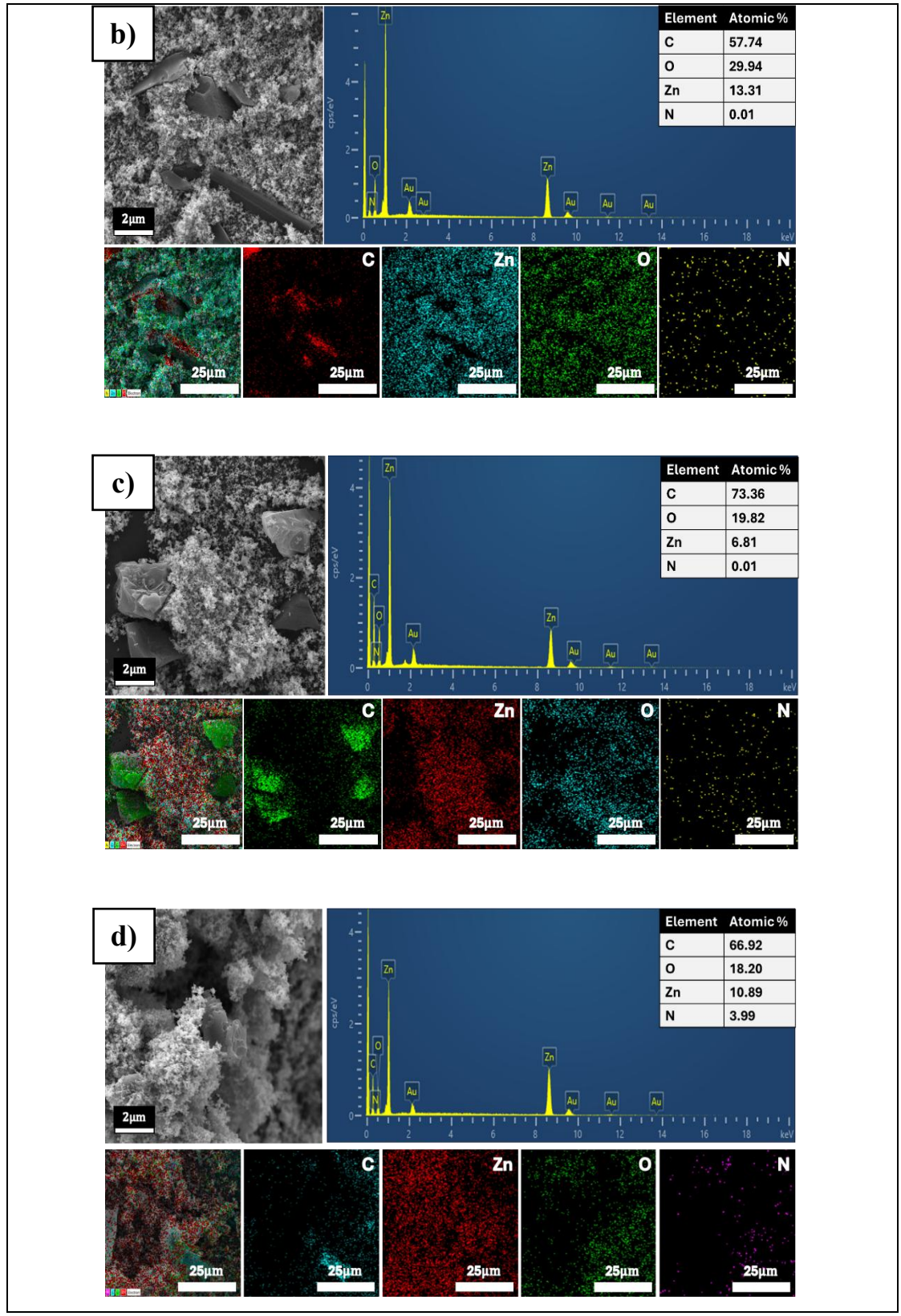
b)
Element Atomic %
C 57.74
O 29.94
Zn 13.31
N 0.01
2µm
C
Zn
O
N
25µm
c)
Element Atomic %
C 73.36
O 19.82
Zn 6.81
N 0.01
2µm
C
Zn
O
N
25µm
d)
Element Atomic %
C 66.92
O 18.20
Zn 10.89
N 3.99
2µm
C
Zn
O
N
25µm

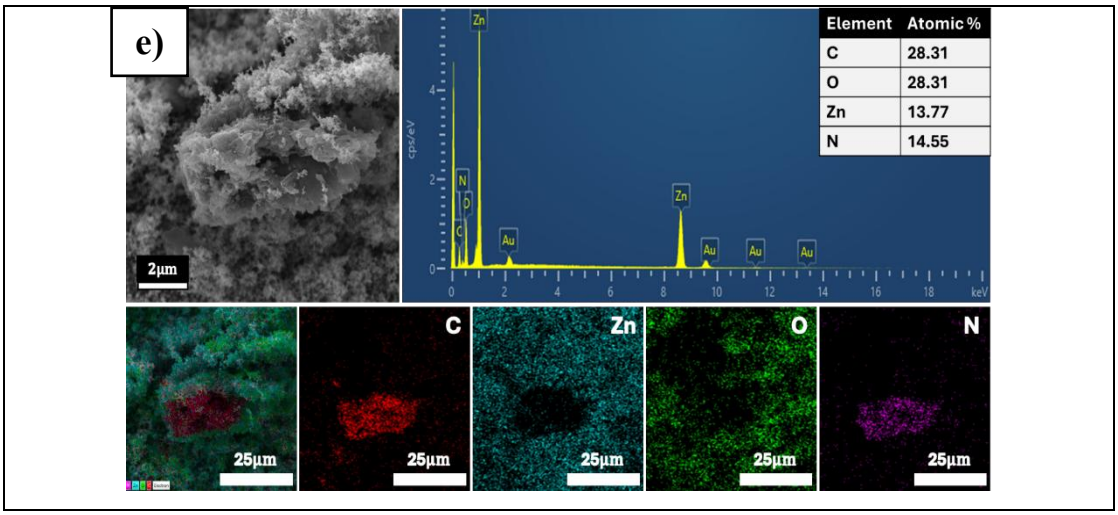

Figure 4.4 SEM-EDX and Mapping Analyses of (a) Pristine g-C_3N_4, b) AZG1, c) AZG2, d) AZG3 and e) AZG4 Composites with Different g-C_3N_4 Contents.

4.2.3 Field Emission Scanning Electron Microscopy (FESEM) Equipped with Energy Dispersive X-ray (EDX)

Field emission scanning electron microscopy equipped with energy dispersive X-ray (FESEM-EDX) analyzer was used to further examine the morphology and compositions of the prepared photocatalysts after SEM analysis. The FESEM morphology for AC-supported ZnO (AZ3) and AC-supported ZnO/g-C_3N_4 (AZG2) composite photocatalyst are shown in Figure 4.5-4.6. AZ3 and AZG2 was chosen to undergo FESEM-EDX as it was the best composite photocatalysts among AC-supported ZnO and AC-supported ZnO/g-C_3N_4 composite photocatalysts.

Figure 4.5a) shown that ZnO filled up the pores of AC and ZnO also seen to be clinging on the surface of AC (Figure 4.5b-c). This is due to the huge particle size different of AC (2-20µm) ZnO (~100nm). ZnO that have been deposited on the surface of AC demonstrated to their high contact and binding with AC. The EDX spectra confirms the presence of C, Zn and O elements with their atomic percentage of 33.08, 29.33 and 37.59, respectively. Besides, the fact that the mapping analysis of C, Zn, and O were overlapped indicates that they are all distributed uniformly on the surface.

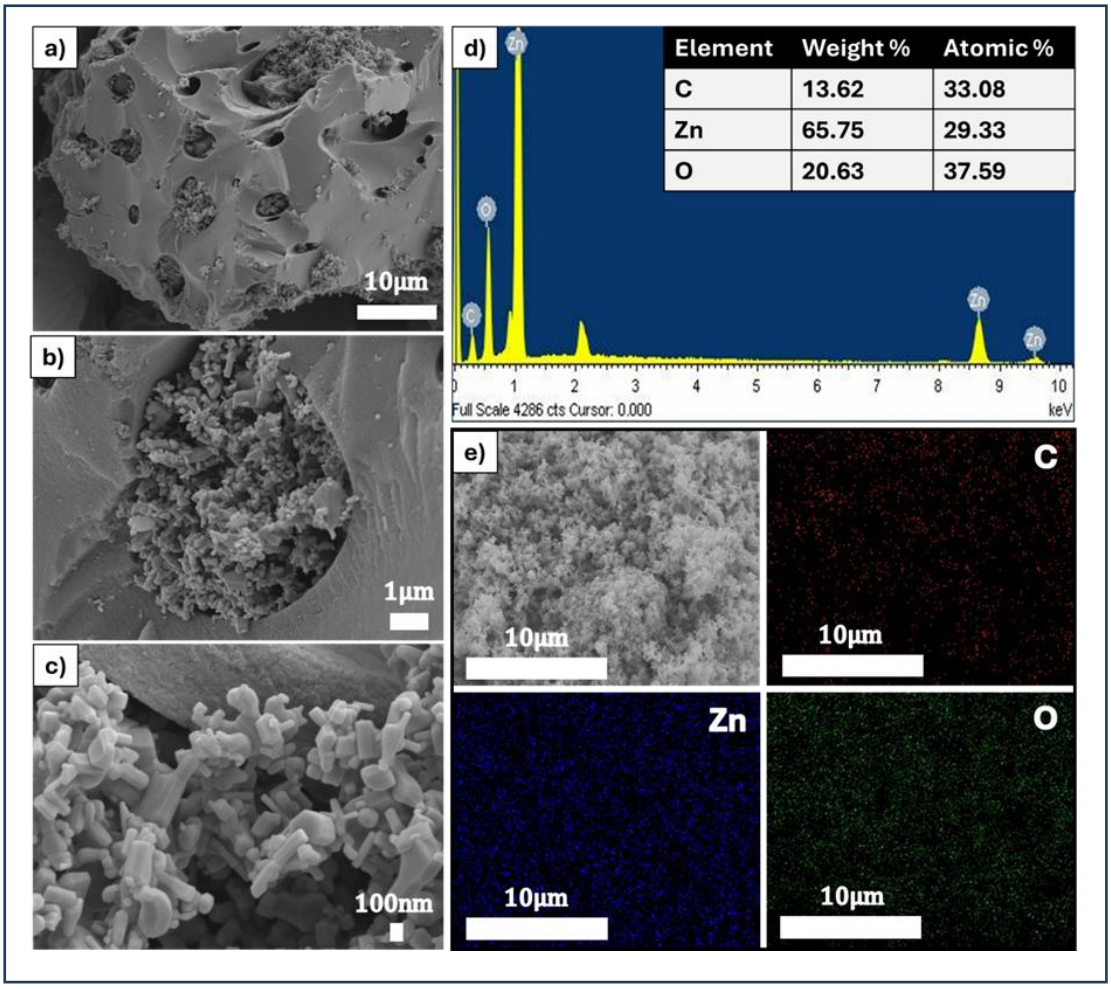

Figure 4.5 FESEM Images of AZ3 with Magnification of a) 2k, b) 10k and c) 30k, d) EDX Spectra and e) Mapping Analysis

Figure 4.6 presents the FESEM images of AC-supported ZnO/g-C_3N_4 composite photocatalyst (AZG2) and its EDX spectra and mapping analysis. As can be seen in Figure 4.6a-c), ZnO particles were laid in uniform manner on the surface of g-C_3N_4. The sheet-like structure of g-C_3N_4 allows many particles of ZnO to lay onto it without changing the original structure of each other. The EDX spectra proved the existence of all elements even with such small amount of g-C_3N_4 was added to the composite, as shown in Figure 4.6d-e). The atomic percentages of each element of C, Zn, O and N are 34.15, 9.48, 54.21 and 2.16, respectively.

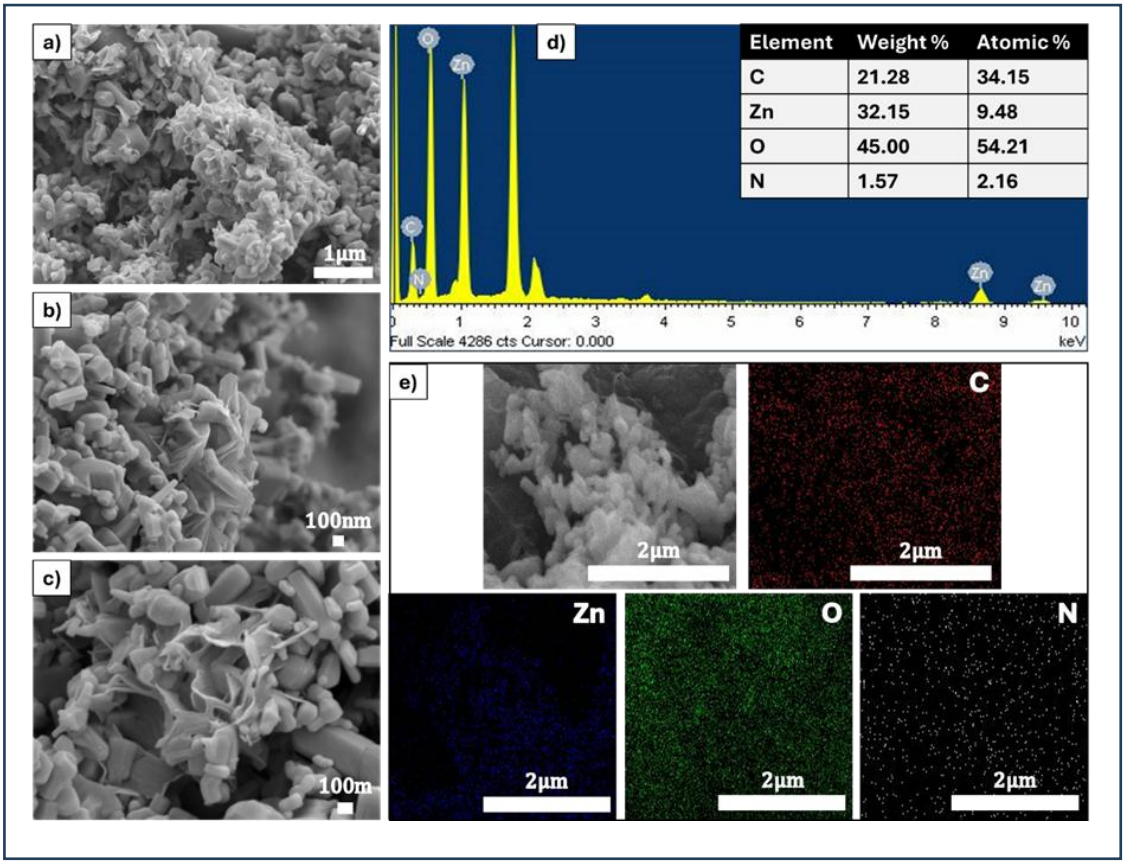

Figure 4.6 FESEM Images of AZG2 with Magnification of a) 20k, b) 30k and c) 50k, d) EDX Spectra and e) Mapping Analysis

4.2.4 N_2 Adsorption-Desorption Analysis

The fitting of N_2 adsorption-desorption isotherms and BET surface area for AC-supported ZnO and AC-supported ZnO/g-C_3N_4 composite photocatalysts is presented in Figure 4.7-4.8. As mentioned earlier, this analysis was done on all of AC-supported ZnO composite photocatalysts and only the most optimum ratio of AC-supported ZnO/g-C_3N_4 composite photocatalyst (AZG2). In Figure 4.7, pristine AC exhibits type I isotherm with H_4 hysteresis loop starting at 0.20 to 1.00 relative pressure (Kim et al., 2023). On the other hand, a type III isotherm in pristine ZnO shows a weak interaction between the adsorbate and the adsorbent (Ismael, 2020a). Pristine g-C_3N_4 presented type IV isotherm with H_3 hysteresis loop starting from 0.3 to 1.00 relative pressure which further indicates the mesoporous materials (Khezami et al., 2024). All of the prepared AC-ZnO composites also exhibit the characteristics of type III isotherm due to a weak adsorbate-adsorbent interaction, with a steep H_3 hysteresis loop at relative pressure ranging from 0.30 to 1.00, further confirm the presence of mesoporous textures

(2–50 nm) (Figure 4.7) (Akir et al., 2017; Inagaki et al., 2019). However, AC-supported ZnO/g-C_3N_4 (AZG2) composite photocatalyst displayed type IV isotherm with H_3 hysteresis loops are present at at around relative pressure 0.2 to 1.0. This loop is frequently seen on aggregates of sheet-like particles that result in slit-shaped pores, indicating that g-C_3N_4 is permeable (Fu et al., 2018; Ismael, 2020). Pristine AC obtained a BET surface area of 554.34 m^2/g with pore diameter of 2.35 nm, pristine g-C_3N_4 with BET surface area of 189.78 m^2/g and pore diameter of 8.84 nm while pristine ZnO with BET surface area of 8.05 m^2/g with pore diameter of 4.73 nm (Figure 4.8a-b). On the other hand, the composite photocatalysts of AZ1, AZ2, AZ3, AZ4 and AZ5 obtained a BET surface area of 36.21, 20.59, 15.12, 9.76 and 7.26 m^2/g with pore diameter of 7.85, 3.05, 7.70, 3.37 and 4.19 nm, respectively (Figure 4.7c-g). The BET surface area of each composite and its pore volume decreased substantially as the amount of ZnO increased from 0.5 up to 2.5 g except for AZ3. These findings are likely to be due to the addition of AC into the composites which is caused by the accumulation of ZnO on the pore of AC (Kim et al., 2023). Confirmed by the FESEM images of AC-supported ZnO composite photocatalyst as ZnO was distributed unevenly and clinging on the surface of AC (Figure 4.5). According to the pore volume distribution curves measured using the Barrett, Joyner, and Halenda (BJH) analysis, all of the composite shows no change in pore volume at a pore diameter with the exception of AZ3 and AZ5, which have a slight increase in pore volume at pore diameter ranges of 3 to 11 nm. These characteristics show that ZnO nanoparticles have been deposited within the pores of AC (Kim et al., 2023). This is explained by the uneven ZnO deposition on the AC blocking the mesopores, which causes the average pore size to decrease (Kim et al., 2023). The SEM image (Figure 4.3c-g) confirms that there was a more uneven ZnO deposition on the surface of AC. This is further supported by BET surface area and BJH analysis, which show that the BET surface area and pore volume of AC-ZnO composites were smaller than those of AC (Table 4.1). However, the specific surface area of AZG2 is 95.58 m^2/g with a pore diameter of 15.08 nm. The AZG2 composite photocatalyst has a higher BET surface area than the pristine ZnO and AC-supported ZnO composite photocatalysts samples indicating that the permeability of g-C_3N_4 could lead to a significant increase in the final product's surface area. In general, the sample's larger surface area helps with light absorption, the adsorption of pollutant, and provides a more active site for the photocatalytic process, which would increases its photocatalytic activity (Garg et al., 2021; Ismael, 2020a).

Table 4.1
BET Surface Area, Total Pore Volume and Average Pore Diameter of Pristine AC and the Composite Photocatalysts.

Photocatalysts	**S_{BET} (m^2/g)**	**Total pore volume (cm^3/g)**	**Average pore diameter (nm)**
Pristine AC	554.34	0.3259	2.35
Pristine ZnO	8.05	-0.0012	4.73
Pristine g-C_3N_4	189.78	0.4180	8.84
AZ1	36.21	0.0297	7.85
AZ2	20.59	0.0276	3.05
AZ3	15.12	0.0170	7.70
AZ4	9.76	0.0147	3.37
AZ5	7.26	0.0102	4.19
AZG2	95.58	0.3564	15.08

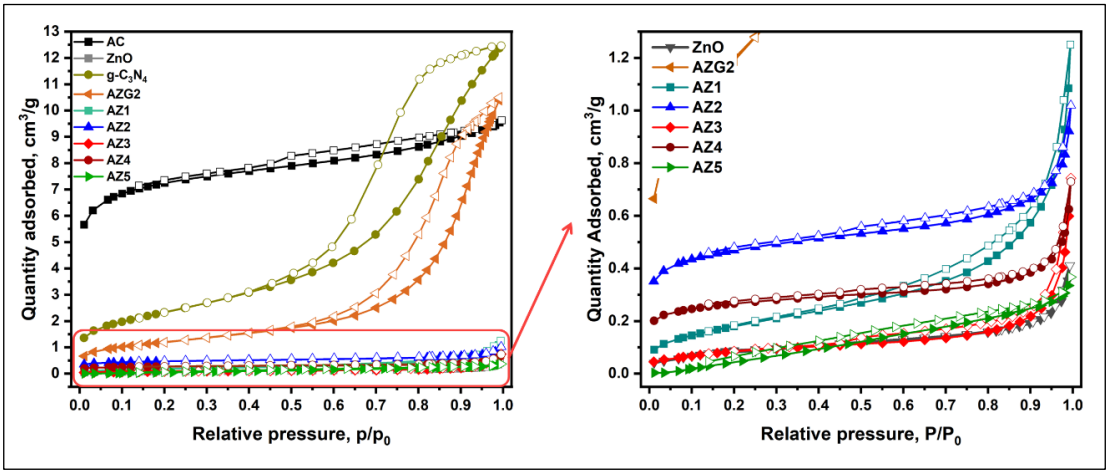

Figure 4.7 N_2 Adsorption–Desorption Isotherms of Pristine AC, Pristine ZnO, Pristine g-C_3N_4, All of AC-ZnO and AC-Supported ZnO/g-C_3N_4 (AZG2) Composite Photocatalysts.

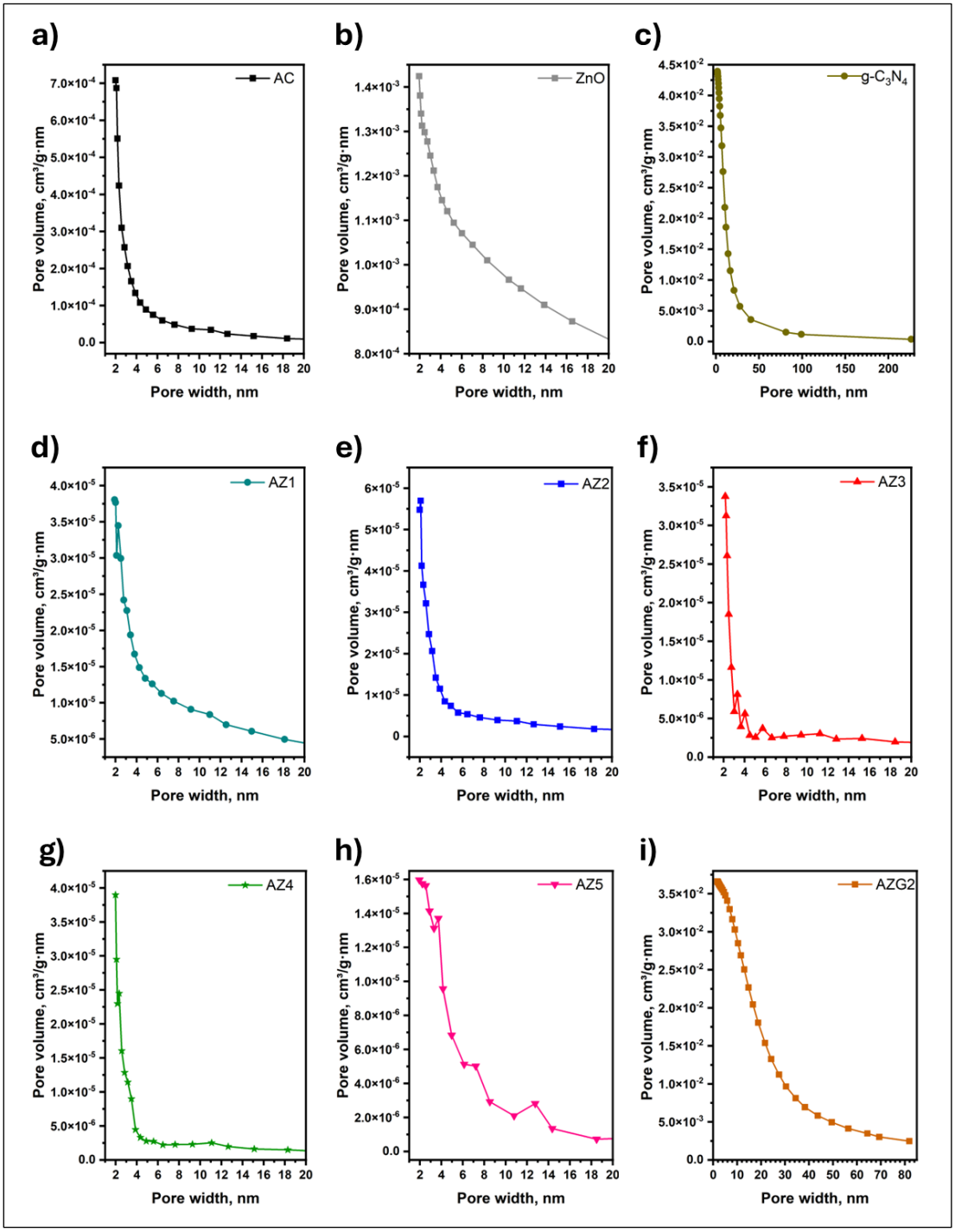

Figure 4.8 BJH Pore Size Distribution of a) Pristine AC b) Pristine ZnO c) AZ1 d) AZ2, e) AZ3, f) AZ4, g) AZ5 and h) AZG2 Composite Photocatalysts.

4.3 Chemical State, Charge Carrier & Optical Analyses

The chemical states and elemental compositions of the photocatalysts were assessed using X-ray photoelectron spectroscopy (XPS) analysis, which revealed information about their bonding properties and surface chemistry. Charge carrier

behaviour, specifically the recombination rates of photogenerated electron-hole pairs, which have a direct impact on photocatalytic efficiency, was examined using photoluminescence spectrophotometer (PL) analysis. Furthermore, the optical characteristics, such as bandgap energy and light absorption capacity, that are crucial for comprehending the photocatalyst's capacity to efficiently use solar energy were ascertained using UV-visible near-infrared spectrophotometry (UV-vis NIR). When taken as a whole, these descriptions offered thorough understandings of the structural and functional characteristics of AC-supported ZnO and AC-supported ZnO/g-C_3N_4 composite photocatalysts.

4.3.1 X-ray Photoelectron Spectroscopy (XPS)

The X-ray photoelectron spectroscopy (XPS) analysis was used to investigate the chemical states and compositions of the AC-supported ZnO (AZ3) composite photocatalyst (Figure 4.9). The C 1s spectra depicts the peaks at 284.4 eV, 285.6 eV and 287.2 eV which are associated to the sp^3 carbon, C-OH bonds, and O-C=O bonds, respectively (Figure 4.9b) (Kim et al., 2023).

The XPS spectra of Zn 2p can be fitted into 2 peaks. The peaks at 1045.1 and 1022.1 eV correspond to the standard values of ZnO with Zn $2p_{1/2}$ and Zn $2p_{3/2}$ splitting. The differences was 23 eV and this values indicate the presence of Zn^{2+} species in the lattice (Figure 4.9c) (Paul et al., 2020; Yin et al., 2015). Meanwhile, the O 1s spectra showed two deconvoluted peaks at 530.9 eV and 532.5 eV (Figure 4.9d). The peak at 530.9 eV is consequent with O^{2-} which is caused by the oxygen vacancies. While the peak at 532.5 eV is due to the surface hydroxyl (-OH) groups of Zn (Fei et al., 2019; Ji et al., 2018; C. Sun et al., 2018; S. Li et al., 2019; H. Li et al., 2022; Mu et al., 2020; Shen et al., 2023).

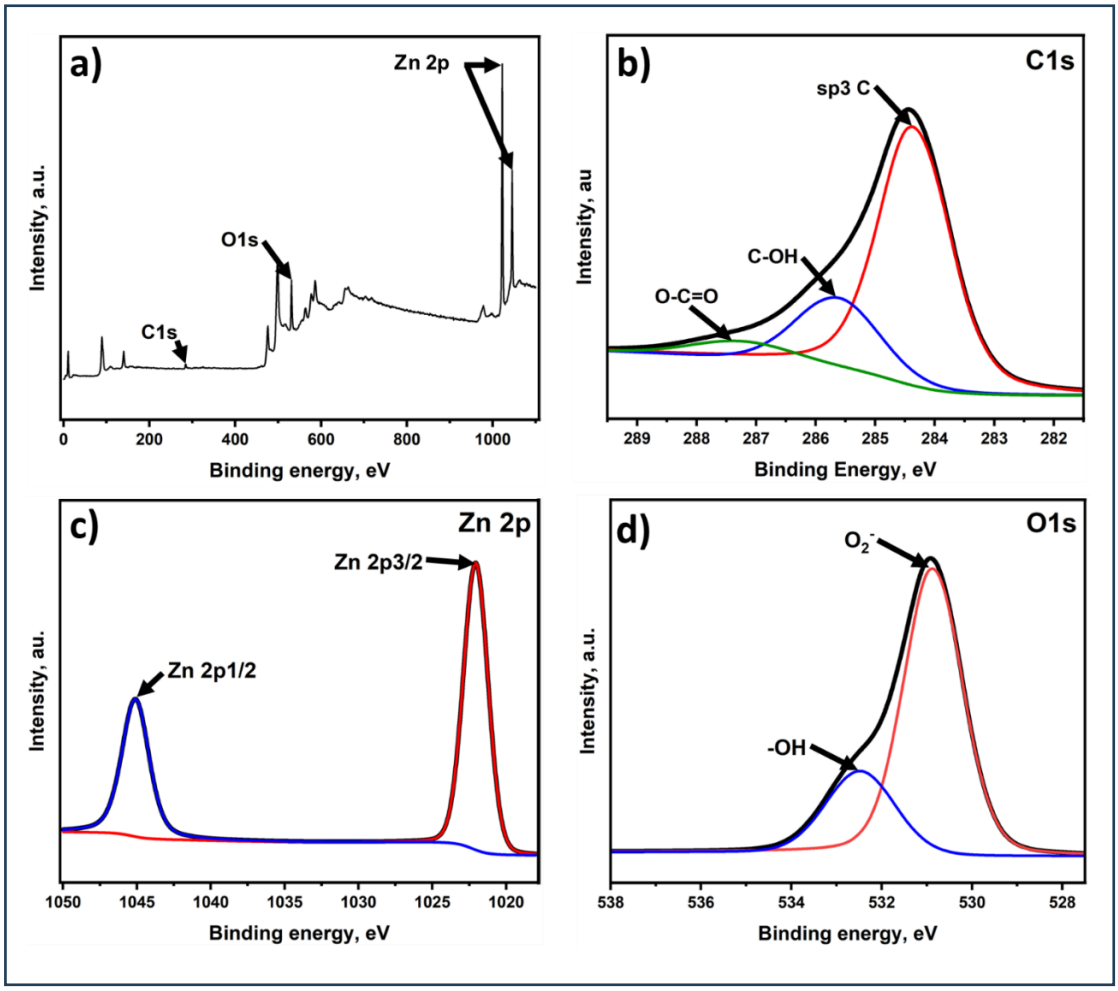

Figure 4.9 X-ray Photoelectron Spectra of (a) Survey Spectrum, (b) C 1s, and (c) Zn 2p, and (d) O 1s Spectrums of AZ3 Composite Photocatalyst.

On the other hand, Figure 4.10 showed the chemical states and compositions of AC-supported ZnO/g-C_3N_4 (AZG2) composite photocatalyst. The XPS spectra for C 1s can be fitted into four individual peaks with binding energy of 283.1 eV, 284.4 eV, 287.0 eV and 288.7 eV respectively. As seen in Figure 4.9, the same peaks of C 1s are present in AZG2 peaks. However, a new peak was identified in the AZG2 spectra at 283.1 eV which was assigned to the C-N-C bond that was associated to sp^3 C–N bond derived from the defects and doping substitution of nitrogen atoms from g-C_3N_4 (Mao et al., 2019).

The XPS spectra of N 1s (Figure 4.10b) can be fitted to one individual peak at 398.2 eV. The peak was assigned to C=N=C namely pyrrolic nitrogen. It's assumed that nitrogen atoms added to the carbon layers particularly the pyrrolic nitrogen atoms are highly bonded and may help to increase reversible specific capacity (Mao et al., 2019; S. Wang et al., 2018).

Meanwhile, the XPS spectra of AZG2 Zn 2p did show the same peaks of AZ2 Zn 2p which are at 1043.9 eV and 1020.8 eV (Figure 4.10c). The ZnO standard values with Zn $2p_{1/2}$ and Zn $2p_{3/2}$ splitting are represented by the peaks. Zn^{2+} species are present in the lattice due to the differences, which was 23 eV (Paul et al., 2020; Yin et al., 2015).

Two peaks at binding energies of 529.6 eV and 530.6 eV were recognised in the curve fitting analysis for O 1s XPS spectra (Figure 4.10d). This peak at 530.9 eV is caused by Zn surface hydroxyl (-OH) groups. Conversely, the peak at 529.6 eV is a result of O^{2-}, which is brought on by oxygen vacancies (Fei et al., 2019; Ji et al., 2018; H. Li et al., 2022; S. Li et al., 2019; Mu et al., 2020; Shen et al., 2023; C. Sun et al., 2018).

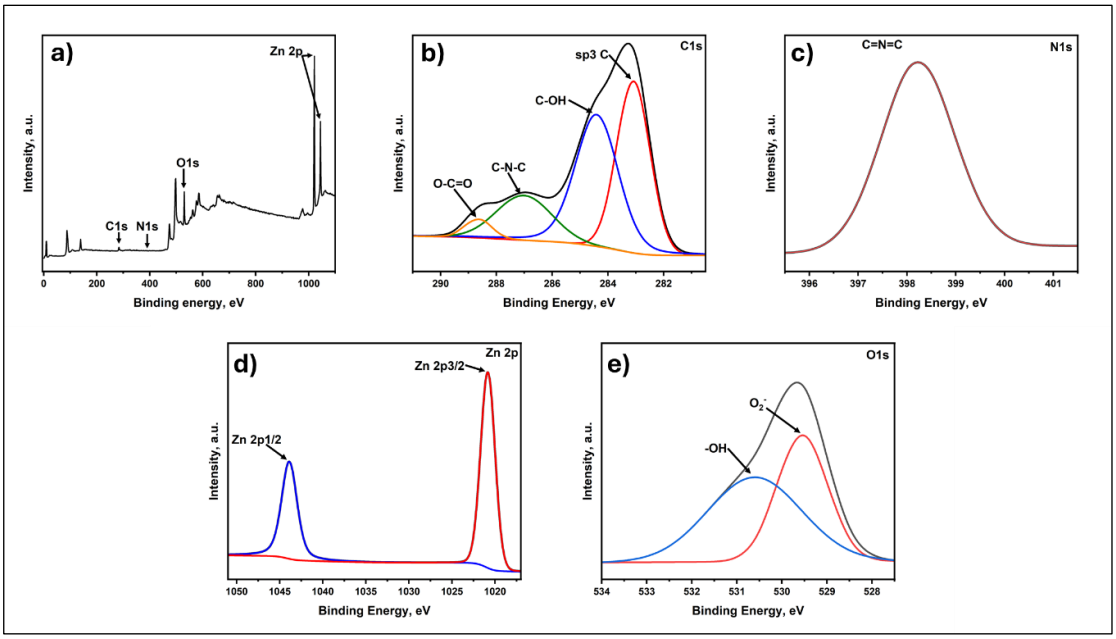

Figure 4.10 X-ray photoelectron Spectra of (a) Survey Spectrum, (b) C 1s, c) N1s and (d) Zn 2p, and (e) O 1s, Spectrums of AZG2 Composite Photocatalyst.

4.3.2 Photoluminescence Spectroscopy (PL)

The separation and recombination processes of the photo-induced electron-hole pairs were examined using the steady-state photoluminescence (PL) spectra. The PL spectra of pristine AC, pristine ZnO, pristine g-C_3N_4, AC-supported ZnO and AC-supported ZnO/g-C_3N_4 composite photocatalyst are shown in Figure 4.11. All of AC-supported ZnO composite photocatalysts had a broad peak at about 530 nm and sharp peak at around 380 nm (Figure 4.11a). These emission peaks are the result of direct

transitions between bands (Chai et al., 2020; B. Liu et al., 2020). Pristine ZnO displayed a broad, powerful deep-level (DL) emission (Luu Thi et al., 2021). In general, high intensity indicates that there has been substantial recombination of electron-hole pairs. The intensity for all AC-ZnO composite reduces significantly as compared to pristine ZnO. Interestingly, the intensity of AC-ZnO composite lowers as the ZnO content rises. This shows that the presence of constant amount of AC does not substantially affect the intensity of the composite photocatalysts. Among the composite photocatalysts, a higher separation efficiency was observed comparatively with a very low ZnO content (0.5 g). All in all, PL analysis indicated a considerable amount of effective charge separation in AC-ZnO composites, demonstrating the improved photoexcited electron-hole separation efficiency in the AC-ZnO composite photocatalysts.

On the other hand, pristine g-C_3N_4 showed a sharp peak at around 450 nm and all of AC-supported ZnO/g-C_3N_4 composite photocatalysts showed comparatively lower intensity than AC-supported ZnO composite photocatalysts. Pristine g-C_3N_4 exhibits a PL signal that is particularly higher than pristine ZnO (Figure 4.11b) due to graphitic carbon nitride's intrinsically fast recombination of photogenerated electrons and holes (Ismael, 2020b). Nevertheless, the PL intensity could be significantly reduced when ZnO and g-C_3N_4 are incorporated in an ideal ratio to create the required composite photocatalyst (Ziaalmolki et al., 2023). Reduced PL intensity in AC-supported ZnO/g-C_3N_4 indicates a suitable charge transfer between the different composites' constituents, which may lead to a significant inhibition of electron hole recombination (Chopan & Chishti, 2023). Additionally, the greatly decreased PL intensity of AC-supported ZnO/g-C_3N_4 show that reducing the unwanted charge carrier recombination may be a benefit of adding even small amounts of g-C_3N_4 to AC-ZnO (Chopan & Chishti, 2023; MuthuKathija et al., 2023b). The AC-supported ZnO/g-C_3N_4 composite photocatalyst may be able to demonstrate superior photocatalytic activity among the synthesised composites as a result of this reduced recombination behaviour (MuthuKathija et al., 2023b).

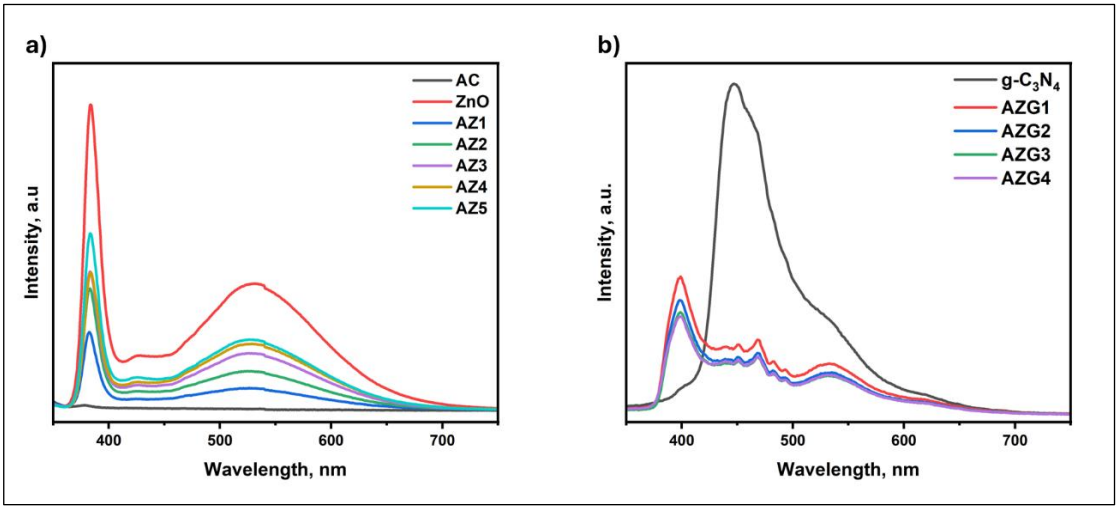

Figure 4.11 PL Spectra of a) Pristine AC, Pristine ZnO, and AC-Supported ZnO Composite Photocatalysts and b) Pristine g-C_3N_4 and AC-Supported/g-C_3N_4 Composite Photocatalysts.

4.3.3 Ultraviolet-Visible Near Infrared Spectroscopy (UV-vis NIR)

Ultraviolet-visible near infrared spectroscopy (UV-vis NIR) was used to examine the optical characteristics of both pristine ZnO and AC-ZnO composite as shown in Figure 4.12. As can be seen in Figure 4.12a, pristine ZnO has a fundamental absorption edge at 385 nm. The band gap energy were estimated from the plots of $F(R)(h\upsilon)^{1/2}$ versus band gap energy ($h\upsilon$) (L. Li et al., 2018). According to their absorption spectra displayed in Figure 4.12b-d, the band gap energies for pristine ZnO, AZ1, AZ2, AZ3, AZ4 and AZ5 composite photocatalysts were 3.25 eV, 3.18 eV, 3.19 eV, 3.18 eV, 3.20 eV, and 3.19 eV, respectively. It was found that the band gap of the AC-ZnO composite photocatalysts slightly decreased when AC was added to ZnO (Garg et al., 2021). The decrease in band gap energy can result to higher photons absorption and a higher formation of photoexcited charge carriers (Luu Thi et al., 2021).

Conversely, pristine g-C_3N_4 has an adsorption edge at around 437 nm. The band gap of pristine g-C_3N_4 and AZG2 composite photocatalyst were 2.7 eV and 3.17 eV respectively. As observed, the addition of g-C_3N_4 (AZG2) to the AC-supported ZnO (AZ3) composite photocatalysts slightly reduced the band gap energy of the AZ3 from 3.18 eV to 3,.17 eV. If the band gap is reduced, the most significant impact is the reduction in the electron-hole recombination behaviour (Jiang et al., 2023; Mao et al., 2019; MuthuKathija et al., 2023b). The formation of a heterojunction structure between ZnO, which has a wide bandgap energy, and g-C_3N_4, which has a narrow bandgap

energy, caused the band gap energy of the composite photocatalysts to decrease (Ismael, 2020a). These results demonstrate that coupling ZnO with g-C_3N_4 enhances ZnO's UV light response by facilitating fast charge transfer and separation between the two materials (L. Li et al., 2018; MuthuKathija et al., 2023). This, in turn, increases the photocatalytic activity of the ZnO/g-C_3N_4 composite. Next, the band gap energy of the composite photocatalysts decreases in comparison to the pristine ZnO, which resolves the issue of the high band gap energy and simultaneously enhances its photocatalytic activity (F. Liu et al., 2019; Q Alfaifi & A Bagabas, 2019).

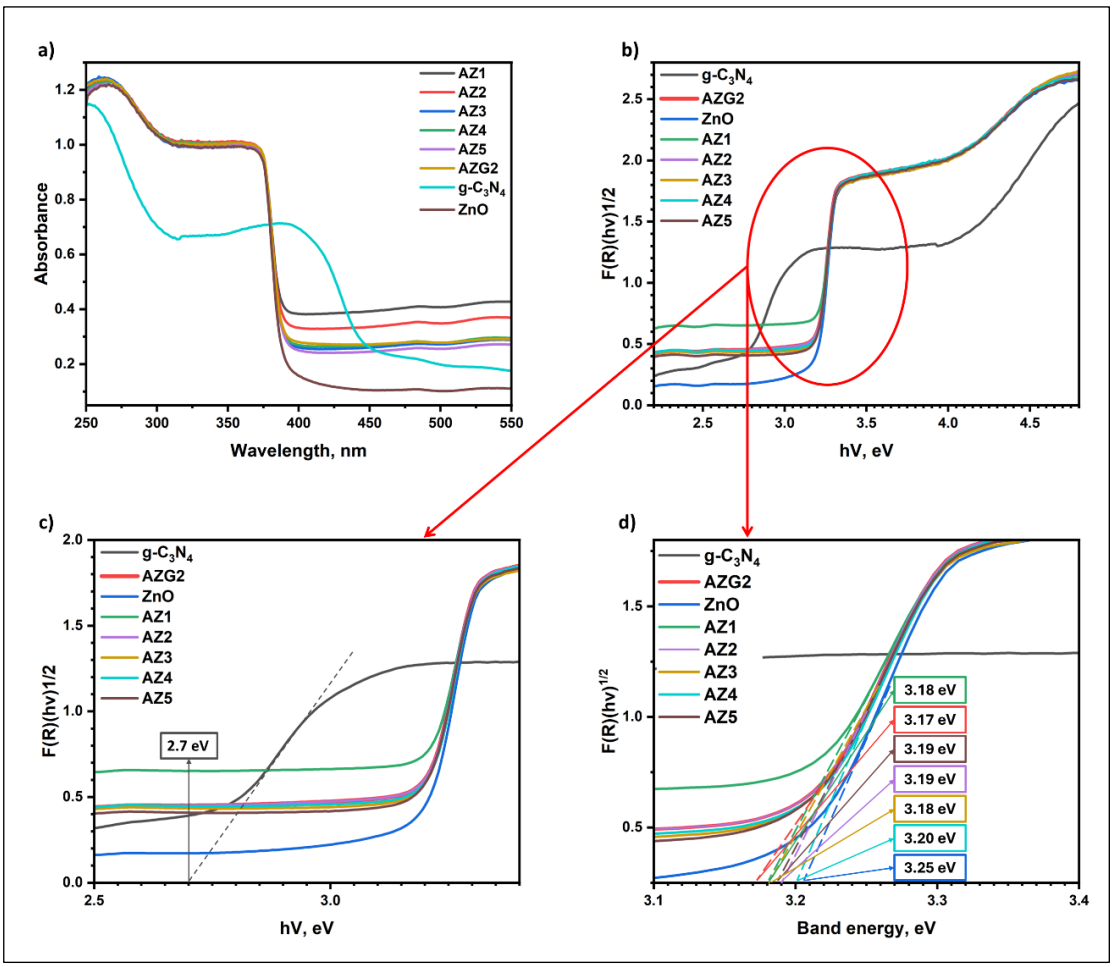

Figure 4.12 (a) UV-vis NIR Spectra of Pristine ZnO, Pristine g-C_3N_4, AC-Supported ZnO and AC-Supported ZnO/g-C_3N_4 Composite Photocatalysts and (b)-(d) Band Gap Energy of Pristine ZnO, AC-Supported ZnO, and AC-Supported ZnO/g-C_3N_4 Composite Photocatalysts Derived from the Plots of $(F(R)(h\upsilon))^{1/2}$ Versus Energy ($h\upsilon$)

4.4 Determination of Acetaminophen (ACE) in Aqueous Phase using UV-vis Spectrophotometer

Prior to the photodegradation of acetaminophen (ACE), the calibration of pristine ACE was conducted to get the maximum absorbance peak (Figure 4.13). The wavelength at λ = 243 nm was chosen as the highest absorbance peak. The wavelength was also used to calculate all of the degradation activity. The ACE concentration 10 mg/L was used as simulated pollutant concentration throughout the degradation activity.

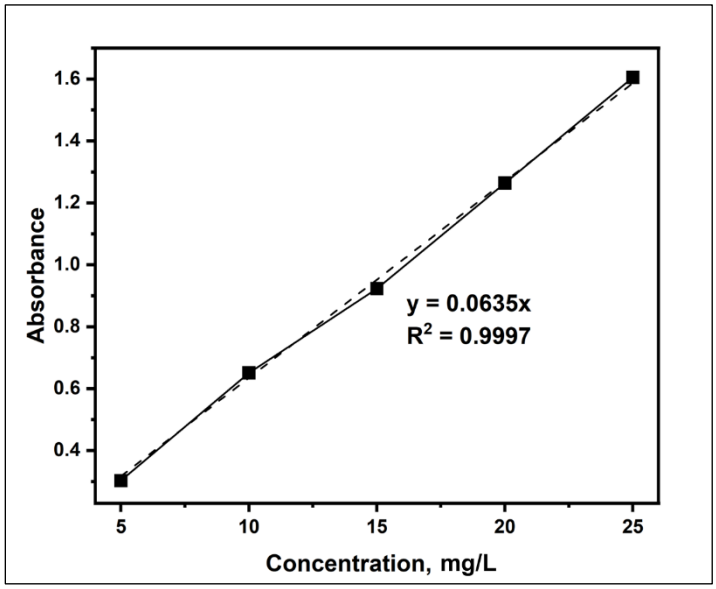

Figure 4.13 Calibration Curve of ACE in Aqueous Phase with Different Concentration Ranging from 5 to 25 mg/L

4.5 Photodegradation of ACE using ZnO, AC-supported ZnO and AC-supported ZnO/g-C_3N_4

4.5.1 Photolysis and Adsorption of ACE in Aqueous Phase

Acetaminophen (ACE) photolysis under low UV light intensity (7 W) revealed very little photocatalytic activity, as shown in Figure 4.14, suggesting that ACE remained stable and did not break down during this process. This demonstrates how resistant it is to direct UV exposure in the specified circumstances. On the other hand, after 240 minutes in the dark, a slight degradation of 16.79% was noted, which was

explained by the composite photocatalyst's activated carbon (AC) adsorption capacity. In the absence of light, the AC was essential in promoting adsorption-driven degradation by facilitating pollutant binding.

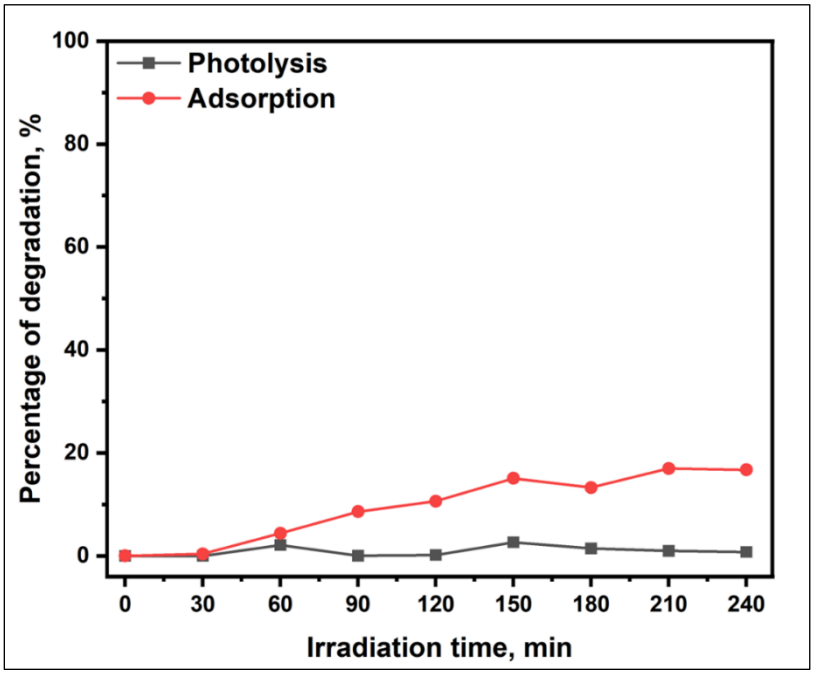

Figure 4.14 Photolysis and Adsorption Activity of ACE Using AC-Supported ZnO/g-C_3N_4 (AZG2) Composite Photocatalyst Under Low UV Light Intensity. [ACE] = 10 mg/L, pH = 5.8, Loading = 0.1 g.

4.5.2 Screening Test

The photodegradation of ACE using pristine ZnO, pristine g-C_3N_4, AC-supported ZnO and AC-supported ZnO/ g-C_3N_4 photocatalysts under low intensity UV light was studied (Figure 4.15). In accordance with preliminary investigations, the amount of the adsorbent had a significant impact on the adsorption process. Thus, determining the minimal adsorbent amount necessary to get the highest ACE removal percentage is crucial. The reaction was carried out with the presence of catalysts under dark conditions for 60 min and shows there is some degradation of ACE. As the ZnO content increases in every AC-supported ZnO composite, the ratio of AC remains the same. This indicates that the higher ZnO content in AC-supported ZnO composite, the smaller amount of AC in the composite. Thus, the difference in degradation percentage varied with different amounts of ZnO in each composite photocatalyst. AZ1 showed the highest degradation of ACE (45%) without UV light exposure as it has the least ZnO

ratio among all composite photocatalyst (Figure 4.15a). However, the degradation percentage only increases linearly after UV light was irradiated. AZ1 has the least ZnO content in comparison with other ratios which cause most of ACE to be adsorbed onto AC rather than surface of ZnO. Accordingly, the decrease in ACE concentration with the presence of AC within irradiation time of 0 to 240 min is faster in the case of AC-supported ZnO than in pristine ZnO. Pristine ZnO only shows total degradation of ACE around 65%, meanwhile the AC-supported ZnO composite photocatalysts reached up to 80% after 120 min of light irradiation. All prepared AC-supported ZnO composite photocatalysts demonstrated a higher degradation percentage compared to pristine ZnO. Surprisingly, the optimum amount of ZnO in the AC-supported ZnO composite photocatalysts AZ3 with ratio of 0.05:1.5 has shown the best results among all ratios (94.78%). It can be observed that the photocatalytic activity and the degradation rate increased alongside the increasing amount of ZnO in the AC-supported ZnO composite photocatalysts. However, as the ZnO increased (>1.5 g), photocatalytic activity and degradation fell significantly. This is due to the accumulation of particles which decrease the surface area and the capacity of the photocatalysts to absorb light which was further confirmed with FESEM images (Figure 4.5) and supported by BET surface area and BJH analysis (Table 4.1). (Steplin Paul Selvin et al., 2018). The amount of ACE degraded for pristine ZnO and all AC-supported ZnO composite photocatalysts can be seen in Figure 4.15a).

However, the percentage of degradation of pristine g-C_3N_4 was very low compared to their counterpart composite photocatalysts because of its high recombination behaviour (Ziaalmolki et al., 2023). On the other hand, the AC-supported ZnO/g-C_3N_4 composite photocatalysts demonstrated higher percentage of degradation (Figure 4.15b) which was attributed by the lower electron-hole pair recombination behaviour which can be explained from the photoluminescence results (Figure 4.11). As can be seen from the degradation results, AC-supported ZnO showed quite a different pattern as compared to AC-supported ZnO/g-C_3N_4 composite photocatalysts. All of the synthesized AC-supported ZnO/g-C_3N_4 showed very little to no degradation of ACE during the adsorption. This could be due to the presence of g-C_3N_4 in the composite. As the g-C_3N_4 has a sheet-like structure, it may have blocked the pores on the AC which resulted in low adsorption during the experiment. However, after UV light was irradiated, the percentage of degradation hiked up dramatically and continued to increase. At 150 min, almost all AC-supported ZnO/g-C_3N_4, reached its

maximum capability to degrade ACE as the percentage of degradation went constant. All AC-supported ZnO/g-C_3N_4 composite photocatalysts showed much better performance as compared to pristine g-C_3N_4 (0.98%). As g-C_3N_4 increased, the percentage of degradation of all composite photocatalysts also increased. Nonetheless, as the amount of g-C_3N_4 went higher (>0.01 g), the percentage of degradation can be seen reduced notably due to the increased exciton production during the destruction process (Ziaalmolki et al., 2023). Nevertheless, the particle aggregation decreased the surface area, which in turn lowered the degradation percentage (Kim et al., 2023; L. Li et al., 2018). Among all the AC-supported ZnO/g-C_3N_4 composite photocatalysts, AZG2 showed the highest degradation percentage. The enhanced photocatalytic activity of the AC-supported ZnO/g-C_3N_4 can be attributed to the synergistic interaction between ZnO and g-C_3N_4 and their optimal band edge positions (Akhundi et al., 2019; Q Alfaifi & A Bagabas, 2019).

Table 4.2
Percentage of Degradation of All Prepared Composite Photocatalysts.

Photocatalysts	**Percentage of degradation, %**	**Amount of ACE degraded, $\frac{mg}{g}$**
Pristine ZnO	77.63	15.91
Pristine g-C_3N_4	0.98	0.20
AZ1	85.07	17.44
AZ2	89.89	18.43
AZ3	94.78	19.43
AZ4	80.58	16.52
AZ5	77.25	15.84
AZG1	75.28	15.43
AZG2	96.17	19.72
AZG3	80.12	16.42
AZG4	75.65	15.51

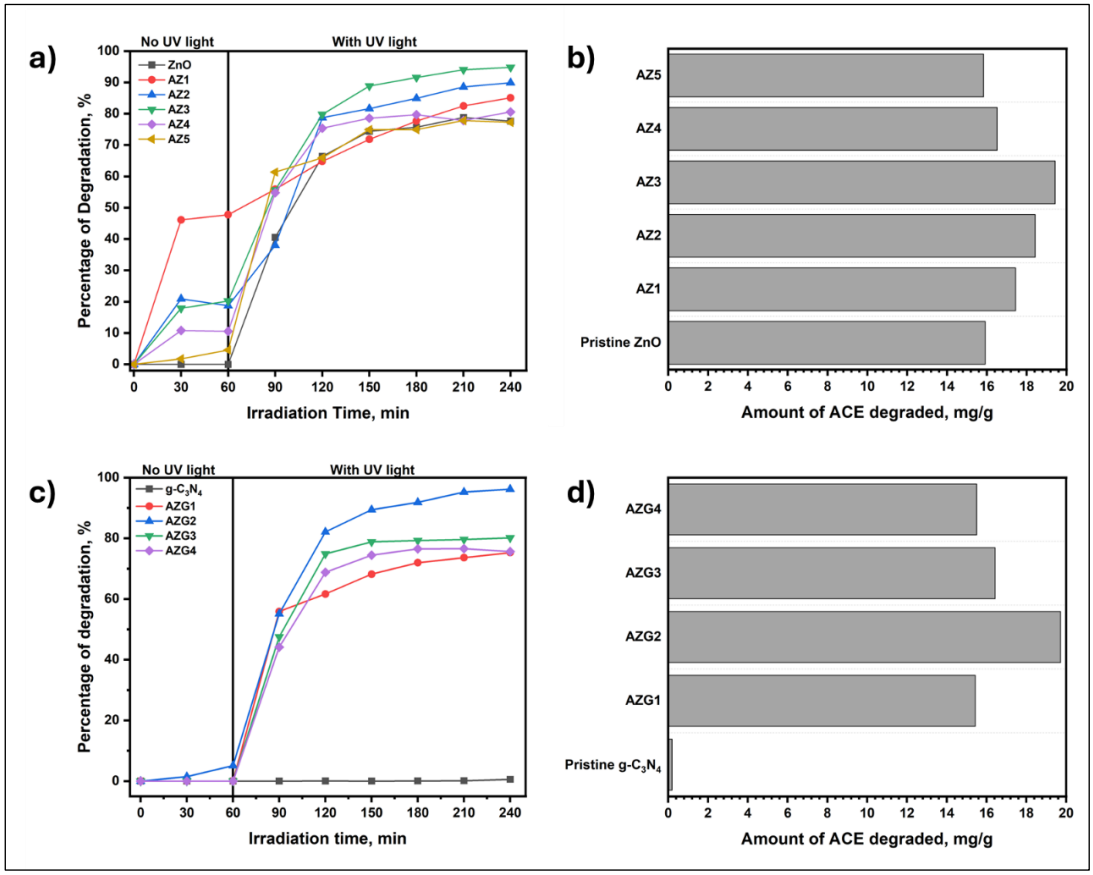

Figure 4.15 a) Degradation Percentages, b) Amount of ACE Degraded by All Prepared AC-Supported ZnO, c) Degradation Percentages and d) Amount of ACE Degraded Using all Prepared AC-Supported ZnO/g-C_3N_4 Composite Photocatalysts. [ACE] = 10 mg/L, pH = 5.8, Loading = 0.1 g.

4.6 Effect of Different Parameters in the Degradation of ACE in Aqueous Phase

4.6.1 Photocatalyst Loading

The photocatalyst loading is crucial as it influences the removal of ACE. Therefore, it is important to determine the best amount of photocatalyst needed to achieve the maximum removal percentage of ACE. The study was carried out using AC-supported ZnO/g-C_3N_4 (AZ2) composite photocatalyst loading ranging from 0.10 to 0.25 g (Figure 4.16). Figure 4.16a shows that the degradation percentage of ACE decreases as loading increases. Photocatalyst loading of 0.10 g achieved the highest degradation percentage (97.17%) after 240 mins of UV light irradiation. However, 0.15 g of photocatalyst loading showed a reduction in degradation percentage as the highest degradation percentage was only 81.27% after 240 mins of UV light irradiation. A

similar situation happened to 0.20 g and 0.25 g photocatalyst loading as it only reached the highest degradation percentage at 77.31% and 80.64% after 240 mins respectively. The amount of ACE degraded of each photocatalyst loadings of 0.10, 0.15, 0.20 and 0.25 g were 19.72, 11.11, 7.92 and 6.61 g respectively. The results showed that further increase of photocatalyst loading above 0.10 g decreases the removal efficiency of ACE. The optimal amount of photocatalyst loading for the photodegradation was 0.10 g as it resulted in 96.17% within 240 min of irradiation.

Theoretically, increased photocatalyst loading promotes the generation of more photoexcited electron-holes and other reactive oxygen species (ROS) that are responsible for molecular breakdown (Bahrami & Nezamzadeh-Ejhieh, 2015). Even so, as the photocatalyst loading increases, the particles agglomerate, the specific surface areas were lowered, and the photocatalytic activity was reduced. According to Hu et al., (2020) the excess catalyst particles might cause a light screening effect, which reduces the surface area of the photocatalyst upon exposure to light irradiation, thus further lowering the photocatalytic effectiveness (Hu et al., 2012). As a result, it was discovered that the optimum catalyst concentration for ACE degradation in this work was 0.10 g due to sufficient number of surface-active sites available for the removal of ACE under our experimental circumstances.

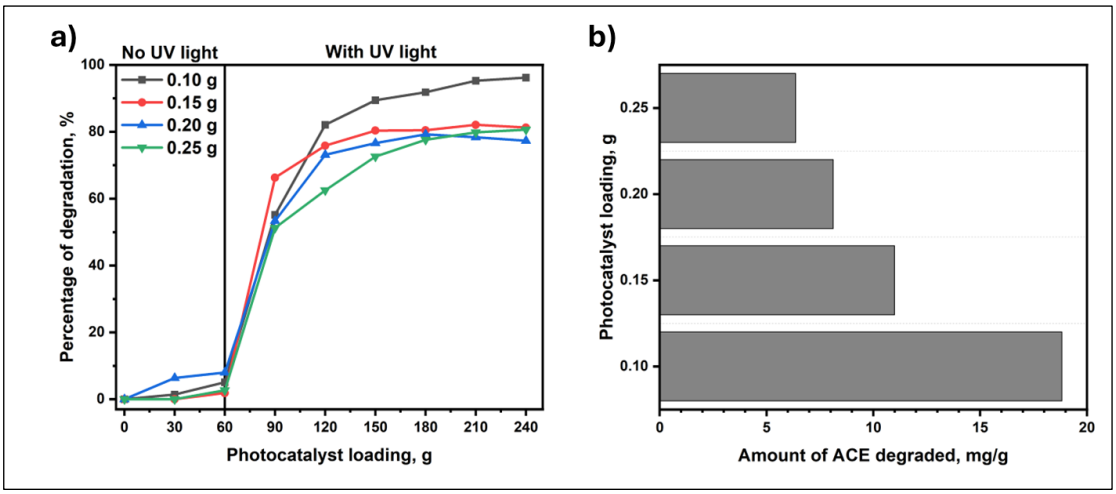

Figure 4.16 a) Degradation Percentages and b) Amount of ACE Degraded Using AC-Supported ZnO/g-C_3N_4 (AZG2) Composite Photocatalyst with Different Photocatalysts Loading. [ACE] = 10 mg/L, pH = 5.8, Loading = 0.10 – 0.25 g.

Table 4.3
Percentage of Degradation and Amount of ACE Degraded for Each Photocatalyst Loading.

Photocatalysts loading, g	Percentage of degradation, %	Amount of ACE degraded, $\frac{mg}{g}$
0.10	96.17	19.72
0.15	81.27	11.11
0.20	77.31	7.92
0.25	80.64	6.61

4.6.2 Initial Concentration

To investigate the effect of the initial ACE concentration on the degradation and removal efficiency, several initial concentrations of 5, 10, 15, and 20 mg/L were used (Figure 4.17). As shown in Figure 4.17a, the ACE degradation and removal effectiveness declined as the initial concentration rose. After 60 mins without UV light irradiation, 5 mg/L initial concentration was observed to have 12.74% degradation percentage of ACE which was contributed by adsorption, but the degradation percentage hiked up to 94.23% after 240 mins of UV light irradiation. The initial percentage of 10 mg/L on the other hand presented lower adsorption of 5.07% after 60 mins without UV light irradiation. Nonetheless, the percentage of degradation achieved the highest at 96.17% after 240 mins of UV light irradiation. For the initial concentration of 15 mg/L, the adsorption was the highest (25.36%). However, the percentage of degradation was only at 87.07% which was the lowest among all the initial concentrations. On the contrary, the adsorption for 20 mg/L of ACE initial concentration after 60 mins was 12.70% and after 240 mins the degradation percentage reached 88.72%. The amount of ACE degraded for 5, 10, 15 and 20 mg/L initial concentrations was 9.61, 19.72, 25.95 and 35.49 g respectively. The highest percentage of degradation of ACE (96.17%) was achieved with using 10 mg/L initial concentration of ACE and the lowest (87.07%) was with 15 mg/L. At low concentrations of pollutants, the rate of degradation typically increases as the concentration of substrate increases because there are enough radicals and holes for the reaction with contaminants at low

substrate concentrations. However, because there aren't enough reactive radicals present, the removal rate drops after the ideal concentration (Ahmad et al., 2024).

Due to the high concentration of ACE particles adsorbed on the surfaces of the photocatalyst, no photons were able to reach the surfaces, reducing the UV screening effect and resulting in drop of degradation rate (Chijioke-Okere et al., 2023). The number of molecules adsorbed on the surface of the photocatalyst increases with the concentration of ACE. Lower degradation efficiency results from this oversaturation since there are fewer active sites available for interaction with ROS (An et al., 2011). The observed decline in degradation and removal efficiency with increasing initial ACE concentrations is well-supported by established theories in photocatalytic research. Active site saturation plays a key role; as the initial concentration rises, the limited active sites on the photocatalyst become overloaded, reducing the interaction between ACE molecules and ROS, as detailed by Salahshoori et al. (2024) and Gusain et al. (2019) (Gusain et al., 2019; Salahshoori et al., 2024). Additionally, increased solution turbidity at higher ACE concentrations impedes UV light penetration, restricting the activation of the photocatalyst surface. This effect, highlighted in studies by Rafiq et al., (2021), explains the reduced generation of ROS throughout the solution at higher pollutant concentrations (Rafiq et al., 2021). Furthermore, competition for ROS among a larger number of ACE molecules at elevated concentrations limits the degradation efficiency per molecule, a phenomenon extensively discussed in studies on multi-pollutant environments (Groeneveld et al., 2023). These mechanisms collectively support the results obtained in earlier, where the optimal ACE concentration of 10 mg/L balanced effective adsorption and degradation.

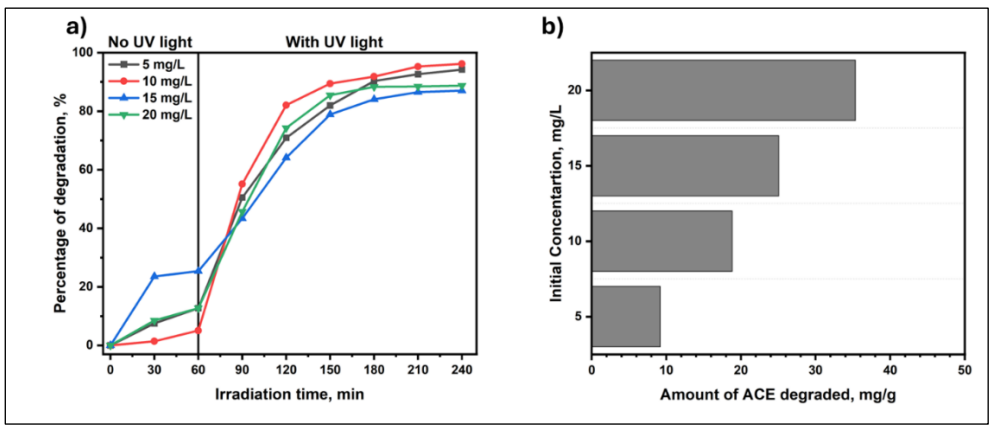

Figure 4.17 a) Degradation Percentages and b) Amount of ACE Degraded Using AC-Supported ZnO/g-C_3N_4 (AZG2) Composite Photocatalysts with Different

Initial Concentration of ACE. [ACE] = 5–10 mg/L, pH = 5.8, Loading = 0.1 g.

Table 4.4
Percentage of Degradation and Amount of ACE Degraded for Each Initial Concentration of ACE.

Initial concentration of ACE, $\frac{mg}{L}$	**Percentage of degradation, %**	**Amount of ACE degraded, $\frac{mg}{g}$**
5	94.23	9.61
10	96.17	19.72
15	87.07	25.95
20	88.72	35.45

4.6.3 Initial pH

In this work, pH has a major impact on the degradation efficiency of ACE degradation during photocatalytic oxidation (Aarab et al., 2020). To investigate the impact of pH on the degradation of ACE, experiments were conducted at various initial pH ranges, 2, 4, 8, 10, and the natural pH of ACE 5.8. Additionally, an initial concentration of 10 mg/L and an ideal dosage of 0.1 g of AC-supported ZnO/g-C_3N_4 (AZG2) composite photocatalyst were employed. Figure 4.18 displays the degradation percentages of ACE at various initial pH values. It can be seen that, at pH of 2, the highest degradation percentage of 99.31% was observed, then steadily declined at pH 4 (86.69%), and then picked up at pH 5.8 (96.17%), corresponding to the pH of natural ACE. However, the pH range in the basic regimes saw a subsequent decrease in ACE degradation with percentage obtained were 79.54%, and 26.93% for pH 8 and 10, respectively. Figure 4.18 illustrates that ACE has a higher capacity to be degraded at pH 2 which is acidic but depicts the lowest capacity in basic regime. However, at natural pH of ACE (5.8) presented high degradation.

The pH at which the net surface charge is neutral is represented by the pH of zero-point charge (pH_{zpc}) of a photocatalyst, such as AC-supported ZnO/g-C_3N_4. Prior research and experimental investigations have demonstrated that the pH_{zpc} is a crucial component in identifying the properties of a photocatalyst's surface charge. The pH_{zpc}

of AC-supported ZnO/g-C_3N_4 was discovered to be 7.5 experimentally. This suggests that at pH values lower than 7.5, the photocatalyst's surface has a positive charge, which enhances its ability to adsorb ACE. The positive charge draws and allows the easier binding of the negatively charged ACE molecules as shown in Equation (4.1) and (4.2) (Sanjeev & Valsan, 2024). Conversely, when the pH exceeds 7.4, the catalyst's surface starts to acquire a negative charge (Katiyar & Saharan, 2023). This negatively charged surface repels the ACE, preventing it from binding to the catalyst. Consequently, less ACE is broken down when the pH rises above 7.5. Through electrostatic interactions, this shift has a direct impact on the photocatalyst's capacity to adsorb charged molecules such as ACE. It shows that the pH of the solution affects the electrostatic interaction between a solution and the photocatalyst surface accordingly (Ramasamy et al., 2023). The positively charged surface of ZnO/g-C_3N_4 aggressively attracts negatively charged ACE molecules at pH values lower than pH_{zpc}. Studies on comparable materials, such as ZnO and TiO_2 composites by Yang et al., 2022 and Kumar et al., 2018, have shown that this advantageous adsorption increases ACE degradation by bringing the target molecules closer to the active sites on the photocatalyst surface (Suneel Kumar et al., 2018; Yang et al., 2022). The charged surface and ACE interaction processes are further demonstrated by equations (4.1) and (4.2), which emphasise the function of the electric double layer in promoting adsorption.

On the other hand, ACE molecules are repelled by the negatively charged surface caused by the dissociation of hydroxyl groups at pH levels higher than 7.5, which restricts their ability to bind to the photocatalyst. The photocatalytic process is less effective as a result of this reluctance. Park et al. (2021) obtained similar results, showing that unfavourable electrostatic interactions cause the efficiency of organic pollutant degradation to decrease when the pH of the solution surpasses the pH_{zpc} of the photocatalyst (Park et al., 2021). Furthermore, surface charge is not the only way that pH affects the photocatalytic process. The pH of the solution also affects the production of ROS, including hydroxyl radicals (•OH). According to research by Groeneveld et al. (2023), alkaline circumstances restrict degradation efficiency by reducing ROS availability, while acidic conditions increase ROS synthesis and improve photocatalytic activity (Groeneveld et al., 2023).

To sum up, the pH of the solution affects the electrostatic interactions and the photocatalytic activity of ZnO/g-C_3N_4 assisted by AC in two ways. These results highlight how crucial pH regulation is for maximising ACE degradation. These findings

are in line with the behaviour of ZnO and g-C_3N_4 composites, where photocatalytic activity was optimised by pH changes (Ibhadon & Fitzpatrick, 2013).

$$ZnOH + H^+ \rightarrow ZnOH_2^+ (pH < pH_{zpc}) \quad (4.1)$$

$$ZnOH + OH^- \rightarrow ZnO^- + H_2O (pH > pH_{zpc}) \quad (4.2)$$

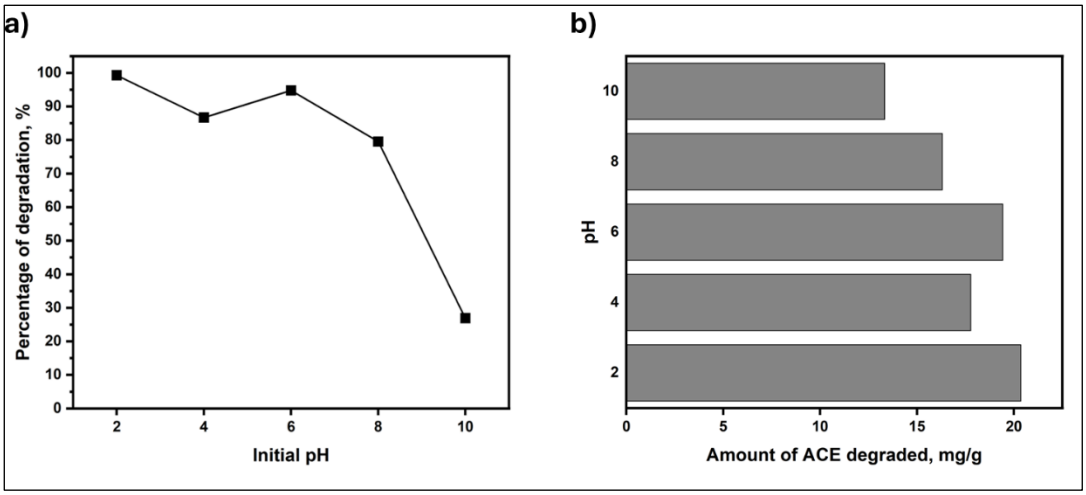

Figure 4.18 a) Degradation Percentages and b) Amount of ACE Degraded Using AC-Supported ZnO/g-C_3N_4 (AZG2) Composite Photocatalysts with Different Initial pH of ACE. [ACE] = 5–10 mg/L, pH = 2–10, Loading = 0.1 g.

Table 4.5
The Percentage of Degradation and Amount of ACE Degraded for Each Initial pH of ACE.

Initial pH of ACE	**Percentage of degradation, %**	**Amount of ACE degraded, $\frac{mg}{g}$**
2	99.31	20.36
4	86.69	17.77
6	96.17	19.72
8	79.54	16.30
10	26.93	13.33

4.7 Photodegradation Mechanism

Radical trapping experiments were conducted to look into the photocatalytic mechanism of AC-supported ZnO/g-C_3N_4 (AZG2) composite photocatalysts. As illustrated in Figure 4.19, ethylenediaminetetraacetic acid (EDTA) served as a scavenger of holes (h^+), p-benzoquinone (pBQ) as a scavenger of superoxide ion radicals (•O_2-), and tert-butanol (tBuOH) as a scavenger of hydroxyl radicals (•OH). The photocatalytic efficiency for AC-supported ZnO/g-C_3N_4 composite photocatalysts has a more notable decline with the addition of pBQ and tBuOH to the solution, however, with the addition of EDTA somewhat dropped the photocatalytic performance. From this data, it shows that the •OH and •O_2- are the main cause for the degradation of ACE, followed by h^+. Theoretically, positive holes are left behind as ZnO absorbs photon energy, stimulating photoexcited electrons to move from the valence band (VB) to the conduction band (CB). The degradation of ACE was attributed to the presence of these radical species by breaking down the bond, converting the ACE molecule into harmless species and small molecules.

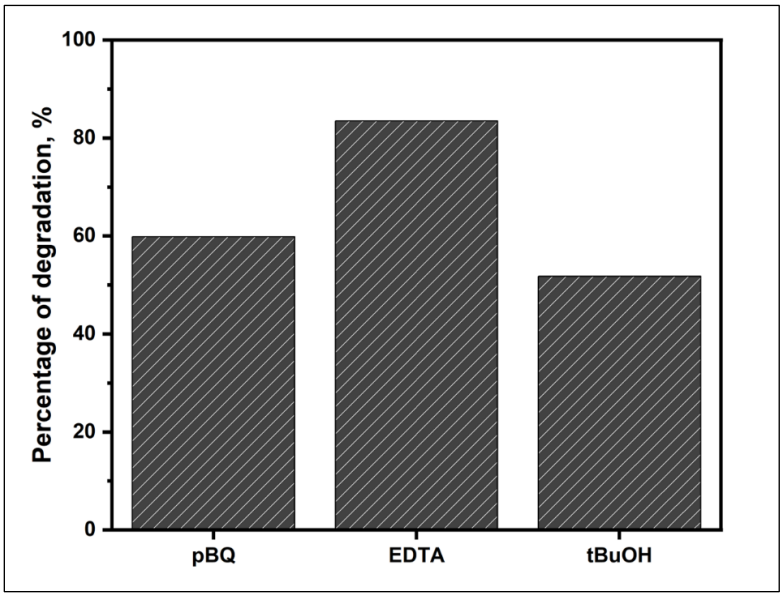

Figure 4.19 Photodegradation of ACE by AC-Supported ZnO/g-C_3N_4 Composite Photocatalyst (AZG2) in the Presence of Different Trapping Agents Under UV Light Irradiation. [ACE] = 10 mg/L, pH = 5.8, Loading = 0.1 g.

Figure 4.20 depicts a potential synergistic mechanism for photocatalysis between AC, ZnO and g-C_3N_4 based on the photodegradation results. The incorporation

of ZnO on the activated carbon support, which increases the photocatalytic activity of ZnO, significantly improved the removal efficiency (Branco et al., 2019; Michelon et al., 2022; Nilsen et al., 2019; Yuan et al., 2019). Effective adsorption of the pollutant onto the porous structure of the carbon is responsible for the enhanced rate constant upon irradiation. The pollutant then spontaneously moves from the AC to the ZnO surface. The pollutant on the ZnO surface under irradiation can decompose more effectively thanks to the process's substantial concentration difference between the two solid phases (Figure 4.20) (Loke et al., 2022). This process demonstrates how ZnO and carbon porosity work together to increase photocatalytic activity. In this instance, this combination of the AC's adsorption ability and the ZnO's photoactivity appears to have a complementary effect in the composite. For photocatalysis to occur without AC, ACE molecules must collide with ZnO and remain in contact. (Loke et al., 2022).

Using the Mulliken electronegativity equation, the valence band (VB) and conduction band (CB) edge values of ZnO and g-C_3N_4 are determined (Praus, 2021; Uddin et al., 2020).The electronegativity (X), band gap energy (E_g), and energy of free electrons on the hydrogen scale (E_e, 4.5 eV) are all represented in the equations below (Equations 4.3 and 4.4). Additionally, the edge potentials for VB and CB are, respectively, E_{CB} and E_{VB}.

$$E_{VB} = X - E_e + 0.5\ E_g \tag{4.3}$$

$$E_{CB} = X - E_e - 0.5\ E_g \tag{4.4}$$

For g-C_3N_4 and ZnO, X is 4.22 and 5.79 eV, respectively (Praus, 2021; Ziaalmolki et al., 2023). Additionally, ZnO and g-C_3N_4 have energy band gaps of 3.25 and 2.70 eV, respectively, based on the samples' UV-vis NIR spectra (Figure 4.12). The values of CB and VB of g-C_3N_4 were determined to be −1.63 and 1.05 eV, respectively. Additionally, ZnO's CB and VB were found to be −0.34 and 2.92 eV, accordingly. ZnO and g-C_3N_4 are excited by UV light, producing multiple excitons. Crucially, the induced holes' redox potential in g-C_3N_4's VB is much lower than the +2.69 eV needed for the production of hydroxyl radicals (Mirzaei et al., 2018). While g-C_3N_4 has a more negative CB potential than zinc oxide (A. Kumar et al., 2018; Ziaalmolki et al., 2023). Due to the morphology of zinc oxide and g-C_3N_4 in the nanocomposite, photogenerated electrons in the CB of g-C_3N_4 transfer to the CB of ZnOs (Mirzaei et al., 2018;

Ziaalmolki et al., 2023). It is possible to move these electrons into the solution and oxidise them further to create $\bullet O_2$- radicals. Because of g-C_3N_4's higher CB, the photoexcited electrons can be efficiently transferred into ZnO's CB, resulting in a successful split of electron-hole pairs and an increase in UV light absorption (Mirzaei et al., 2018). ZnO and g-C_3N_4 form an n-n heterojunction at the interface because they are both n-type semiconductors (Ziaalmolki et al., 2023). Electrons travel from higher CB to lower CB and holes from lower VB to higher VB in type II heterojunction (Mirzaei et al., 2018).

In theory, photon energy is absorbed and the electrons (e^-) at the VB are excited to the CB when the composite photocatalyst is exposed to light of the desired wavelength (sufficient energy) (Chopan & Chishti, 2023; Torkamani et al., 2024). A hole (h^+) is made in the valence band during this process. As a result of this process, the photo-excited state forms and an e^- and h^+ pair is produced. The hole is used to oxidise donor molecules, and the excited electron is used to reduce an acceptor (Ziaalmolki et al., 2023). Superoxide radical anions ($\bullet O_2$-) and hydroxyl radicals ($\bullet$OH) are created during the photodegradation process (Y. Wang et al., 2020).

As illustrated in Figure 4.20, charge transfer on the semiconductor surface reacts with dissolved oxygen, water, or the organic target compound (ACE) to produce ·OH and $\cdot O_2^-$ radicals. Emphasis is placed on the critical roles that ·OH and $\cdot O_2^-$ play in the composite photocatalysts' ACE degradation. These radicals convert pollutants—particularly ACE—into molecules that are safe for the environment when they are interaction with them. When AZG2 is exposed to UV light (7 W), electrons in its VB absorb energy and get excited to the CB, leaving behind positively charged holes in the VB (Equation 4.5). This step generates electron-hole pairs, which are essential for initiating redox reactions on the photocatalyst surface. $\cdot O_2^-$ radicals form when the dissolved oxygen in the solution combines with the photogenerated electrons in the CB (Equation 4.6). $\cdot O_2^-$ radicals are extremely reactive substances that aid in the decomposition of organic contaminants such as ACE. ·OH are produced when the hydroxide ions (OH^-) in the solution react with the holes in the VB (Equation 4.7). Strong oxidising agents that can break down organic molecules are ·OH. Additional ·OH can be produced by further reacting the $\cdot O_2^-$ radicals created in Equation 4.6 with protons (Equation 4.8). The oxidative capacity of AZG2 is increased by this reaction, which increases the generation of ·OH radicals. Then, ACE molecules are attacked and

oxidised by the ·OH radicals produced in steps (Equation 4.7) and (Equation 4.8), resulting in their degradation into smaller, non-toxic products (Equation 4.9). ACE is successfully eliminated from the solution in this step, which is the central component of the photocatalytic process (Jiang et al., 2023).

$$AZG2 + h\nu\ (UV) \rightarrow AZG2 + (e_{CB}^{-} + h_{VB}^{+}) \tag{4.5}$$

$$O_2 + e_{CB}^{-} \rightarrow \cdot O_2^{-} \tag{4.6}$$

$$OH^{-} + h_{VB}^{+} \rightarrow \cdot OH \tag{4.7}$$

$$\cdot O_2^{-} + 2\,H^{+} \rightarrow 2 \cdot OH \tag{4.8}$$

$$OH + ACE \rightarrow \text{Degraded products} \tag{4.9}$$

Throughout the photocatalytic process, photoexcited electrons move from the VB of g-C_3N_4 to its CB and then transfer to the CBs of ZnO and AC. This results in the formation of holes in the VB and electrons in the CB, which prevent recombination and promote effective charge separation (Ziaalmolki et al., 2023). The accumulated electrons react with O_2, producing $\cdot O_2^{-}$. Consequently, ·OH and $\cdot O_2^{-}$ radicals play a crucial role in enhancing the photocatalytic activity of the AZG composite (Hemavibool et al., 2022; Y. Wang et al., 2020). Moreover, an additional factor that enhances photocatalytic performance is the higher photon absorption capacity of the AC-supported ZnO/g-C_3N_4 composite photocatalyst (MuthuKathija et al., 2023a). More electrons and holes are produced as a result, which promotes a more reaction between the holes and H_2O and raises the amount of ·OH that is produced (Torkamani et al., 2024; Ziaalmolki et al., 2023). As a result, the photocatalytic action of the AC-supported ZnO/g-C_3N_4 composite photocatalyst was significantly improved by the suggested photocatalytic mechanisms and it was consistent with the previously reported study by Asadzadeh-Khaneghah and Habibi-Yangjeh., (2020) (Ziaalmolki et al., 2023).

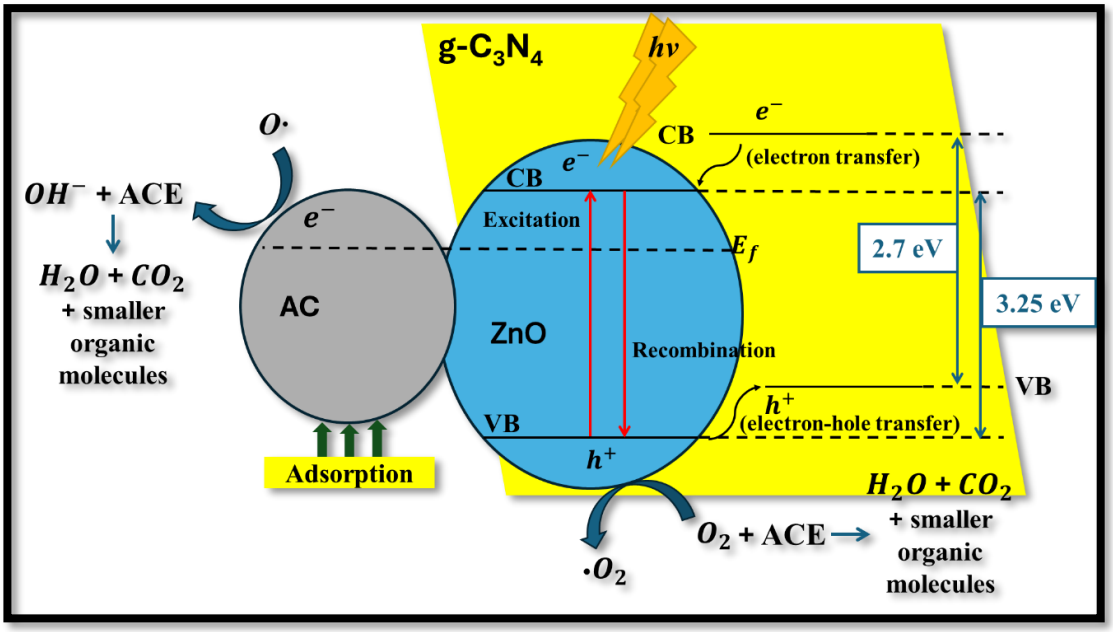

Figure 4.20 Schematic Illustration of the Photogenerated Electron-Hole Pair Separation and Transfer over AC-Supported ZnO/g-C_3N_4 Composite Photocatalysts Irradiated to UV Light for the Degradation of ACE.

4.8 Kinetic of ACE using ZnO, AC-supported ZnO and AC-supported ZnO/g-C_3N_4

4.8.1 Screening Test

The linear plots of ln (C_0/C_t) versus irradiation of time, t of ACE are shown in Figure 4.21-4.24. The pseudo first-order rate constant, degradation rate and correlation factors values are tabulated in Table 4.6-4.9. The kinetics of the ACE degradation by the prepared photocatalysts was studied based on the Langmuir– Hinshelwood (L–H) kinetic model (J. Liu et al., 2023). The pseudo-first-order model assumes that ACE molecule is adsorbed on the photocatalyst surface before it undergoes photodegradation (Behravesh et al., 2020). It can be observed that AZ3 had the highest degradation percentage among AC-supported ZnO while AZG2 for the AC-supported ZnO/g-C_3N_4 composite photocatalysts with each degradation rate of 0.1286 mg/L•min^{-1} and 0.1390 mg/L•min^{-1} respectively.

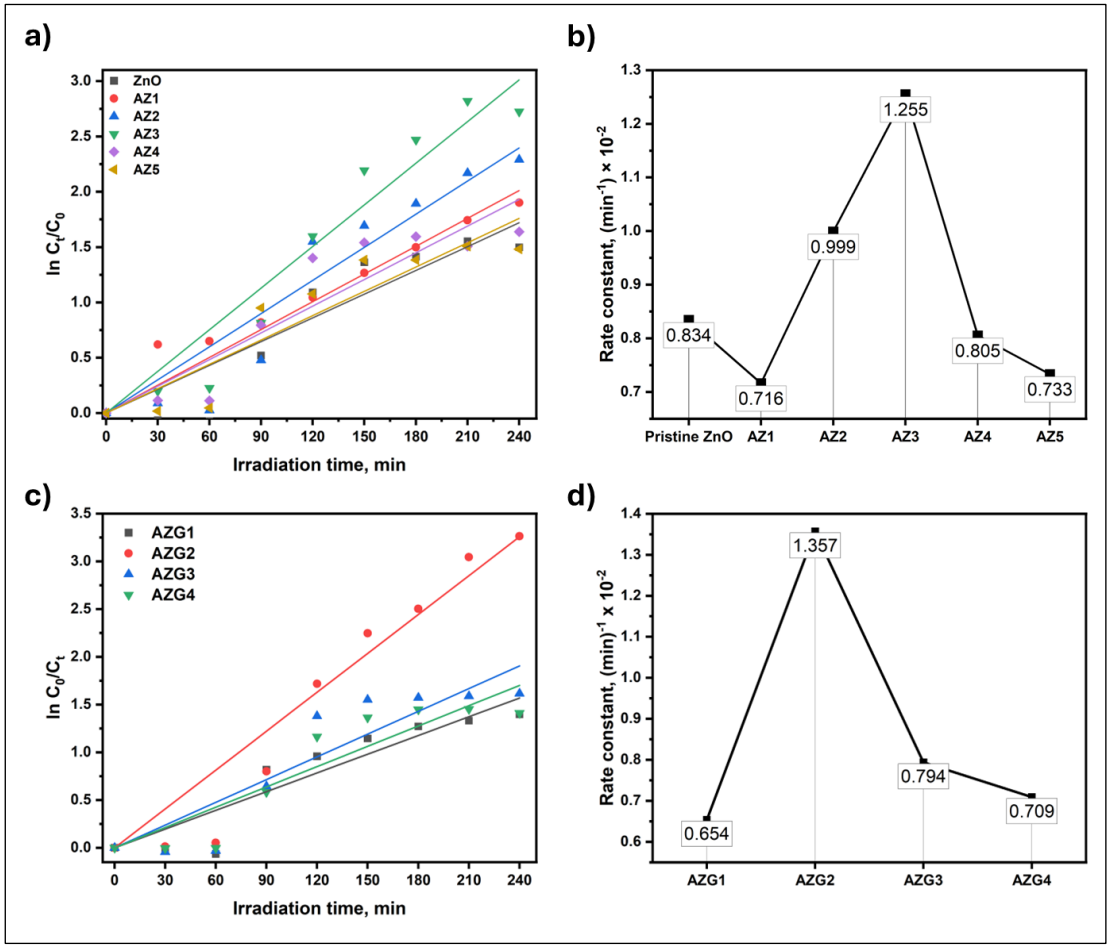

Figure 4.21 a) Kinetics of the Degradation of ACE Using Pristine ZnO and AC-Supported ZnO Composite Photocatalysts, b) Rate Constants by AC-Supported ZnO Composite Photocatalysts, c) Kinetics of the Degradation of ACE Using AC-Supported ZnO/g-C_3N_4 Composite Photocatalysts and d) Rate Constants by AC-Supported ZnO/g-C_3N_4 Composites Photocatalysts. [ACE] = 10 mg/L, pH = 5.8, Loading = 0.1 g.

Table 4.6
Rate Constant, Rate, and Correlation Factors Values of all Prepared Composites Photocatalysts.

Photocatalysts	**Rate constant, k_1 (min^{-1}) x 10^{-2}**	**Rate (mg/L•min^{-1})**	**Correlation factors, R^2**
Pristine ZnO	0.834	0.0855	0.9867
AZ1	0.716	0.0734	0.9448
AZ2	0.999	0.1024	0.9612
AZ3	1.255	0.1286	0.9772
AZ4	0.805	0.0825	0.9519

Photocatalysts	Rate constant, k_1 (min^{-1}) x 10^{-2}	Rate (mg/L•min^{-1})	Correlation factors, R^2
AZ5	0.733	0.0751	0.9764
AZG1	0.654	0.0670	0.9454
AZG2	1.357	0.1390	0.9683
AZG3	0.794	0.0814	0.9300
AZG4	0.709	0.0727	0.9382

4.9 Effect of Different Parameters on the Kinetic of ACE in the Aqueous Phase

4.9.1 Photocatalysts Loading

Figure 4.22 showed the kinetics and rate constants of ACE degradation using AC-supported ZnO/g-C_3N_4 with different photocatalysts loadings. As a result, we found that, in our experimental setup, 0.10 g of photocatalyst loading is ideal for ACE degradation. 0.10 g of photocatalyst loading depicts the highest degradation efficiency compared to other photocatalyst loadings (0.15, 0.20, 0.25) g. Table 4.7 also showed the rate for 0.10 g photocatalyst was at 0.1391 mg/L•min^{-1}. However, as the loading increased to 0.15, 0.20 and 0.25 g, the rate of degradation was observed to reduce significantly to 0.0876, 0.0788 and 0.0077 mg/L•min^{-1}. The rate constants also presented that photocatalyst loading 0.10 g was the highest (1.357 min^{-1}) while 0.25 g photocatalyst loading has the lowest rate constant (0.075 min^{-1}) (Figure 4.22b). This was due to sufficient number of available active sites that cause ACE degradation at 0.10 g. However as loading increases, more composite photocatalyst particles agglomerate in the working solution, reducing its surface area and ability to absorb light, which slows down the rate of degradation (Aminuddin et al., 2021; F. Liu et al., 2019). The optimal photocatalyst loading is 0.10 g as the rate constant for was the highest among all loadings which is 1.357 min^{-1} (Figure 4.22b).

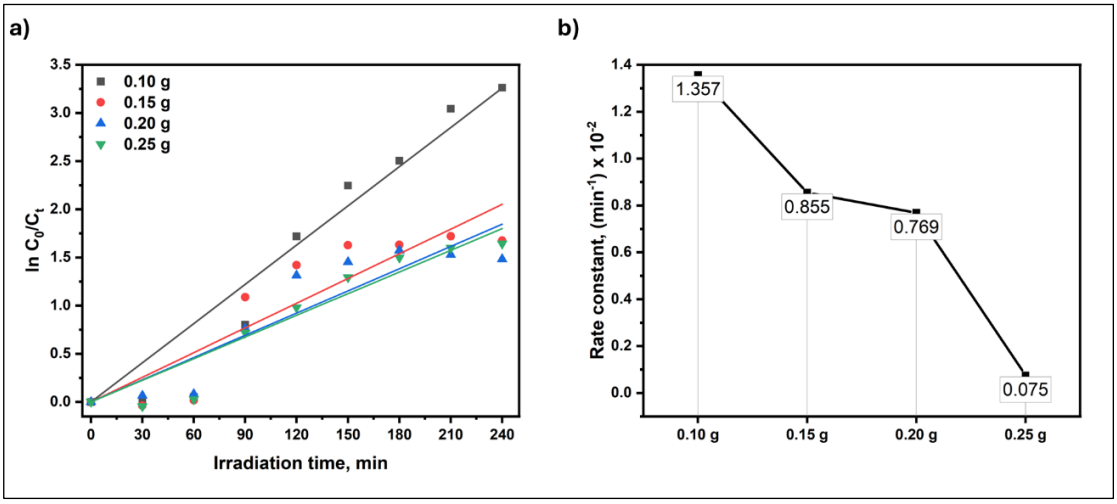

Figure 4.22 a) Kinetics of the Degradation of ACE and b) Rate Constants by AZ-Supported ZnO/g-C_3N_4 (AZG2) Composite Photocatalysts with Different Photocatalysts Loading. [ACE] = 10 mg/L, pH = 5.8, Loading = 0.1 – 0.25 g.

Table 4.7
Rate Constant, Rate, and Correlation Factors Values of AC-supported ZnO/g-C_3N_4 Composite Photocatalysts (AZG2) with Different Photocatalyst Loading. [ACE] = 10 mg/L, pH = 5.8, Loading = 0.1 – 0.25 g.

Photocatalysts loading, g	**Rate constant, k_1 (min^{-1}) x 10^{-2}**	**Rate (mg/L•min^{-1})**	**Correlation factors, R^2**
0.10	1.357	0.1391	0.9711
0.15	0.855	0.0876	0.9395
0.20	0.769	0.0788	0.9483
0.25	0.075	0.0077	0.9685

4.9.2 Initial Concentration

Figure 4.23 showed the rate of ACE degradation with respect to the effect of initial concentration of working concentration. Figure 4.22a showed that the 10 mg/L initial concentration has the highest efficiency in degrading ACE compared to other initial concentrations. The rate for the degradation of ACE with different initial concentrations shown quite high rate of 5 mg/L (1.162 mg/L•min^{-1}) and increased up to 1.357 mg/L•min^{-1} after the concentration was increased to 10 mg/L. However, 20 mg/L of initial concentration showed drastic reduction to 0.099 mg/L•min^{-1} and the same case

happened with 25 mg/L initial concentration of ACE. The rate constant obtained for 5, 10, 15 and 20 mg/L initial concentration of ACE were 0.9755, 0.9711, 0.9571 and 0.9855 min^{-1}. According to Figure 4.23, it can be said that as the concentration increased, the rate of reaction decreased. This demonstrated that the effectiveness of AC-supported ZnO/ composite photocatalysts have reduced in degrading higher concentration of ACE. As a result, the ideal starting concentration was determined to be 10 mg/L with rate constant of 1.306 min^{-1} (Figure 4.23b).

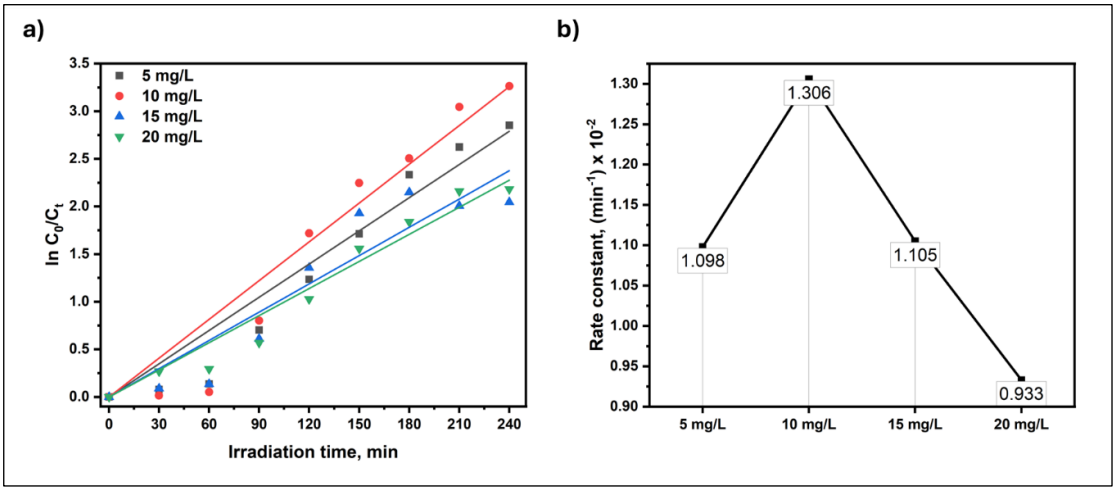

Figure 4.23 a) Kinetics of the Degradation of ACE and b) Rate Constants by AZ-Supported ZnO/g-C_3N_4 (AZG2) Composite Photocatalysts with Different ACE Initial Concentration. [ACE] = 5–10 mg/L, pH = 5.8, Mass = 0.1 g.

Table 4.8
Rate Constant, Rate, and Correlation Factors Values of AC-supported ZnO/g-C_3N_4 Composite Photocatalysts (AZG2) with Initial Concentration of ACE. [ACE] = 5 – 20 mg/L, pH = 6.8, Loading = 0.10 g

Initial concentration, mg/L	**Rate constant, k_1 (min^{-1}) x 10^{-2}**	**Rate (mg/L•min^{-1})**	**Correlation factors, R^2**
5	1.162	0.0593	0.9755
10	1.357	0.1391	0.9711
15	0.099	0.0148	0.9571
20	0.923	0.1846	0.9855

4.9.3 Initial pH

The degradation of the best ratio of AC-supported ZnO/g-C_3N_4 composite photocatalysts was further measured at different initial pH of working solutions ranging from 2-10 as illustrated in Figure 4.24. From the experimental results, the rate of ACE degradation was observed to be very high at pH 2 which indicates a rapid degradation rate (Figure 4.24). This implies that the photocatalytic activity is enhanced in an acidic environment, possibly as a result of increased ACE adsorption onto the positively charged photocatalyst surface. However, the rate reduced significantly at pH 4. This may be because as the pH approaches the pH_{zpc} of the photocatalyst, there is less electrostatic attraction. Yet the rate spiking up back at pH 6 showing an improved degradation rate which may be connected to the best photocatalyst performance around the pH_{zpc}, where charge separation and production of ROS are at their highest. Then the rate decreased gradually at pH 8 – 10. At these pH values, the negatively charged ACE molecules are probably repelled by the photocatalyst's negatively charged surface, which lowers adsorption and photocatalytic efficiency. Table 4.9 summarized the rate constant, rate, and correlation factors values of AC-supported ZnO/g-C_3N_4 composite photocatalysts.

Results in Figure 4.24 showed that pH has a major effect on photocatalytic performance by affecting the photocatalyst's surface charge and the availability of superoxide and hydroxyl radicals. Alkaline conditions (pH 8–10) decrease activity because of repulsion and reduced ROS formation, whereas acidic conditions (pH 2) maximise ACE degradation because of increased electrostatic attraction. A balance between charge interactions and catalytic efficiency is suggested by the intermediate spike at pH 6 which is the natural pH of ACE in aqueous phase.

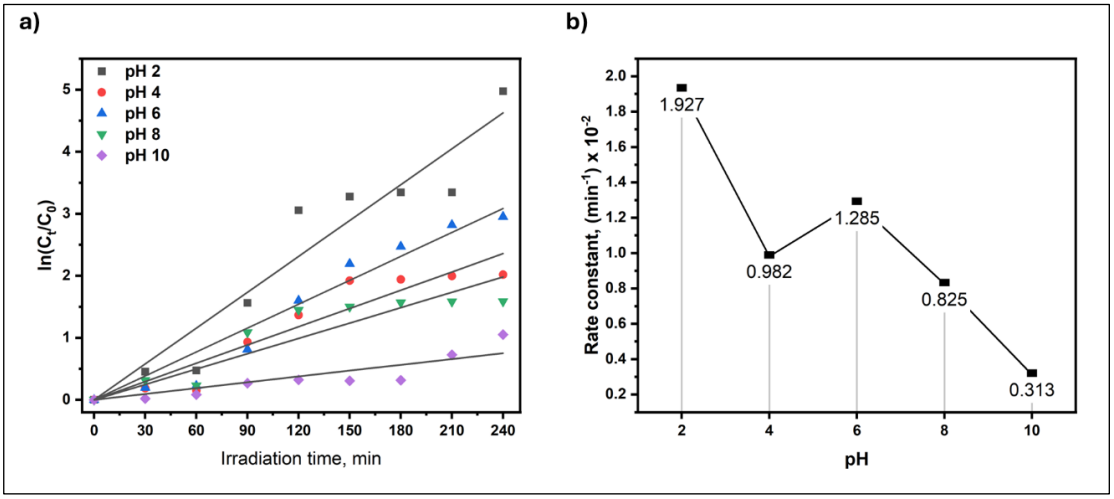

Figure 4.24 a) Kinetics of the Degradation of ACE and b) Rate Constants by AZ-Supported ZnO/g-C_3N_4 (AZG2) Composite Photocatalysts with Different Initial pH of ACE. [ACE] = 10 mg/L, pH = 2 – 10, Loading = 0.1 g.

Table 4.9
Rate Constant, Rate, and Correlation Factors Values of AC-Supported ZnO/g-C_3N_4 Composite Photocatalysts (AZG2) with Different Initial pH of ACE. [ACE] = 10 mg/L, pH = 2 – 10, Loading = 0.10 g

Initial pH of ACE	**Rate constant, k_1 (min^{-1}) x 10^{-2}**	**Rate (mg/L•min^{-1})**	**Correlation factors, R^2**
2	1.927	0.1975	0.9704
4	0.982	0.1007	0.9633
6	1.285	0.1317	0.9789
8	0.825	0.0845	0.9441
10	0.313	0.0321	0.8859

4.10 Recyclability of AC-supported ZnO/g-C_3N_4 Composite Photocatalysts

The stability and practicality of the potential AC-supported ZnO/g-C_3N_4 composite photocatalyst for a long-run was investigated. The AZG2 composite photocatalyst was collected and reused in the next cycle without any pre-treatment procedures between each cycle. Fresh ACE aqueous solution (10 mg/L) was added to the new cycle after earlier reaction cessation. Figure 4.25 depicts that the AZG2 composite could be used up to five cycles with more than 84% photodegradation

efficiency. The decrease in degradation efficiency could be due to the loss of samples during the recycling reaction. It can be concluded that the catalyst possesses high stability during the photocatalytic degradation of ACE under UVC irradiation and it could have the potential for practical water remediation process.

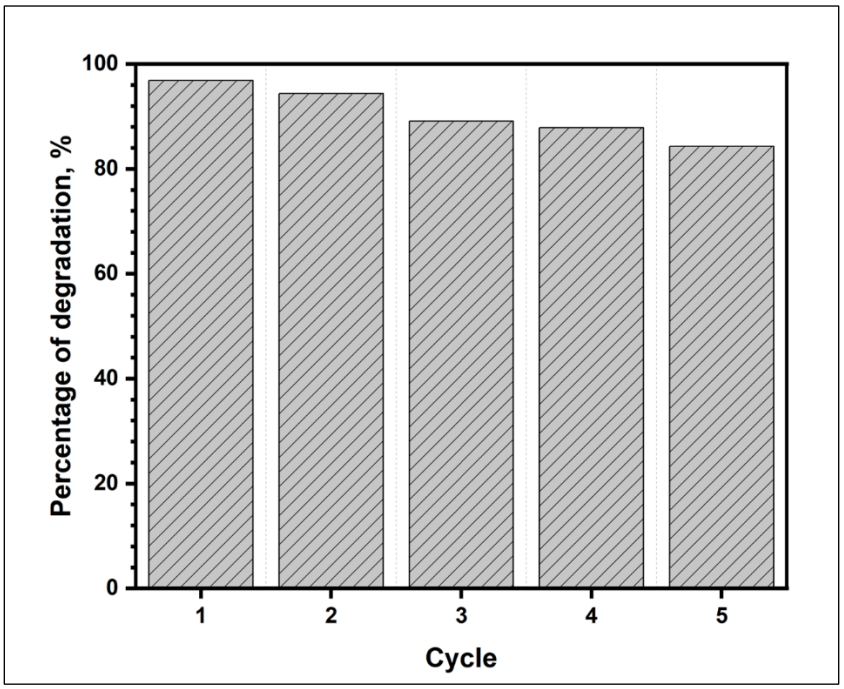

Figure 4.25 Recyclability of AZ-Supported ZnO/g-C_3N_4 (AZG2) Composite Photocatalysts Under Low Intensity UV Light Irradiation. [ACE] = 10 mg/L, pH = 6.8, Mass = 0.1 g.

CHAPTER 5
CONCLUSION

5.1 Conclusion

Through this study, two novel photocatalysts, AC-supported ZnO and AC-supported ZnO/g-C_3N_4, were successfully synthesised and characterised, indicating their potential for the photocatalytic degradation of ACE, a model organic pollutant. These materials were prepared using a methodical process that guaranteed excellent catalytic performance and reusability. The structural, morphological, and optical characteristics of the photocatalysts were validated using characterization methods such as X-ray diffraction (XRD) analysis, scanning electron microscopy (SEM) and field scanning electron microscopy (FESEM) equipped with Energy Dispersive X-ray (EDX), N_2 adsorption-desorption analysis and Brunauer–Emmett–Teller (BET) surface area, X-ray photoelectron spectroscopy (XPS), photoluminescence spectroscopy (PL) and UV-near infrared spectroscopy (UV-NIR). Kinetic study was also carried out on every parameter tested. A promising candidate for photocatalytic applications, the AC-ZnO composite's surface area, light absorption capacity, and charge separation efficiency were all greatly increased by the addition of g-C_3N_4. AZG2 was chosen as the best photocatalysts composite with percentage of degradation of 96.17% at under the optimal conditions of photocatalyst loading of 0.1 g, initial concentration of ACE of 10 mg/L and initial pH of 5.8.

ACE degradation optimal parameters were determined by evaluating the photocatalytic performance of AC-supported ZnO and AC-supported ZnO/g-C_3N_4 under different conditions such as photocatalyst loading, reusability, radical scavenger and initial concentration and initial pH of ACE. An ideal dosage is crucial for optimising degradation efficiency while preventing excessive material waste, according to the catalyst loading study. It was discovered that pH was important; the photocatalysts' surface characteristics promoted pollutant adsorption and improved interaction with reactive oxygen species, resulting in maximum activity under acidic conditions (pH 2). Higher pollutant levels reduced removal efficiency, probably as a result of fewer active sites and less reactive species production, according to the effect of initial ACE concentration. Scavenger studies verified that the primary reactive species in charge of

ACE degradation were superoxide and hydroxyl radicals (·OH). Furthermore, both photocatalysts demonstrated outstanding stability and reusability over several cycles with negligible efficiency loss, making them economical and environmentally friendly for real-world uses.

According to kinetic analysis, ACE degraded in accordance with a pseudo-first-order reaction model. In comparison to AC-supported ZnO, AC-supported ZnO/g-C_3N_4 showed noticeably higher rate constants, suggesting increased catalytic activity. The synergistic interaction between ZnO, AC, and g-C_3N_4 is responsible for the superior performance of AC-supported ZnO/g-C_3N_4. AC added adsorption support which immensely helped improving the degradation efficiency of the composite photocatalyst. On the other hand, the interaction between ZnO and g-C_3N_4 then enhanced charge transfer, expanded the number of active sites available, and encouraged pollutant adsorption. Because of these characteristics, AC-supported ZnO/g-C_3N_4 is the photocatalyst that performs the best in this investigation.

In summary, the results of this study show that effective, stable, and recyclable photocatalysts have been successfully developed for the degradation of ACE from aqueous environments. The findings highlight AC-supported ZnO/g-C_3N_4's potential as a cutting-edge material for environmental remediation, providing a balance between sustainability and high performance. Future research aimed at improving photocatalyst compositions and operating conditions to increase the degradation efficiency of different pollutants in practical applications will have a solid basis thanks to this work.

5.2 Recommendations

The study demonstrates that ZnO/g-C_3N_4 composite photocatalysts supported by AC can efficiently degrade endocrine-disrupting compound (EDC) pollutants, including ACE. By improving adsorption and photocatalytic efficiency, this combination solves important environmental issues. Future research is necessary to improve material properties, assess performance in practical settings, and gain a deeper understanding of the underlying photocatalytic mechanisms. The wider applicability and sustainability of these innovative photocatalysts will also be confirmed by broadening the scope to include other common pollutants that contribute to environmental contamination. Here are some suggestions for additional research:

a) Using alternative adsorbent and photocatalyst systems.

A synergistic effect can be achieved by combining other photocatalysts that are active in the presence of UV or visible light with adsorbents like agricultural waste, chitosan, zeolite, porous materials, and other carbonaceous compounds. Combining highly effective adsorbents like chitosan, zeolite, agricultural waste, porous materials, or other carbonaceous compounds with photocatalysts that are active under UV or visible light can have a synergistic effect. By utilising the advantages of both materials, this combination optimises the removal of EDC pollutants. While the photocatalysts aid in the pollutants' breakdown when exposed to light, the adsorbents quickly bind and concentrate the pollutants on their surface. By accelerating the removal of pollutants, this complementary action improves efficiency and shortens the time needed for water treatment procedures. This strategy is appropriate for extensive environmental remediation applications since it also adheres to eco-friendly standards by using sustainable adsorbents, such as agricultural waste.

b) Photodegradation of other organic and inorganic compounds.

To assess the photocatalytic activity and efficacy of AC-supported ZnO/g-C_3N_4 composite photocatalysts, other EDCs that are frequently present in wastewater, such as triclosan, phthalates, bisphenol A, and different pharmaceutical products, could be used as extra test pollutants. Examining these substances would give a thorough grasp of the photocatalyst's potential for wider wastewater treatment applications. These studies would also help evaluate its adaptability, compare its performance to that of other photocatalysts, and guarantee that it can be used in real-world situations involving a variety of persistent contaminants in municipal and industrial wastewater streams.

c) Photocatalyst optimisation measures.

Several operational parameters can be adjusted to improve the photocatalyst's performance by using response surface methodology (RSM) and optimisation techniques. This thorough development procedure guarantees that, under particular circumstances, the photocatalyst will operate at its highest efficiency. After being

refined, the photocatalyst can be used directly in industrial water treatment procedures, providing an efficient and environmentally friendly way to get rid of pollutants. This method ensures that the produced photocatalyst satisfies industrial requirements for versatility, effectiveness, and environmental compatibility by bridging laboratory-scale research with real-world applications.

d) Study the degradation activity on real wastewater.

The photodegradation of real wastewater can be carried out especially from hospital or pharmaceutical industry which contained several pharmaceutical residues. Since hospitals and pharmaceutical industries frequently contain persistent pharmaceutical residues like ACE and antibiotics, the AC-supported ZnO/g-C_3N_4 photocatalyst exhibits great promise for treating actual wastewater. These pollutants can be effectively degraded into less hazardous byproducts thanks to its large surface area, effective charge separation, and increased production of ROS. Because of this, it is perfect for solving complex effluent problems where traditional treatment techniques are insufficient. Furthermore, the photocatalyst's recyclability lends credence to its viability for extensive use, providing an economical and sustainable means of reducing pharmaceutical pollution in practical settings.

REFERENCES

Aarab, N., Hsini, A., Essekri, A., Laabd, M., Lakhmiri, R., & Albourine, A. (2020). Removal of an emerging pharmaceutical pollutant (metronidazole) using PPY-PANi copolymer: Kinetics, equilibrium and DFT identification of adsorption mechanism. *Groundwater for Sustainable Development*, *11*, 100416. https://doi.org/10.1016/j.gsd.2020.100416

Ahmad, I., Bousbih, R., Mahal, A., Khan, W. Q., Aljohani, M., Amin, M. A., Jafar, N. N. A., Jabir, M. S., Majdi, H., Alshomrany, A. S., Shaban, M., Ali, I., & Bayahia, H. (2024). Recent progress in ZnO-based heterostructured photocatalysts: A review. *Materials Science in Semiconductor Processing*, *180*(January). https://doi.org/10.1016/j.mssp.2024.108578

Ajiboye, T. O., Oyewo, O. A., & Onwudiwe, D. C. (2021). Adsorption and photocatalytic removal of Rhodamine B from wastewater using carbon-based materials. *FlatChem*, *29*(June). https://doi.org/10.1016/j.flatc.2021.100277

Akhundi, A., Habibi-Yangjeh, A., Abitorabi, M., & Rahim Pouran, S. (2019). Review on photocatalytic conversion of carbon dioxide to value-added compounds and renewable fuels by graphitic carbon nitride-based photocatalysts. *Catalysis Reviews - Science and Engineering*, *61*(4), 595–628. https://doi.org/10.1080/01614940.2019.1654224

Akir, S., Hamdi, A., Addad, A., Coffinier, Y., Boukherroub, R., & Dakhlaoui Omrani, A. (2017). Facile synthesis of carbon-ZnO nanocomposite with enhanced visible light photocatalytic performance. *Applied Surface Science*, *400*, 461–470. https://doi.org/10.1016/j.apsusc.2016.12.212

Ameta, R., Solanki, M. S., Benjamin, S., & Ameta, S. C. (2018). *Photocatalysis*. https://doi.org/10.1016/B978-0-12-810499-6.00006-1

Ameta, S. C. (2018). *Advanced oxidation processes for wastewater treatment; introduction*. 1–12. https://doi.org/10.1016/B978-0-12-810499-6.00001-2

Aminuddin, N. F., Nawi, M. A., Bahrudin, N. N., & Jawad, A. H. (2021). Iron ion assisted photocatalytic-adsorptive removal of acid orange 52 by immobilized TiO2/polyaniline bilayer photocatalyst. *Applied Surface Science Advances*, *6*(August), 100180. https://doi.org/10.1016/j.apsadv.2021.100180

Amornpitoksuk, P., Suwanboon, S., & Randorn, C. (2018). Photocatalytic activities of silver compound modified activated carbon@ZnO: Novel ternary composite

visible light-driven photocatalysts. *Materials Science in Semiconductor Processing*, *84*(May), 50–57. https://doi.org/10.1016/j.mssp.2018.05.005

An, T., An, J., Yang, H., Li, G., Feng, H., & Nie, X. (2011). Photocatalytic degradation kinetics and mechanism of antivirus drug-lamivudine in TiO 2 dispersion. *Journal of Hazardous Materials*, *197*, 229–236. https://doi.org/10.1016/j.jhazmat.2011.09.077

Asadzadeh-Khaneghah, S., & Habibi-Yangjeh, A. (2020). g-C3N4/carbon dot-based nanocomposites serve as efficacious photocatalysts for environmental purification and energy generation: A review. *Journal of Cleaner Production*, *276*, 124319. https://doi.org/10.1016/j.jclepro.2020.124319

Ayoub, H., Roques-carmes, T., Potier, O., Koubaissy, B., & Pontvianne, S. (2018). *Iron-impregnated zeolite catalyst for efficient removal of micropollutants at very low concentration from Meurthe river*.

Ayu, D. G., Gea, S., Telaumbanua, D. J., Fazlur, A., Piliang, R., Harahap, M., Yen, Z., Goei, R., Iing, A., & Tok, Y. (2023). *Photocatalytic Degradation of Methylene Blue Using N - Doped ZnO / Carbon Dot (N-ZnO / CD) Nanocomposites Derived from Organic Soybean*. https://doi.org/10.1021/acsomega.2c07546

Bahrami, M., & Nezamzadeh-Ejhieh, A. (2015). Effect of the supported ZnO on clinoptilolite nano-particles in the photodecolorization of semi-real sample bromothymol blue aqueous solution. *Materials Science in Semiconductor Processing*, *30*, 275–284. https://doi.org/10.1016/j.mssp.2014.10.006

Basheer, A. A. (2018). Chemical chiral pollution: Impact on the society and science and need of the regulations in the 21st century. *Chirality*, *30*(4), 402–406. https://doi.org/10.1002/chir.22808

Behravesh, S., Mirghaffari, N., Alemrajabi, A. A., Davar, F., & Soleimani, M. (2020). Photocatalytic degradation of acetaminophen and codeine medicines using a novel zeolite-supported TiO2 and ZnO under UV and sunlight irradiation. *Environmental Science and Pollution Research*, *27*(21), 26929–26942. https://doi.org/10.1007/s11356-020-09038-y

Biswas, U., Kanti, T., Islam, T., Rani, P., & Idris, A. M. (2025). *International Journal of Biological Macromolecules Role of humic acid for climate change adaptation measures to boost up sustainable agriculture and soil health : A potential review*. *313*(April).

Bozetine, H., Meziane, S., Aziri, S., Berkane, N., Allam, D., Boudinar, S., & Hadjersi,

T. (2021). Facile and green synthesis of a ZnO / CQDs / AgNPs ternary heterostructure photocatalyst : study of the methylene blue dye photodegradation. *Bulletin of Materials Science*, *0123456789*. https://doi.org/10.1007/s12034-021-02353-1

Branco, G. S., Melo, A. G., Ricci, J. M. B., Digmayer, M., de Jesus, L. W. O., Habibi, H. R., & Nóbrega, R. H. (2019). Effects of GnRH and the dual regulatory actions of GnIH in the pituitary explants and brain slices of Astyanax altiparanae males. *General and Comparative Endocrinology*, *273*(February 2018), 209–217. https://doi.org/10.1016/j.ygcen.2018.08.006

Branco, G. S., Moreira, R. G., Borella, M. I., Camargo, M. de P., Muñoz-Peñuela, M., Gomes, A. D. O., & Tolussi, C. E. (2021). Nonsteroidal anti-inflammatory drugs act as endocrine disruptors in Astyanax lacustris (Teleostei: Characidae) reproduction: An ex vivo approach. *Aquatic Toxicology*, *232*(September 2020). https://doi.org/10.1016/j.aquatox.2021.105767

Brillas, E., & Manuel Peralta-Hernández, J. (2023). Removal of paracetamol (acetaminophen) by photocatalysis and photoelectrocatalysis. A critical review. *Separation and Purification Technology*, *309*(November 2022). https://doi.org/10.1016/j.seppur.2022.122982

Carofiglio, M., Barui, S., Cauda, V., & Laurenti, M. (2020). *Doped Zinc Oxide Nanoparticles : Synthesis , Characterization and Potential Use in Nanomedicine*.

Chai, B., Yan, J., Fan, G., Song, G., & Wang, C. (2020). In situ fabrication of CdMoO4/g-C3N4 composites with improved charge separation and photocatalytic activity under visible light irradiation. *Chinese Journal of Catalysis*, *41*(1), 170–179. https://doi.org/10.1016/S1872-2067(19)63383-8

Chauhan, P. S., Kant, R., Rai, A., Gupta, A., & Bhattacharya, S. (2019). Facile synthesis of ZnO/GO nanoflowers over Si substrate for improved photocatalytic decolorization of MB dye and industrial wastewater under solar irradiation. *Materials Science in Semiconductor Processing*, *89*(August 2018), 6–17. https://doi.org/10.1016/j.mssp.2018.08.022

Chegeni, M., Mousavi, Z., Soleymani, M., & Dehdashtian, S. (2020). Removal of aspirin from aqueous solutions using graphitic carbon nitride nanosheet: Theoretical and experimental studies. *Diamond and Related Materials*, *101*(October 2019), 107621. https://doi.org/10.1016/j.diamond.2019.107621

Chen, D., Cheng, Y., Zhou, N., Chen, P., Wang, Y., Li, K., Huo, S., Cheng, P., Peng,

P., Zhang, R., Wang, L., Liu, H., Liu, Y., & Ruan, R. (2020). *Photocatalytic degradation of organic pollutants using TiO 2 -based photocatalysts : A review*. *268*.

Chijioke-Okere, M., Abdullah, A. H., Mohd Hir, Z. A., Alinnor, J. I., & Oguzie, E. E. (2023). Efficient photodegradation of paracetamol by integrated PES-ZnO photocatalyst sheets. *Inorganic Chemistry Communications*, *148*(December 2022), 110377. https://doi.org/10.1016/j.inoche.2022.110377

Chopan, N. A., & Chishti, H. T. N. (2023). Polypyrrole-decorated ZnO/g-C3N4 S-scheme photocatalyst for rhodamine B dye degradation: Mechanism and antibacterial activity. *Materials Today Chemistry*, *32*. https://doi.org/10.1016/j.mtchem.2023.101643

Chubenko, E., Gerasimenko, I., Bondarenko, V., & Zhigulin, D. (2019). Zinc Oxide Nanostructures Doped with Transition Metals: Fabrication and Properties. *International Journal of Nanoscience*, *18*(3–4), 1–4. https://doi.org/10.1142/S0219581X19400453

Das, A., Adak, M. K., Mahata, N., & Biswas, B. (2021). Wastewater treatment with the advent of TiO 2 endowed photocatalysts and their reaction kinetics with scavenger effect. *Journal of Molecular Liquids*, *338*(May), 116479. https://doi.org/10.1016/j.molliq.2021.116479

de Moraes, N. P., dos Santos, G. S., Neves, G. C., Valim, R. B., da Silva Rocha, R., Landers, R., Caetano Pinto da Silva, M. L., & Rodrigues, L. A. (2020). Development of Nb2O5-doped ZnO/Carbon xerogel photocatalyst for the photodegradation of 4-chlorophenol. *Optik*, *219*(July), 165238. https://doi.org/10.1016/j.ijleo.2020.165238

Di, G., Zhu, Z., Dai, Q., Zhang, H., Shen, X., & Qiu, Y. (2020). *Wavelength-dependent effects of carbon quantum dots on the photocatalytic activity of g-C 3 N 4 enabled by LEDs*. *379*(May 2019).

dos Santos, A. J., Kronka, M. S., Fortunato, G. V., & Lanza, M. R. V. (2021). Recent advances in electrochemical water technologies for the treatment of antibiotics: A short review. *Current Opinion in Electrochemistry*, *26*. https://doi.org/10.1016/j.coelec.2020.100674

Elhalil, A., Elmoubarki, R., Farnane, M., Machrouhi, A., Sadiq, M., Mahjoubi, F. Z., Qourzal, S., & Barka, N. (2018). Photocatalytic degradation of caffeine as a model pharmaceutical pollutant on Mg doped ZnO-Al2O3 heterostructure.

Environmental Nanotechnology, Monitoring and Management, *10*(October 2017), 63–72. https://doi.org/10.1016/j.enmm.2018.02.002

Fei, W., Song, Y., Li, N., Chen, D., Xu, Q., Li, H., He, J., & Lu, J. (2019). Fabrication of visible-light-active ZnO/ZnFe-LDH heterojunction on Ni foam for pollutants removal with enhanced photoelectrocatalytic performance. *Solar Energy*, *188*(May), 593–602. https://doi.org/10.1016/j.solener.2019.06.037

Feng, Xianyong, Wang, P., Hou, J., Qian, J., Wang, C., & Ao, Y. (2018). Oxygen vacancies and phosphorus codoped black titania coated carbon nanotube composite photocatalyst with efficient photocatalytic performance for the degradation of acetaminophen under visible light irradiation. *Chemical Engineering Journal*, *352*(June), 947–956. https://doi.org/10.1016/j.cej.2018.06.037

Feng, Xiangbo, Zhu, J., Song, K., Zeng, J., Zhou, X., Guo, X., Lin, K., Cuihong Zhang, Xie, C., & Shi, J. W. (2024). Insight into the reasons for enhanced NH3-SCR activity and SO2 tolerance of Mn-Co layered oxides. *Separation and Purification Technology*, *336*(December 2023). https://doi.org/10.1016/j.seppur.2024.126285

Fu, J., Yu, J., Jiang, C., & Cheng, B. (2018). g-C3N4-Based Heterostructured Photocatalysts. *Advanced Energy Materials*, *8*(3), 1–31. https://doi.org/10.1002/aenm.201701503

Gao, W., Zhang, S., Wang, G., Cui, J., Lu, Y., Rong, X., & Gao, C. (2022). A review on mechanism, applications and influencing factors of carbon quantum dots based photocatalysis. *Ceramics International*, *48*(24), 35986–35999. https://doi.org/10.1016/j.ceramint.2022.10.116

Garg, R., Gupta, R., & Bansal, A. (2021). Synthesis of g-C3N4/ZnO nanocomposite for photocatalytic degradation of a refractory organic endocrine disrupter. *Materials Today: Proceedings*, *44*, 855–859. https://doi.org/10.1016/j.matpr.2020.10.787

Girija Shankar, E., Aishwarya, M., Khan, A., Kumar, A. B. V. K., & Yu, J. S. (2021). Efficient solar light photocatalytic degradation of commercial pharmaceutical drug and dye using rGO-PANI assisted c-ZnO heterojunction nanocomposites. *Ceramics International*, *47*(17), 23770–23780. https://doi.org/10.1016/j.ceramint.2021.03.206

Groeneveld, I., Kanelli, M., Ariese, F., & van Bommel, M. R. (2023). Parameters that

affect the photodegradation of dyes and pigments in solution and on substrate – An overview. *Dyes and Pigments*, *210*(November 2022). https://doi.org/10.1016/j.dyepig.2022.110999

Gunnarsson, L., Snape, J. R., Verbruggen, B., Owen, S. F., Kristiansson, E., Margiotta-Casaluci, L., Österlund, T., Hutchinson, K., Leverett, D., Marks, B., & Tyler, C. R. (2019). Pharmacology beyond the patient – The environmental risks of human drugs. *Environment International*, *129*(May), 320–332. https://doi.org/10.1016/j.envint.2019.04.075

Guo, Y., Ao, Y., Wang, P., & Wang, C. (2019). Photocatalysts With Enhanced Visible-Light-Driven Performance Towards Carbamazepine Degradation. *Applied Catalysis B: Environmental*, *254*(February), 479–490.

Guo, Y., Wang, P., Qian, J., Hou, J., Ao, Y., & Wang, C. (2018). Construction of a composite photocatalyst with significantly enhanced photocatalytic performance through combination of homo-junction with hetero-junction. *Catalysis Science and Technology*, *8*(2), 486–498. https://doi.org/10.1039/c7cy02027a

Gusain, R., Gupta, K., Joshi, P., & Khatri, O. P. (2019). Adsorptive removal and photocatalytic degradation of organic pollutants using metal oxides and their composites: A comprehensive review. *Advances in Colloid and Interface Science*, *272*. https://doi.org/10.1016/j.cis.2019.102009

Haibo, O., Feng, H. J., Cuiyan, L., Liyun, C., & Jie, F. (2013). Synthesis of carbon doped ZnO with a porous structure and its solar-light photocatalytic properties. *Materials Letters*, *111*, 217–220. https://doi.org/10.1016/j.matlet.2013.08.081

Hemavibool, K., Sansenya, T., & Nanan, S. (2022). Enhanced Photocatalytic Degradation of Tetracycline and Oxytetracycline Antibiotics by BiVO4 Photocatalyst under Visible Light and Solar Light Irradiation. *Antibiotics*, *11*(6), 761. https://doi.org/10.3390/antibiotics11060761

Hir, Z. A. M., Alam, N. M. F. H. N. B., Shaari, A. So., & Rafaie, H. A. (2022). One-Pot Sol-Gel Synthesis of a Zinc Oxide-Reduced Graphene Oxide Composite: Photocatalysis and Kinetics Studies using a Fuzzy Inference System. *Malaysian Journal of Chemistry*, *24*(2), 37–46.

Hir, Z. A. M., Nik Badrul Alam, N. M. F. H., Shaari, A. S., & Rafaie, H. A. (2022). One-Pot Sol-Gel Synthesis of a Zinc Oxide-Reduced Graphene Oxide Composite: Photocatalysis and Kinetics Studies using a Fuzzy Inference System. *Malaysian Journal of Chemistry*, *24*(2), 37–46.

https://doi.org/10.55373/mjchem.v24i2.46

Hojamberdiev, M., Czech, B., Göktaş, A. C., Yubuta, K., & Kadirova, Z. C. (2020). SnO2@ZnS photocatalyst with enhanced photocatalytic activity for the degradation of selected pharmaceuticals and personal care products in model wastewater. *Journal of Alloys and Compounds*, *827*. https://doi.org/10.1016/j.jallcom.2020.154339

Hu, X. Y., Fan, J., Zhang, K. L., & Wang, J. J. (2012). Photocatalytic removal of organic pollutants in aqueous solution by Bi4NbxTa(1-x)O8I. *Chemosphere*, *87*(10), 1155–1160. https://doi.org/10.1016/j.chemosphere.2012.02.023

Hung, C. H., Chiang, P. C., Yuan, C., & Chou, C. Y. (2001). Photocatalytic degradation of azo dye in TiO2 suspended solution. *Water Science and Technology*, *43*(2), 313–320. https://doi.org/10.2166/wst.2001.0105

Ibhadon, A., & Fitzpatrick, P. (2013). Heterogeneous Photocatalysis: Recent Advances and Applications. *Catalysts*, *3*(1), 189–218. https://doi.org/10.3390/catal3010189

Inagaki, M., Tsumura, T., Kinumoto, T., & Toyoda, M. (2019). Graphitic carbon nitrides (g-C3N4) with comparative discussion to carbon materials. *Carbon*, *141*, 580–607. https://doi.org/10.1016/j.carbon.2018.09.082

Ismael, M. (2020a). The photocatalytic performance of the ZnO/g-C3N4 composite photocatalyst toward degradation of organic pollutants and its inactivity toward hydrogen evolution: The influence of light irradiation and charge transfer. *Chemical Physics Letters*, *739*(November 2019). https://doi.org/10.1016/j.cplett.2019.136992

Ismael, M. (2020b). The photocatalytic performance of the ZnO/g-C3N4 composite photocatalyst toward degradation of organic pollutants and its inactivity toward hydrogen evolution: The influence of light irradiation and charge transfer. *Chemical Physics Letters*, *739*, 136992. https://doi.org/10.1016/j.cplett.2019.136992

Jacques, C. V. (2017). Heterogeneous Catalysis on Metal Oxides. *Catalysts 7*. https://doi.org/10.3390/catal7110341

Ji, M., Liu, Y., Di, J., Chen, R., Chen, Z., Xia, J., & Li, H. (2018). *N-CQDs accelerating surface charge transfer of Bi 4 O 5 I 2 hollow nanotubes with broad spectrum photocatalytic activity*. *237*(June), 1033–1043.

Jiang, Y., Xi, H., Li, L., Wang, Z., & Yang, C. (2023). Mechanism of action of the

heterojunction structure of the photocatalyst ZnO-g-C3N4@TiO2 and its application to the degradation of acetaminophen. *Journal of Photochemistry and Photobiology A: Chemistry*, *445*(July). https://doi.org/10.1016/j.jphotochem.2023.115010

Kanakaraju, D., Glass, B. D., & Oelgemöller, M. (2018). Advanced oxidation process-mediated removal of pharmaceuticals from water: A review. *Journal of Environmental Management*, *219*, 189–207. https://doi.org/10.1016/j.jenvman.2018.04.103

Katiyar, J., & Saharan, V. K. (2023). Enhanced photocatalytic degradation of reactive blue 21 dye and textile dyeing effluent by synthesized SmFeO3-rGO photocatalyst in combination with ultrasonication: Characterization and performance evaluation. *Journal of Water Process Engineering*, *56*(June). https://doi.org/10.1016/j.jwpe.2023.104314

Khezami, L., Bessadok, A., Ali, M., Aissa, B., Ahmed, A. H., Modwi, A., Benhamadi, N., & Amine, A. (2024). *Revolutionizing dye removal : g-C 3 N 4 -Modified ZnO nanocomposite for exceptional adsorption of basic fuchsin dye*. *164*(January).

Kim, S., Kim, S., & Lee, S. (2023). Activated carbon modified with polyethyleneimine and MgO: Better adsorption of aldehyde and production of regenerative VOC adsorbent using a photocatalyst. *Applied Surface Science*, *631*(March), 157565. https://doi.org/10.1016/j.apsusc.2023.157565

Kodom, K., Attiogbe, F., & Kuranchie, F. A. (2021). Assessment of removal efficiency of pharmaceutical products from wastewater in sewage treatment plants: A case of the sewerage systems Ghana limited, Accra. *Heliyon*, *7*(11), e08385. https://doi.org/10.1016/j.heliyon.2021.e08385

Krishnakumar, B., Alsalme, A., Alharthi, F. A., Mani, D., Anandan, K., Amutha, P., & Sobral, A. J. F. N. (2021). Synthesis , characterization of gelatin assisted ZnO and its effective utilization of toxic azo dye degradation under direct sunlight. *Optical Materials*, *113*(January), 110854. https://doi.org/10.1016/j.optmat.2021.110854

Kumar, A., Kumar, A., Sharma, G., Al-Muhtaseb, A. H., Naushad, M., Ghfar, A. A., & Stadler, F. J. (2018). Quaternary magnetic BiOCl/g-C3N4/Cu2O/Fe3O4 nano-junction for visible light and solar powered degradation of sulfamethoxazole from aqueous environment. *Chemical Engineering Journal*, *334*(October 2017), 462–478. https://doi.org/10.1016/j.cej.2017.10.049

Kumar, R., Singh, K., Kumar, P., & Kaur, A. (2023). *Highly porous activated carbon prepared from the bio-waste of yellow mustard seed for high-capacity supercapacitor applications*. *304*(February), 1–9.

Kumar, Suneel, Dhiman, A., Sudhagar, P., & Krishnan, V. (2018). ZnO-graphene quantum dots heterojunctions for natural sunlight-driven photocatalytic environmental remediation. *Applied Surface Science*, *447*, 802–815. https://doi.org/10.1016/j.apsusc.2018.04.045

Kumar, Sushant, Singh, P. K., Deep, V., Singh, A., Strza, K., Singh, D., Yahya, M. Z. A., Savilov, S. V, Singh, P., & Singh, M. K. (2023). *In-situ N / O-heteroatom enriched micro- / mesoporous activated carbon derived from natural waste honeycomb and paper wasp hive and its application in quasi-solid-state supercapacitor*. *72*(August).

Latha, P., Prakash, K., & Karuthapandian, S. (2017). Enhanced visible light photocatalytic activity of CeO 2 /alumina nanocomposite: Synthesized via facile mixing-calcination method for dye degradation. *Advanced Powder Technology*, *28*(11), 2903–2913. https://doi.org/10.1016/j.apt.2017.08.017

Lauretta, R., Sansone, A., Sansone, M., Romanelli, F., & Appetecchia, M. (2019). Endocrine disrupting chemicals: Effects on endocrine glands. *Frontiers in Endocrinology*, *10*(March), 1–7. https://doi.org/10.3389/fendo.2019.00178

Leng, L., Wei, L., Xiong, Q., Xu, S., Li, W., Lv, S., Lu, Q., Wan, L., Wen, Z., & Zhou, W. (2020). Use of microalgae based technology for the removal of antibiotics from wastewater: A review. *Chemosphere*, *238*. https://doi.org/10.1016/j.chemosphere.2019.124680

Li, H., Ding, J., Cai, S., Zhang, W., Zhang, X., Wu, T., Wang, C., Foss, M., & Yang, R. (2022). *Plasmon-enhanced photocatalytic properties of Au / ZnO nanowires*. *583*(October 2021).

Li, Jiade, Fang, W., Yu, C., Zhou, W., Zhu, L., & Xie, Y. (2015). Ag-based semiconductor photocatalysts in environmental purification. *Applied Surface Science*, *358*, 46–56. https://doi.org/10.1016/j.apsusc.2015.07.139

Li, Jianxin, Wang, Y., Wang, Y., Guo, Y., Zhang, S., Song, H., Li, X., Gao, Q., Shang, W., Hu, S., Zheng, H., & Li, X. (2023). *Nano Materials Science MXene Ti 3 C 2 decorated g-C 3 N 4 / ZnO photocatalysts with improved photocatalytic performance for CO 2 reduction*. *5*(December 2022), 237–245.

Li, K., Chen, J., Ao, Y., & Wang, P. (2021). Preparation of a ternary g-C3N4-

CdS/Bi4O5I2 composite photocatalysts with two charge transfer pathways for efficient degradation of acetaminophen under visible light irradiation. *Separation and Purification Technology*, *259*(August 2020). https://doi.org/10.1016/j.seppur.2020.118177

Li, L., Sun, S. Q., Wang, Y. X., & Wang, C. Y. (2018). Facile synthesis of ZnO/g-C3N4 composites with honeycomb-like structure by H2 bubble templates and their enhanced visible light photocatalytic performance. *Journal of Photochemistry and Photobiology A: Chemistry*, *355*, 16–24. https://doi.org/10.1016/j.jphotochem.2017.12.016

Li, S., Ezugwu, C. I., Zhang, S., Xiong, Y., & Liu, S. (2019). Co-doped MgAl-LDHs nanosheets supported Au nanoparticles for complete catalytic oxidation of HCHO at room temperature. *Applied Surface Science*, *487*(May), 260–271. https://doi.org/10.1016/j.apsusc.2019.05.083

Li, X., Zhang, L., Yang, Z., Wang, P., Yan, Y., & Ran, J. (2020). Adsorption materials for volatile organic compounds (VOCs) and the key factors for VOCs adsorption process: A review. *Separation and Purification Technology*, *235*, 116213. https://doi.org/10.1016/j.seppur.2019.116213

Lia, J., Wang, Y., Li, X., Gao, Q., & Zhang, S. (2021). A facile synthesis of high-crystalline g-C3N4 nanosheets with closed self-assembly strategy for enhanced photocatalytic H2 evolution. *Journal of Alloys and Compounds*, *881*(SPEC. ISS.), 1–9. https://doi.org/10.1016/j.jallcom.2005.05.002

Liu, B., Wang, J., Sun, H., Wu, Z., Yao, C., Liao, Q., Wei, Z., Yang, W., Zhang, X., Meng, H., Woo, H. Y., & Guo, X. (2020). A Terpolymer Acceptor Enabling All-Polymer Solar Cells with a Broad Donor:Acceptor Composition Tolerance and Enhanced Stability. *Solar RRL*. https://doi.org/10.1002/solr.202000436

Liu, F., Nguyen, T. P., Wang, Q., Massuyeau, F., Dan, Y., & Jiang, L. (2019). Construction of Z-scheme g-C3N4/Ag/P3HT heterojunction for enhanced visible-light photocatalytic degradation of tetracycline (TC) and methyl orange (MO). *Applied Surface Science*, *496*(August), 143653. https://doi.org/10.1016/j.apsusc.2019.143653

Liu, J., Gao, Y., Zhang, Z., Dang, R., El Houda Tiri, R. N., MuhammedBekmezci, Bayat, R., Darabi, R., & Sen, F. (2023). Photocatalytic activity of TiO2-ZnO/g-C3N4 nanocomposites for methylene orange and Rhodamine B dyes removal from water and photocatalytic hydrogen generation. *Chemosphere*, *339*(March).

https://doi.org/10.1016/j.chemosphere.2023.139426

Loaiza-ambuludi, S., Panizza, M., Oturan, N., & Oturan, M. A. (2014). *Removal of the anti-inflammatory drug ibuprofen from water using homogeneous photocatalysis*. *224*, 29–33.

Loke, J. Y., Mohd Zaki, R. S., & Setiabudi, H. D. (2022). Photocatalytic degradation of methylene blue using ZnO supported on wood waste-derived activated carbon (ZnO/AC). *Materials Today: Proceedings*, *57*, 1315–1321. https://doi.org/10.1016/j.matpr.2021.12.535

Low, J., Yu, J., Jaroniec, M., Wageh, S., & Al-Ghamdi, A. A. (2017). Heterojunction Photocatalysts. *Advanced Materials*, *29*(20), 1–20. https://doi.org/10.1002/adma.201601694

Lu, L., Lv, Z., Si, Y., Liu, M., & Zhang, S. (2018). Recent progress on band and surface engineering of graphitic carbon nitride for artificial photosynthesis. *Applied Surface Science*, *462*, 693–712. https://doi.org/10.1016/j.apsusc.2018.08.131

Luu Thi, L. A., Neto, M. M., Van, T. P., Nguyen Ngoc, T., Nguyen Thi, T. M., Nguyen, X. S., & Nguyen, C. T. (2021). In Situ g-C3N4@Zno Nanocomposite: One-Pot Hydrothermal Synthesis and Photocatalytic Performance under Visible Light Irradiation. *Advances in Materials Science and Engineering*, *2021*, 17–20. https://doi.org/10.1155/2021/6651633

Mandade, P. (2021). Introduction, basic principles, mechanism, and challenges of photocatalysis. *Handbook of Nanomaterials for Wastewater Treatment: Fundamentals and Scale up Issues*, 137–154. https://doi.org/10.1016/B978-0-12-821496-1.00016-7

Mao, J., Chen, M., Deng, Y., Liu, H., Ju, Z., Xing, Z., & Cao, X. (2019). Synthesis of uniform silica nanospheres wrapped in nitrogen-doped carbon nanosheets with stable lithium-ion storage properties. *Journal of Materials Science*, *54*(19), 12767–12781. https://doi.org/10.1007/s10853-019-03812-1

Mariana, M., S, A. K. H. P., Mistar, E. M., Bashir, E., Alfatah, T., Danish, M., & Amayreh, M. (2021). Journal of Water Process Engineering Recent advances in activated carbon modification techniques for enhanced heavy metal adsorption. *Journal of Water Process Engineering*, *43*(June), 102221. https://doi.org/10.1016/j.jwpe.2021.102221

Maryam, B., Buscio, V., Odabasi, S. U., & Buyukgungor, H. (2020). A study on

behavior, interaction and rejection of Paracetamol, Diclofenac and Ibuprofen (PhACs) from wastewater by nanofiltration membranes. *Environmental Technology and Innovation*, *18*. https://doi.org/10.1016/j.eti.2020.100641

Mashayekh-Salehi, A., Moussavi, G., & Yaghmaeian, K. (2017). Preparation, characterization and catalytic activity of a novel mesoporous nanocrystalline MgO nanoparticle for ozonation of acetaminophen as an emerging water contaminant. *Chemical Engineering Journal*, *310*, 157–169. https://doi.org/10.1016/j.cej.2016.10.096

Mashuri, S. I. S., Ibrahim, M. L., Kasim, M. F., Mastuli, M. S., Rashid, U., Abdullah, A. H., Islam, A., Asikin-Mijan, N., Tan, Y. H., Mansir, N., Kaus, N. H. M., & Hin, T. Y. Y. (2020). Photocatalysis for organic wastewater treatment: From the basis to current challenges for society. *Catalysts*, *10*(11), 1–29. https://doi.org/10.3390/catal10111260

Mehta, A., Colusso, E., Kraxner, J., Galusek, D., Bernardo, E., & Ash, F. (2022). Waste-derived glass as a precursor for inorganic polymers : From foams to photocatalytic destructors for dye removal. *Ceramics International*, *March*. https://doi.org/10.1016/j.ceramint.2022.06.059

Mehwish, H., Aroosh, K., Meng, D., Ruan, X., Akhter, M., & Cui, X. (2025). *A review on modified ZnO to address environmental challenges through photocatalysis : Photodegradation of organic pollutants*. *48*(December 2024).

Melchionna, M., & Fornasiero, P. (2020). Updates on the Roadmap for Photocatalysis. *ACS Catalysis*, *10*(10), 5493–5501. https://doi.org/10.1021/acscatal.0c01204

Michelon, A., Bortoluz, J., Raota, C. S., & Giovanela, M. (2022). Agro-industrial residues as biosorbents for the removal of anti-inflammatories from aqueous matrices : An overview. *Environmental Advances*, *9*(April), 100261. https://doi.org/10.1016/j.envadv.2022.100261

Mirzaee, R., Darvishi Cheshmeh Soltani, R., Khataee, A., & Boczkaj, G. (2019). Combination of air-dispersion cathode with sacrificial iron anode generating Fe 2+ Fe 3+2 O 4 nanostructures to degrade paracetamol under ultrasonic irradiation. *Journal of Molecular Liquids*, *284*, 536–546. https://doi.org/10.1016/j.molliq.2019.04.033

Mirzaei, A., Chen, Z., Haghighat, F., & Yerushalmi, L. (2018). Hierarchical magnetic petal-like Fe3O4-ZnO@g-C3N4 for removal of sulfamethoxazole, suppression of photocorrosion, by-products identification and toxicity assessment.

Chemosphere, *205*, 463–474. https://doi.org/10.1016/j.chemosphere.2018.04.102

Mondal, K., & Sharma, A. (2016). Recent advances in the synthesis and application of photocatalytic metal-metal oxide core-shell nanoparticles for environmental remediation and their recycling process. *RSC Advances*, *6*(87), 83589–83612. https://doi.org/10.1039/c6ra18102c

Mu, R., Ao, Y., Wu, T., Wang, C., & Wang, P. (2020). Synthesis of novel ternary heterogeneous anatase-TiO2 (B) biphase nanowires/Bi4O5I2 composite photocatalysts for the highly efficient degradation of acetaminophen under visible light irradiation. *Journal of Hazardous Materials*, *382*(July 2019). https://doi.org/10.1016/j.jhazmat.2019.121083

Mukhair, H., Halim Abdullah, A., Adlan Mohd Hir, Z., Syazwani Osman, N., Zainal, Z., & Hong Ngee, L. (2023). In-depth investigation on the photostability and charge separation mechanism of Ag3PO4/g-C3N4 photocatalyst towards very low visible light intensity. *Journal of Molecular Liquids*, *376*, 121494. https://doi.org/10.1016/j.molliq.2023.121494

Munusamy, S., Sivaranjan, K., Sabhapathy, P., Narayanan, V., Mohammad, F., & Sagadevan, S. (2021). Enhanced electrochemical and photocatalytic activity of g-C3N4-PANI-PPy nanohybrids. *Synthetic Metals*, *272*(October 2020), 116669. https://doi.org/10.1016/j.synthmet.2020.116669

Munyengabe, A., Ndibewu, P. P., Sibali, L. L., & Ngobeni, P. (2022). Polymeric nanocomposite materials for photocatalytic detoxification of polycyclic aromatic hydrocarbons in aquatic environments-A review. *Results in Engineering*, *15*(May). https://doi.org/10.1016/j.rineng.2022.100530

MuthuKathija, M., Muthukrishnan, R. M., Renuka Devee, D., Kader, S. M. A., Rama, V., & Badhusha, M. S. M. (2023a). A novel biogenic method to synthesis a ternary (ZnO-Ag)/g-C3N4 nanocomposite with an enhanced photocatalytic and antibacterial activities. *Inorganic Chemistry Communications*, *154*(May). https://doi.org/10.1016/j.inoche.2023.110877

MuthuKathija, M., Muthukrishnan, R. M., Renuka Devee, D., Kader, S. M. A., Rama, V., & Badhusha, M. S. M. (2023b). A novel biogenic method to synthesis a ternary (ZnO-Ag)/g-C3N4 nanocomposite with an enhanced photocatalytic and antibacterial activities. *Inorganic Chemistry Communications*, *154*(March). https://doi.org/10.1016/j.inoche.2023.110877

Nassri, I., khattabi rifi, S., Sayerh, F., & Souabi, S. (2023). Occurrence, pollution

sources, and mitigation prospects of Antibiotics, anti-inflammatories, and endocrine disruptors in the aquatic environment. *Environmental Nanotechnology, Monitoring & Management*, *20*(June), 100878. https://doi.org/10.1016/j.enmm.2023.100878

Nilsen, E., Smalling, K. L., Ahrens, L., Gros, M., Miglioranza, K. S. B., Picó, Y., & Schoenfuss, H. L. (2019). Critical review: Grand challenges in assessing the adverse effects of contaminants of emerging concern on aquatic food webs. *Environmental Toxicology and Chemistry*, *38*(1), 46–60. https://doi.org/10.1002/etc.4290

Ohore, O. E., & Songhe, Z. (2019). Endocrine disrupting effects of bisphenol A exposure and recent advances on its removal by water treatment systems. A review. *Scientific African*, *5*. https://doi.org/10.1016/j.sciaf.2019.e00135

Ouriques Brasileiro, I. L., Madeira, V. S., Lopes-Moriyama, A. L., & Rodrigues de Almeida Ramalho, M. L. (2023). Addition of g-C3N4 to ZnO and ZnFe2O4 to improve photocatalytic degradation of emerging organic pollutants. *Ceramics International*, *49*(3), 4449–4459. https://doi.org/10.1016/j.ceramint.2022.09.331

Oyim, J., Amuhaya, E., Matshitse, R., Mack, J., & Nyokong, T. (2022). *Integrated photocatalyst adsorbents based on porphyrin anchored to activated carbon granules for water treatment*. *8*.

Pant, B., Park, M., & Park, S. J. (2020). Hydrothermal synthesis of Ag2CO3-TiO2 loaded reduced graphene oxide nanocomposites with highly efficient photocatalytic activity. *Chemical Engineering Communications*, *207*(5), 688–695. https://doi.org/10.1080/00986445.2019.1615470

Park, J. K., Rupa, E. J., Arif, M. H., Li, J. F., Anandapadmanaban, G., Kang, J. P., Kim, M., Ahn, J. C., Akter, R., Yang, D. C., & Kang, S. C. (2021). Synthesis of zinc oxide nanoparticles from Gynostemma pentaphyllum extracts and assessment of photocatalytic properties through malachite green dye decolorization under UV illumination-A Green Approach. *Optik*, *239*(December 2020), 1–11. https://doi.org/10.1016/j.ijleo.2020.166249

Paul, D. R., Gautam, S., Panchal, P., Nehra, S. P., Choudhary, P., & Sharma, A. (2020). ZnO-Modified g-C3N4: A Potential Photocatalyst for Environmental Application. *ACS Omega*, *5*(8), 3828–3838. https://doi.org/10.1021/acsomega.9b02688

Phong Vo, H. N., Le, G. K., Hong Nguyen, T. M., Bui, X. T., Nguyen, K. H., Rene, E.

R., Vo, T. D. H., Thanh Cao, N. D., & Mohan, R. (2019). Acetaminophen micropollutant: Historical and current occurrences, toxicity, removal strategies and transformation pathways in different environments. *Chemosphere*, *236*. https://doi.org/10.1016/j.chemosphere.2019.124391

Phuruangrat, A., Yayapao, O., Thongtem, T., & Thongtem, S. (2014). Synthesis and characterization of europium-doped zinc oxide photocatalyst. *Journal of Nanomaterials*, *2014*. https://doi.org/10.1155/2014/367529

Praus, P. (2021). On electronegativity of graphitic carbon nitride. *Carbon*, *172*, 729–732. https://doi.org/10.1016/j.carbon.2020.10.074

Q Alfaifi, M., & A Bagabas, A. (2019). Preparation, characterization, and application in water purification of g-C3N4/I-TiO2 composite photocatalysts. *Advanced Material Science*, *4*(1), 1–10. https://doi.org/10.15761/ams.1000148

Qi, Kemin, Ye, Y., Wei, B., Li, M., Lun, Y., Xie, X., & Xie, H. (2022). *N-CQDs from reed straw enriching charge over BiO 2 − x / BiOCl p-n heterojunction for improved visible-light-driven photodegradation of organic pollutants*. *432*(March).

Qi, Kezhen, Cheng, B., Yu, J., & Ho, W. (2017). Review on the improvement of the photocatalytic and antibacterial activities of ZnO. *Journal of Alloys and Compounds*, *727*, 792–820. https://doi.org/10.1016/j.jallcom.2017.08.142

Qiu, J., Li, M., Ding, M., & Yao, J. (2022). Cellulose tailored semiconductors for advanced photocatalysis. *Renewable and Sustainable Energy Reviews*, *154*(September 2021), 111820. https://doi.org/10.1016/j.rser.2021.111820

Qiu, P., Park, B., Choi, J., Thokchom, B., Pandit, A. B., & Khim, J. (2018). A review on heterogeneous sonocatalyst for treatment of organic pollutants in aqueous phase based on catalytic mechanism. *Ultrasonics Sonochemistry*, *45*, 29–49. https://doi.org/10.1016/j.ultsonch.2018.03.003

Rafaie, H. A., Nor, R. M., Azmina, M. S., Ramli, N. I. T., & Mohamed, R. (2017). *Decoration of ZnO microstructures with Ag nanoparticles enhanced the catalytic photodegradation of methylene blue dye*. *5*(April), 3963–3972.

Rafiq, A., Ikram, M., Ali, S., Niaz, F., Khan, M., Khan, Q., & Maqbool, M. (2021). Photocatalytic degradation of dyes using semiconductor photocatalysts to clean industrial water pollution. *Journal of Industrial and Engineering Chemistry*, *97*, 111–128. https://doi.org/10.1016/j.jiec.2021.02.017

Ramachandran, A., & Jaeschke, H. (2019). Acetaminophen Hepatotoxicity. *Seminars*

in Liver Disease, *39*(2), 221–234. https://doi.org/10.1055/s-0039-1679919

Ramasamy, B., Jeyanthi, J., & Chinnaiyan, P. (2023). Fe-TiO2 and Ag-ZnO mediated visible light photocatalysis for atenolol and acetaminophen removal – A comparative study and modeling. *Environmental Nanotechnology, Monitoring and Management*, *19*(January), 1–11. https://doi.org/10.1016/j.enmm.2023.100779

Ravichandran, K., Kalpana, K., Uma, R., Sindhuja, E., & seelan, K. S. (2018). Cost-effective fabrication of ZnO/g-C3N4 composite film coated stainless steel meshes for visible light responsive photocatalysis. *Materials Research Bulletin*, *99*(November 2017), 268–280. https://doi.org/10.1016/j.materresbull.2017.11.010

Reddy, P. V. L., Kim, K. H., Kavitha, B., Kumar, V., Raza, N., & Kalagara, S. (2018). Photocatalytic degradation of bisphenol A in aqueous media: A review. *Journal of Environmental Management*, *213*, 189–205. https://doi.org/10.1016/j.jenvman.2018.02.059

Reddy Pullagurala, V. L., Adisa, I. O., Rawat, S., Kim, B., Barrios, A. C., Medina-Velo, I. A., Hernandez-Viezcas, J. A., Peralta-Videa, J. R., & Gardea-Torresdey, J. L. (2018). Finding the conditions for the beneficial use of ZnO nanoparticles towards plants-A review. *Environmental Pollution*, *241*, 1175–1181. https://doi.org/10.1016/j.envpol.2018.06.036

Reza, K. M., Kurny, A., & Gulshan, F. (2017). Parameters affecting the photocatalytic degradation of dyes using TiO2: a review. *Applied Water Science*, *7*(4), 1569–1578. https://doi.org/10.1007/s13201-015-0367-y

Reza, M. S., Yun, C. S., Afroze, S., Radenahmad, N., Bakar, M. S. A., Saidur, R., Taweekun, J., & Azad, A. K. (2020). Preparation of activated carbon from biomass and its' applications in water and gas purification, a review. *Arab Journal of Basic and Applied Sciences*, *27*(1), 208–238. https://doi.org/10.1080/25765299.2020.1766799

Sa-nguanprang, S., Phuruangrat, A., Thongtem, T., & Thongtem, S. (2020). Characterization and photocatalysis of visible-light-driven Dy-doped ZnO nanoparticles synthesized by tartaric acid-assisted combustion method. *Inorganic Chemistry Communications*, *117*(April), 107944. https://doi.org/10.1016/j.inoche.2020.107944

Salahshoori, I., Yazdanbakhsh, A., Namayandeh Jorabchi, M., Kazemabadi, F. Z.,

Khonakdar, H. A., & Mohammadi, A. H. (2024). Recent advances and applications of stimuli-responsive nanomaterials for water treatment: A comprehensive review. *Advances in Colloid and Interface Science*, *333*(September). https://doi.org/10.1016/j.cis.2024.103304

Sambaza, S. S., Maity, A., & Pillay, K. (2020). *Polyaniline-Coated TiO 2 Nanorods for Photocatalytic Degradation of Bisphenol A in Water*. https://doi.org/10.1021/acsomega.0c00628

Sanjeev, N. O., & Valsan, A. E. (2024). Photocatalytic and antibacterial activity of green synthesized and immobilized zinc oxide nanoparticles for the removal of sulfadiazine and acetaminophen: Effect of operational parameters and degradation pathway. *Journal of Environmental Chemical Engineering*, *12*(3). https://doi.org/10.1016/j.jece.2024.112649

Sboui, M., Niu, W., Li, D., Lu, G., Zhou, N., Zhang, K., & Pan, J. H. (2022). Fabrication of electrically conductive TiO2/PANI/PVDF composite membranes for simultaneous photoelectrocatalysis and microfiltration of azo dye from wastewater. *Applied Catalysis A: General*, *644*(May), 118837. https://doi.org/10.1016/j.apcata.2022.118837

Selvaraj, V., Swarna Karthika, T., Mansiya, C., & Alagar, M. (2021). An over review on recently developed techniques, mechanisms and intermediate involved in the advanced azo dye degradation for industrial applications. *Journal of Molecular Structure*, *1224*. https://doi.org/10.1016/j.molstruc.2020.129195

Shen, J., Shi, A., Lu, J., Lu, X., Zhang, H., & Jiang, Z. (2023). Optimized fabrication of Cu-doped ZnO/calcined CoFe–LDH composite for efficient degradation of bisphenol a through synergistic visible-light photocatalysis and persulfate activation: Performance and mechanisms. *Environmental Pollution*, *323*(January). https://doi.org/10.1016/j.envpol.2023.121186

Sin, J. C., Lam, S. M., Mohamed, A. R., & Lee, K. T. (2012). Degrading endocrine disrupting chemicals from wastewater by tiO 2 photocatalysis: A review. *International Journal of Photoenergy*, *2012*. https://doi.org/10.1155/2012/185159

Singh, N. B., Nagpal, G., Agrawal, S., & Rachna. (2018). Water purification by using Adsorbents: A Review. *Environmental Technology and Innovation*, *11*, 187–240. https://doi.org/10.1016/j.eti.2018.05.006

Singh, S., Kumar, V., Dhanjal, D. S., Datta, S., Kaur, S., Romero, R., & Singh, J.

(2021). 9 - Degradation of pesticides in wastewater using heterogeneous photocatalysis. In *Advance Oxidation Processes for Effluent Treatment Plants*. Elsevier Inc. https://doi.org/10.1016/B978-0-12-821011-6.00009-8

Soltani, R. D. C., Miraftabi, Z., Mahmoudi, M., Jorfi, S., Boczkaj, G., & Khataee, A. (2019). Stone cutting industry waste-supported zinc oxide nanostructures for ultrasonic assisted decomposition of an anti-inflammatory non-steroidal pharmaceutical compound. *Ultrasonics Sonochemistry*, *58*(July). https://doi.org/10.1016/j.ultsonch.2019.104669

Steplin Paul Selvin, S., Ganesh Kumar, A., Sarala, L., Rajaram, R., Sathiyan, A., Princy Merlin, J., & Sharmila Lydia, I. (2018). Photocatalytic Degradation of Rhodamine B Using Zinc Oxide Activated Charcoal Polyaniline Nanocomposite and Its Survival Assessment Using Aquatic Animal Model. *ACS Sustainable Chemistry and Engineering*, *6*(1), 258–267. https://doi.org/10.1021/acssuschemeng.7b02335

Stukenborg, J. B., Mitchell, R. T., & Söder, O. (2021). Endocrine disruptors and the male reproductive system. *Best Practice and Research: Clinical Endocrinology and Metabolism*, *35*(5), 1–13. https://doi.org/10.1016/j.beem.2021.101567

Su, K., Liu, H., Gao, Z., Fornasiero, P., & Wang, F. (2021). Nb2O5-Based Photocatalysts. *Advanced Science*, *8*(8), 1–25. https://doi.org/10.1002/advs.202003156

Sun, C., Xu, Q., Xie, Y., Ling, Y., & Hou, Y. (2018). Designed synthesis of anatase-TiO2 (B) biphase nanowire/ZnO nanoparticle heterojunction for enhanced photocatalysis. *Journal of Materials Chemistry A*, *6*(18), 8289–8298. https://doi.org/10.1039/c7ta10274g

Sun, Y., Zhang, W., Li, Q., Liu, H., & Wang, X. (2023). *Preparations and applications of zinc oxide based photocatalytic materials*. *2*(May).

Sundaram, I. M., Kalimuthu, S., & Ponniah, G. P. (2017). Highly active ZnO modified g-C3N4 Nanocomposite for dye degradation under UV and Visible Light with enhanced stability and antimicrobial activity. *Composites Communications*, *5*(July), 64–71. https://doi.org/10.1016/j.coco.2017.07.003

Tahir, M. B., Sohaib, M., Sagir, M., & Rafique, M. (2022). Role of Nanotechnology in Photocatalysis. *Encyclopedia of Smart Materials*, 578–589. https://doi.org/10.1016/b978-0-12-815732-9.00006-1

Tang, M., Ao, Y., Wang, C., & Wang, P. (2020). Rationally constructing of a novel

dual Z-scheme composite photocatalyst with significantly enhanced performance for neonicotinoid degradation under visible light irradiation. *Applied Catalysis B: Environmental*, *270*(February). https://doi.org/10.1016/j.apcatb.2020.118918

Tisler, S., Tüchsen, P. L., & Christensen, J. H. (2022). Non-target screening of micropollutants and transformation products for assessing AOP-BAC treatment in groundwater. *Environmental Pollution*, *309*(July), 119758. https://doi.org/10.1016/j.envpol.2022.119758

Torkamani, R., Aslibeiki, B., Darbandi, M., & Naghshara, H. (2024). The Effect of Particle Size on Photocatalytic Degradation of Oxytetracycline by ZnO Nanoparticles. *Journal of Water and Environmental Nanotechnology*, *9*(2), 186–195. https://doi.org/10.22090/jwent.2024.02.05

Tsai, Y. S., Chen, J. R., Lee, C. H., Kuo, C. C., Lin, Y. H., Wang, C. C., Chang, Y. C., Wu, Y. C. S., & Chen, H. (2022). Morphologies and material properties of ZnO nanotubes, ZnO/ZnS core-shell nanorods, and ZnO/ZnS core-shell nanotubes. *Ceramics International*, *48*(5), 7232–7239. https://doi.org/10.1016/j.ceramint.2021.11.283

Uddin, M. T., Hoque, M. E., & Chandra Bhoumick, M. (2020). Facile one-pot synthesis of heterostructure SnO 2 /ZnO photocatalyst for enhanced photocatalytic degradation of organic dye. *RSC Advances*, *10*(40), 23554–23565. https://doi.org/10.1039/D0RA03233F

Uma, R., Ravichandran, K., Sriram, S., & Sakthivel, B. (2017). Cost-effective fabrication of ZnO/g-C3N4 composite thin films for enhanced photocatalytic activity against three different dyes (MB, MG and RhB). *Materials Chemistry and Physics*, *201*, 147–155. https://doi.org/10.1016/j.matchemphys.2017.08.015

Wang, C., Zhu, J., Wu, X., Xu, H., Song, Y., Yan, J., & Song, Y. (2014). Photocatalytic degradation of bisphenol A and dye by graphene-oxide / Ag 3 PO 4 composite under visible light irradiation. *Ceramics International*, *40*(6), 8061–8070. https://doi.org/10.1016/j.ceramint.2013.12.159

Wang, S., Liu, B., Zhi, G., Gong, X., & Zhang, J. (2018). Diverse nitrogen-doped 2D layered mesoporous MoS 2 /reduced graphene oxide composites with superior structural features for enhancing the performance of lithium ion batteries. *Applied Surface Science*, *458*(February), 954–963. https://doi.org/10.1016/j.apsusc.2018.07.075

Wang, Y., Li, X., Yang, Y., Yang, J., Zhang, N., Wu, X., & Li, X. (2020). Visible

light degradation and separation of RhB by magnetic Fe3O4/ZnO/g-C3N4 nanoparticles. *Journal of Materials Science: Materials in Electronics*, *31*(7), 5187–5197. https://doi.org/10.1007/s10854-020-03078-3

Weldekirstos, H. D., Mengist, T., Belachew, N., & Mekonnen, M. L. (2024). Enhanced photocatalytic degradation of methylene blue dye using fascily synthesized g-C3N4/CoFe2O4 composite under sun light irradiation. *Results in Chemistry*, *7*(August 2023). https://doi.org/10.1016/j.rechem.2024.101306

Wilkinson, J. L., Boxall, A. B. A., Kolpin, D. W., Leung, K. M. Y., Lai, R. W. S., Wong, D., Ntchantcho, R., Pizarro, J., Mart, J., Echeverr, S., Garric, J., Chaumot, A., Gibba, P., Kunchulia, I., Seidensticker, S., Lyberatos, G., Morales-salda, J. M., & Kang, H. (2022). *Pharmaceutical pollution of the world ' s rivers*. *119*(8), 1–10. https://doi.org/10.1073/pnas.2113947119/-/DCSupplemental.Published

Wu, Y., Chen, C., He, S., Zhao, X., Huang, S., Zeng, G., You, Y., Cao, Y., & Niu, L. (2021). In situ preparation of visible-light-driven carbon quantum dots/NaBiO3 hybrid materials for the photoreduction of Cr(VI). *Journal of Environmental Sciences (China)*, *99*, 100–109. https://doi.org/10.1016/j.jes.2020.06.016

Xu, J., & Ma, S. (2023). High-efficiency photocatalytic degradation of RhB by protonation of g-C3N4 with Ag-loaded TiO2 nanofibers. *Journal of Crystal Growth*, *617*(May). https://doi.org/10.1016/j.jcrysgro.2023.127290

Yang, H., Yang, B., Chen, W., & Yang, J. (2022). Preparation and Photocatalytic Activities of TiO2-Based Composite Catalysts. *Catalysts*, *12*(10). https://doi.org/10.3390/catal12101263

Yin, L., Wang, Z., Lu, L., Wan, X., & Shi, H. (2015). Universal degradation performance of a high-efficiency AgBr/Ag 2 CO 3 photocatalyst under visible light and an insight into the reaction mechanism. *New Journal of Chemistry*, *39*(6), 4891–4900. https://doi.org/10.1039/C5NJ00385G

Youssef, Z., Colombeau, L., Yesmurzayeva, N., Baros, F., Vanderesse, R., Hamieh, T., Toufaily, J., Frochot, C., & Roques-Carmes, T. (2018). Dye-sensitized nanoparticles for heterogeneous photocatalysis: Cases studies with TiO2, ZnO, fullerene and graphene for water purification. *Dyes and Pigments*, *159*, 49–71. https://doi.org/10.1016/j.dyepig.2018.06.002

Yu, H. L., Liu, L. Q., Zhou, Y. W., Xue, X. L., Yuan, X. H., Shen, Y. G., Liu, Z. Q., Chen, H. M., & Huang, C. L. (2023). Photocatalysis performance enhancement of Ag2O/Al-doped ZnO heterojunction by introducing ZnO nanorod array.

Ceramics International, *49*(7), 10513–10524. https://doi.org/10.1016/j.ceramint.2022.11.238

Yuan, X., Floresyona, D., Aubert, P. H., Bui, T. T., Remita, S., Ghosh, S., Brisset, F., Goubard, F., & Remita, H. (2019). Photocatalytic degradation of organic pollutant with polypyrrole nanostructures under UV and visible light. *Applied Catalysis B: Environmental*, *242*, 284–292. https://doi.org/10.1016/j.apcatb.2018.10.002

Yue, Y., Yue, X., Tang, X., Han, L., Wang, J., Wang, S., & Du, C. (2024). *Heliyon Synergistic adsorption and photocatalysis study of TiO 2 and activated carbon composite*. *10*(May).

Zhang, F., Wang, X., Liu, H., Liu, C., Wan, Y., Long, Y., & Cai, Z. (2019). Recent advances and applications of semiconductor photocatalytic technology. *Applied Sciences (Switzerland)*, *9*(12). https://doi.org/10.3390/app9122489

Zhang, Q., Wang, B. X., Yu, Y. B., Chen, B. Y., & Hong, J. ming. (2020). Sulfur doped-graphene for enhanced acetaminophen degradation via electro-catalytic activation: Efficiency and mechanism. *Science of the Total Environment*, *715*. https://doi.org/10.1016/j.scitotenv.2020.136730

Zhao, H., Li, G., Tian, F., Jia, Q., Liu, Y., & Chen, R. (2019). g-C3N4 surface-decorated Bi2O2CO3 for improved photocatalytic performance: Theoretical calculation and photodegradation of antibiotics in actual water matrix. *Chemical Engineering Journal*, *366*, 468–479. https://doi.org/10.1016/j.cej.2019.02.088

Zhu, J., Zhang, T., Yang, Y., & Huang, R. (2020). A comprehensive review on emerging artificial neuromorphic devices. *Applied Physics Reviews*, *7*(1). https://doi.org/10.1063/1.5118217

Ziaalmolki, S., Aslibeiki, B., Zarei, M., Torkamani, R., & Sarkar, T. (2023). Enhanced visible-light-driven photocatalysis via magnetic nanocomposites: A comparative study of g-C3N4, g-C3N4/Fe3O4, and g-C3N4/Fe3O4/ZnO. *Materials Today Communications*, *37*(October). https://doi.org/10.1016/j.mtcomm.2023.107340

APPENDICES

APPENDIX 1

Calculation for the preparation of Acetaminophen (ACE) working solution

i. Preparation of stock solution of 100 ppm

100 ppm = 100mg/L = **0.1 g/L**

0.1 g of ACE was put in 1 L volumetric flask and filled with distilled water to the mark.

ii. *Preparation of standard solution 10 ppm

$M_1V_1 = M_2V_2$

(100 ppm) x V_1 = (10 ppm) x (1000 mL)

V_1 = **100 mL**

*The equation applies for the preparation of other concentration of ACE (5 ppm, 15 ppm and 20 ppm)

AUTHOR'S PROFILE

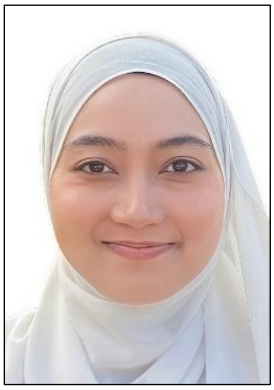

Nurul Izzati Binti Izhar obtained Bachelor of Science in Industrial Chemical Technology (Hons.) in 2021 from Universiti Sains Islam Malaysia, Negeri Sembilan. Her BSc thesis regarding using one of chemometric techniques which is Principal Component Analysis (PCA) and with the help of Fourier Transform Infrared (FTIR) spectroscopy to estimate the percentage of lard in the heated mixtures of edible fats of bovine and vegetable.

LIST OF PUBLICATION:

Izhar, N. I., Hir, Z. A. M., Rafaie, H. A., & Daud, S. Influence of ZnO content on activated carbon/ZnO for enhanced acetaminophen removal under very low light intensity: Kinetics, operational variables, and radical trapping response. Kuwait Journal of Science 52.2, 2025. 100391.

Izhar, N. I., Hir, Z. A. M., Daud, S., & Rafaie, H. A. Physicochemical Characterization of Zno/g-C_3N_4 for Photo-Removal of Methyl Orange under Low UV-light Intensity. Malaysian Journal of Analytical Sciences, 2024. Vol 28 No 2: 365 - 375

Izhar, N. I., Hir, Z. A. M., Sazman, N. S. N., Azaludin, N. R. M., Daud, S., & Rafaie, H. A. Polymer-Based Photocatalysts for Pharmaceutical Wastewater Treatment. Advanced Materials for Pharmaceutical Wastewater Treatment. CRC Press, 2024. 219-256.

Sazman, N. S. N., Izhar, N. I., Mohamad Azaludin, N. R., Daud, S., Ahmad Rafaie, H., & Mohd Hir, Z. A. Valorization of Wood Waste as Biosorbent for the Removal of Organic and Inorganic Contaminants in Water. In *Wood Waste Management and Products*, 2023. (pp. 59-78). Singapore: Springer Nature Singapore.